A programmable chemical computer with memory and pattern recognition

Juan Manuel Parrilla Gutierrez,[1] Soichiro Tsuda,[1+] Abhishek Sharma,[1+] Geoffrey J. T. Cooper,[1] Gerardo Aragon-Camarasa,[1] Kevin Donkers[1] and Leroy Cronin[1]*

[1]School of Chemistry, The University of Glasgow, University Avenue, Glasgow G12 8QQ, UK, *Corresponding author email: Lee.Cronin@glasgow.ac.uk

+ these authors contributed equally

Once Sentence Summary: A programmable chemical computer with memory that can perform pattern recognition using a reaction-diffusion reaction is demonstrated.

Abstract: Current electronic computers are limited by the cost of fabrication and power dissipation. In contrast, computers that use chemical reactions can scale beyond current technology as the processing unit and memory are combined, performing computations through chemical reactions, yet their lack of programmability limits their practical use. We present a programmable chemical computer comprising of a 5 by 5 array of cells filled with a switchable oscillating chemical (Belousov–Zhabotinsky, BZ) reaction. Each cell can be addressed using magnetic stirrer bars in the 'on' or 'off state, with the weakly interconnected cells giving up to $2^{(5x5)}$ different programmable chemical input states, and this yields more than 10^{22} chemical states. By programming the array, we were able to demonstrate chemically encoded and addressable memory, and we were able to create a chemical autoencoder for pattern recognition that was able to achieve the equivalent of around one million operations per second.

Main text: Over the last 50 years computers have become ubiquitous, essential for many aspects of modern life. During this period their processing power has increased manifold, but the paradigm used has remained the same keeping the processor and memory separate (*1*, *2*), and using binary state electronic switches (*3*, *4*). Systems based upon quantum effects

promise to solve problems intractable for conventional computers (*5*, *6*), but they are yet to reach their full potential. However, nature exploits the parallelism of collective networks (*7*–*9*) by developing systems able to process information despite large amounts of noise (*10*). Furthermore, it has been demonstrated that even non-living chemical systems can implement computations (*11*–*16*).

Herein, we show that a chemical computer, which utilizes individually addressed but fully interconnected cells of a chemical oscillating Belousov–Zhabotinsky (BZ) reaction as the data processing medium (*17*), can be programmed to achieve flexible and multi-purpose computation by using individually controlled stirring speeds as user code input (Figure 1 and SM1). Our computer architecture relies on data storage and information processing via electron transfer between molecules of $[Fe(Bpy)_3]^{2/3+}$ as a catalyst for the BZ reaction (*18*) and an indicator where the oxidized regions containing Fe(III) are blue, and the reduced states containing Fe(II) species are red. To achieve programmability, we designed a platform that controls the inputs as oscillations of the BZ reaction at local sites in a grid ("cells") by externally controlling the oscillations in each cell with a magnetic stirrer, where cells are only triggered when a stirrer is turned on. The output from the array is produced by recording a video of to monitor the oscillation states of the reaction in the individual cells. As a result, programming the platform can be done to exploit the chemical states arising from interactions between spatiotemporal excitation patterns (*19*). This means that the excited waves generated at a cell can propagate to neighboring cells by setting phase and oscillation frequency of active cells controlling their stirrer speed and initial time, and eventually form a globally synchronized oscillation pattern.

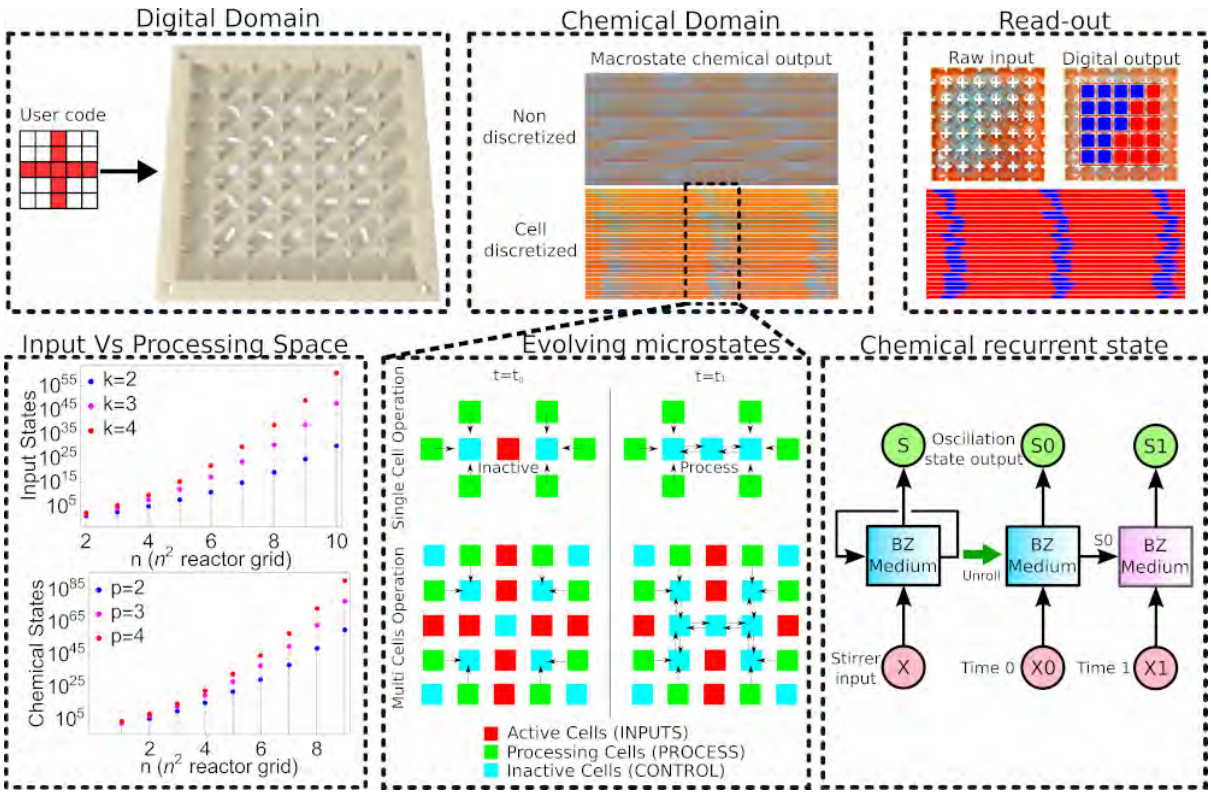

Figure 1. Chemical computer paradigm. (Digital Domain) In the current platform the user can input the code as a 5 by 5 grid of data. This grid of data will define which stirrers oscillate, and also their speed. (Chemical Domain) Based on the selected grid, oscillating waves will appear in the platform. If the cells are discretized, these oscillations will localize. (Read-out) Using a camera and machine learning the states of the chemical computer are read by a digital computer. (Input Vs Processing Space) Input States plot shows the scaling of the number of input states with the number of BZ cells on the experimental platform at different PWM stirring inputs (k^{nxn}, where k can be 2, 3 and 4). (Chemical States) shows scaling of the number of chemical states (defined by initial phase and frequency of BZ oscillations, see SI) with the number of BZ cells on the experimental platform at a different number of measurable oscillation frequencies ($2^{nxn}p^{nxn}$ where p can be 2, 3 and 4). (Evolving microstates) Because the cells are weakly connected, their oscillations will convolve, and be able to perform complex computations by controlling the stirring speeds into (a) active cells – fast stirring – for inputs, (b) process cells – slow stirring (c) inactive cells – no stirring (see SI) (Chemical recurrent state) Because the BZ oscillations have memory, the global state of the medium not only depends on the input, but also on the state of previous iterations.

We propose that our automated BZ system can be used as a programmable chemical computing system, exploiting the excitability and bistability of the oscillating chemical reaction. We demonstrate programmability by performing different computational tasks in our BZ platform, such as memory, and a chemical Neural Network capable of pattern recognition. Our digital-chemical computing system consists of four components (see Figure

1 and see methods). (i) The BZ reactor cell grid can be customized to the desired geometry depending on the experiment. In addition, by changing the size of the opening gap between neighbouring cells it is possible to control the global propagation of BZ excitation (see Figure 2). When the gap size was large enough, the whole BZ medium generates coherent excitation wave patterns. (ii) A magnetic stirrer array consisting of 25 motors to control the stirrer bars within the BZ reactor cells. (iii) A control interface connected to a computer and the magnetic stirrer array. The rotation speed of each stirrer can be individually controlled therefore, the local oscillations of the BZ reaction at a given cell can be individually addressed. (iv) The BZ reaction in the cells was monitored by a camera mounted above the grid. The camera was connected to a computer which analyzed the BZ reaction in real-time, and classified each cell as excited (blue) or non-excited state (red) (see Methods).

Ferroin, $[Fe(Bpy)_3]^{2/3+}$ was chosen as the sole catalyst since this gives simple oscillations and the colour change between the reduced form (red) and the oxidized form (blue) is distinct and easily tracked optically. The other chemical components used were sulfuric acid, malonic acid and potassium bromate (see the SI for a description of how the solutions were prepared). To control the reaction, we exploited the fact that bulk oscillations of the BZ reaction break down and may become chaotic with short-lived or completely suppressed oscillations when they are not stirred (*20*). Thus, the excitation of an individual BZ cell in the grid can be controlled by activating a stirrer placed in the cell. To stir cells and drive patterns in the resulting oscillations, the platform described in Figure 1 was used, where each cell contained a stirring bar and was directly placed above a motor with a pair of opposing magnets attached to its shaft. This way, the stirring could be turned on and BZ oscillatory excitation waves generated only in specific cells. Defining which cells were stirred and which were not (i.e. input pattern) could then impact the formation of excitation wave patterns on the chemical

system, see Figure 2. This is because the stirred cells are more likely to generate oscillatory excited waves, which propagated to neighbouring cells and eventually formed a globally synchronized wave pattern. The speed of stirrers in the grid could be individually controlled and input patterns with different stirrer speeds could result in different global wave patterns of BZ reaction. Once a cell oscillates by being stirred, it will continue to oscillate long after the stirring is stopped. Depending on the concentration of potassium bromate the number of oscillations that can occur without physical actuation can arrive up to eight repetitions (see SI). This property can be used for short-term information storage, where the BZ platforms acts similar to a volatile memory, akin to computer RAM. By pairing the system programmability using the mechanical stirrers, and the system memory via the BZ medium, the platform keeps processing and memory residing in the same space.

By using grids of discrete but fluidically-connected cells, we were able to control the propagation of wave patterns from a cell to a neighbouring cell. The basic starting design for the platform comprised a 7 × 7 grid, where only the middle 5 × 5 cells were used. To control the interaction between cells, we first designed and fabricated a prototype array of BZ cell grid using a 3D printer which had a “v” shape opening between cells. The BZ reaction volume used was 70 ml, which filled the arena to three quarters of its height, well above the “v” opening. With this design, it was found that oscillations did not propagate to neighbouring cells and the platform acted similarly to a display screen, where only the cells that were enabled flashed in blue, while the other ones remained red (Fig. 2 Top-Left and SM2). To facilitate improved interaction between cells, we removed the “v” shaped part of the opening, leaving only the corners of each cell to define it (Fig. 2 Top-Right). This way the fluid from an activated cell would propagate to its neighbours when stirred, and we could, for example, activate a cell that was disabled by stirring (and therefore activating) its neighbours.

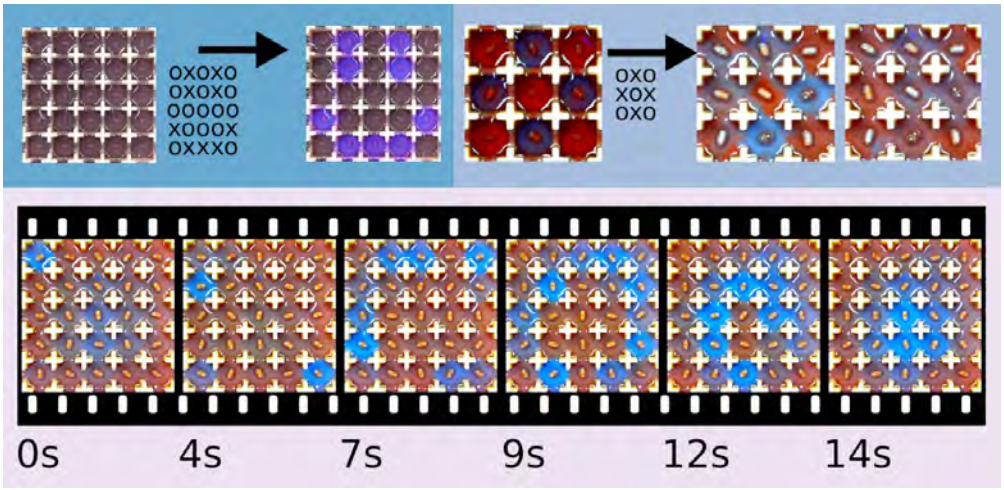

Figure 2 Controlling the oscillating cells. In this figure, every video frame is accompanied by a matrix of "x" and "o". This matrix indicates if in that given frame a motor was enabled (marked with a "x") or disabled (marked with a "o"). (Top-left) With a v-shape opening between cells, we could flash images like in a display screen. Here, for example, it was flashed a smiley emoji. (Top-right) The main drawback of this v-shape opening between cells is that very little fluid was transferred between them, as can be seen in B-left. Thus we decided to completely open the gap, see B-right, and this allowed for a better connection between cells, and in this way we achieved the objective of enabling a cell which was disabled just by enabling its surrounding cells. (Bottom) Once the cells are weakly connected, they will generate coherent patterns. (Note: the oscillations in the top-left image have been had the contrast enhanced, but the movie SM2 shows the oscillations with raw video).

To implement a chemical computer, we exploited the fact that when all of the stirrers were activated, globally synchronized wave patterns emerged from the system. The emergence of globally synchronized patterns comes from two properties of the BZ reaction: (1) Sustained oscillation: once activated, a BZ reaction tends to sustain its oscillation even after the stirrer is off (see SM3). Thus, each cell can be considered as an oscillator. (2) Signal convolution: the BZ excitation waves generated at a cell propagate to neighbouring cells where another excitation waves are generated. The waves collide and interact to form a synchronized oscillation. Thus, the whole BZ grid system can be viewed as a coupled oscillator system, or more in general, as a chemical dynamical system that consistently converts stirrer input patterns into patterns of excitation waves.

An example of the emergence of global oscillations can be seen on Figure 3. Here, the columns marked as “on” rotated at a high speed, while the other ones rotated at a slower speed. Setting “on” only the left-most or the right-most column, we discovered that the stirrer motion generated a unidirectionally propagating pattern: when the right-most column was “on”, oscillating waves were generated from the bottom-left corner to the top-right one, while when the left-most column was on, a similar but mirrored pattern emerged. In order to better study this, a dataset was created using similar stirring patterns to the ones just described, and this dataset was then used to train a Recurrent Neural Network (RNN) using “Long short-term memory” cells. This RNN was able to emulate the behaviour of simple input stirring patterns as the ones just described, see Figure 3. Nevertheless, it failed to emulate more complex patterns, with, for example, different disconnected sources of oscillations. This showed the potential of our chemical computer of producing results beyond what can be achieved with current state-of-the-art technologies.

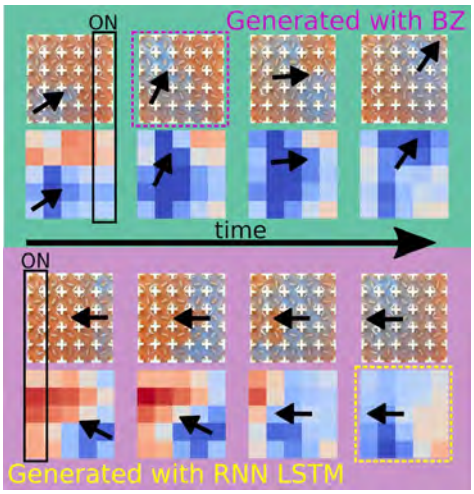

Figure 3 Studying the behaviour of unidirectional wave oscillations. When only activating one column at high speed while keeping all the other hands at a lower speed, the platform produced unidirectional wave patterns. For example, when activating the right-most column at high speed, the system produced waves from left to right, while when activating the left-most column at high speed, it produced waves from right to left. Using a dataset of similar stirring patterns, a RNN was trained to emulate the oscillations generated by the BZ platform. In this plots, blue means that a cell oscillates, while red means it did not. The trained RNN was able of emulating some of the basic input patterns.

To perform more complex tasks such as pattern recognition and data encoding, we interfaced our chemical computer to an Artificial Neural Network, which was used as computing output layer to discover and discern the BZ computational space. The wave propagation patterns described before were found to be reproducible between parallel experiments, which indicates that our BZ platform can consistently convert an input pattern into a wave propagation pattern. Detection and interpretation of such propagating patterns was relatively easy with simple input patterns, but it increasingly becomes more complicated to human interpreters as the input patterns become complex. However, the complex patterns generated were neither random, nor impossible to distinguish between them, because the BZ system generates consistent outputs in response to the same input pattern.

To exploit this feature, we adapted the 'reservoir computing' scheme (*21*) using the BZ platform (Figure 4, B). Namely, the system's output is interfaced with a neural network which is used to classify different input patterns based on the wave they generate. The generated wave propagation patterns were input into a neural network layer after being processed using image processing in order to identify the BZ oscillations (Figure 4, A). To capture the temporal dynamics of the wave propagation patterns, a sliding window over 100 time points (~ 50 seconds) was used to create a dataset with 2500 features (25 cells × 100 time points). We first used ten different input patterns representing digital numbers from zero to nine (see SI) with 1500 training data points and 300 test data points, which gave correct answers with 98.6% accuracy against the test dataset.

This result suggests that the BZ system produces consistent patterns upon a specific input pattern that can be distinguished by a machine learning algorithm (which may be too complicated for the human eye). In other words, the BZ system satisfies the "echo state property" of reservoir computing (*22*); i.e. each cell within its "reservoir" neighbours produces a nonlinear response signal which is combined into a desired output signal by

means of linear combinations of these response signals in the BZ grid. In contrast, when using the reservoir system without the BZ reaction, but replaced with pure water, the output neural network is not capable of classifying the patterns because the dynamics of the water are not sufficient to project input patterns into higher dimensional space (see SI).

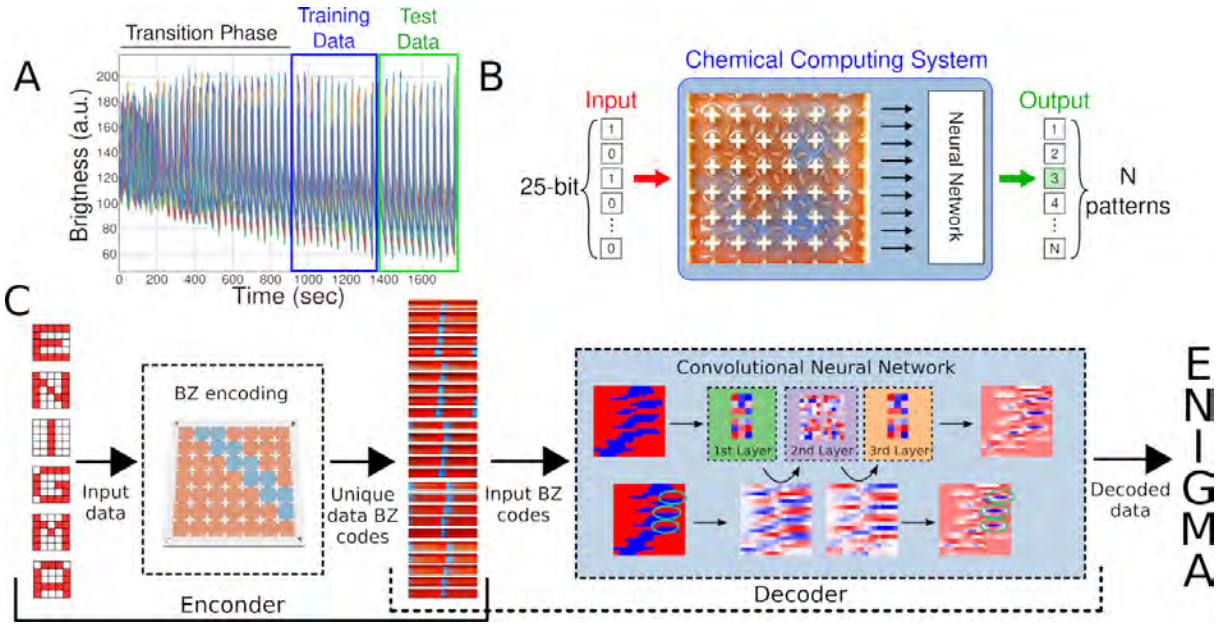

Figure 4 Pattern classification and data encoding by BZ reaction and machine learning. (A) An example output pattern of the BZ reaction system. The data after the transition phase (~15 min) was used for pattern recognition, which was further split into two parts as training and test date, respectively. (B) Schematic for BZ reaction grid data analysis using reservoir computing scheme. (C) Schematic showing the full working pipeline of our system. Initially the user selects a pattern to flash, and this pattern is binarised in 5 by 5 matrix. This matrix is used as a source for the PWM generator, and this will eventually generate a global oscillation. These oscillations are then enconded into a machine learning model, and decode when needed for pattern recognition. In order to decode it a CNN was used. It contained three convolutional layers with filters of 3 by 3, 5 by 5 and 3 by 3. In the bottom row there it can be seen how we speculate that the CNN learns how to classify a given input by finding the points of the oscillations where it contains a bigger phase difference.

To prove that during the pattern recognition process our BZ platform acted like a chemical computer, we performed a similar experiment, but in this case the BZ platform was replaced by a Fully-connected Neural Network (FNN) -which had been trained to digitally produce BZ oscillations from input motor patterns, see Figure 5 Top-left. This way, the FNN had as

inputs the different motor patterns, it then digitally generated a BZ oscillation, and then this BZ oscillation was classified using a Convolutional Neural Network (CNN) (Figure 5 Top-Right). This is effectively the same process detailed in Figure 4C, but by-passing the BZ medium and using a neural network instead. The CNN correctly labelled the different BZ oscillations, both the ones generated through the BZ medium, and the ones generated with the FNN. This unequivocally means that our platform is acting like a chemical computer because it is developing the same role as a neural network, specifically we can consider this to be acting like a chemical autoencoder.

To benchmark the effective computational power exhibited by the 25-cell BZ system, we should consider the number of logical operations that the equivalent artificial neural network would need to do in order to encode the patterns, and how this is manifested in the silicon substrate, see SI. Given that the BZ platform has 2^{25} binary stirring pattern states and around 3.77×10^{22} chemical states, this seemed a reasonable challenge. It was possible to use an autoencoder that had three layers of 50-10-50 neurons, with 25 inputs and 625 outputs that would give outcomes with similar accuracy. The total number of operations can be evaluated to be of the order of 60 M operations using around 32 M logic gates, which would need 100 M transistors. The total time the chemical-computer needed to decode the pattern is around 60 seconds worth of data which equates to around 1 M operations per second whilst only consuming 1.56 W of power.

We show our chemical computer serves as a sophisticated system in which the dynamics or functions that are theoretically difficult to infer can be calculated within the computation space defined by our BZ-driven cellular chemical computer. For example, the system can be exploited as encoding device, see Figure 4, and we have tested the described chemical encoding machine, and in our tests it could distinguish a total of 26 patterns reliably, with up

to 96% accuracy (see SI). This was achieved by addressing the cells individually, generating oscillations at localized positions, yet are weakly connected in a shared medium, creating a network of coupled oscillators, similar to, for example, the oscillatory neural computer network (*23*).

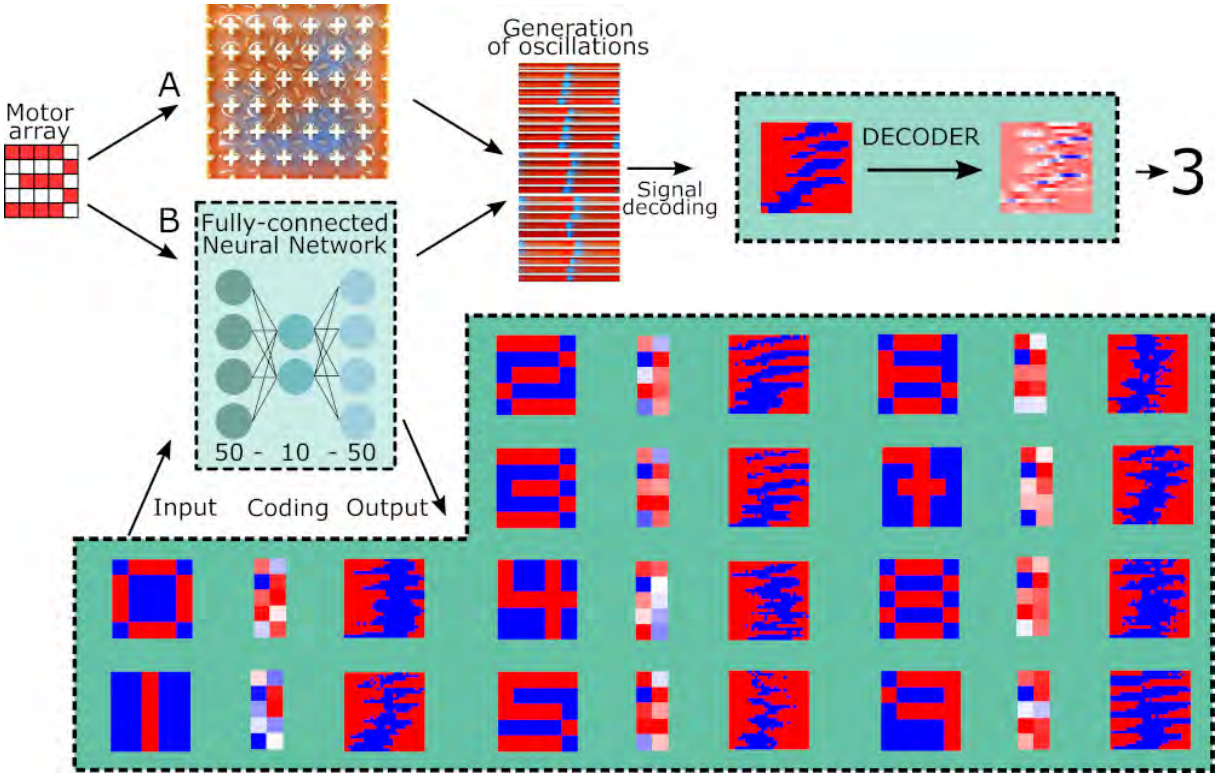

Figure 5 Comparing the BZ oscillations produced by an Autoenconder and by the BZ platform. (Top-left) Flow diagram of the pattern recognition process. The "A" path uses the BZ medium as described on Figure 4. The "B" path uses a Fully-connected Neural Network (FNN) which has been trained beforehand in order to digitally produce BZ oscillations from motor patterns. (Top-right) Once the oscillations were generated using the BZ platform or the FNN, they were correctly decoded using a model as shown on Figure 4. (Bottom) Digitally generated BZ oscillations using the FNN. For each case, the input shown is the motor pattern used, and the output shown is the BZ oscillation obtained. In these BZ oscillation plots the blue colour represents when the oscillation happens. The X axis means time, and the Y axis means location – each of the 25 cells. The coding represents the hidden layer of the FNN.

In a 5 by 5 grid as defined, and in the case of binary stirrer inputs, there are a total of 2^{25} (33,554,432) different states. The effect of stirring rate on the BZ oscillation frequency and amplitude has been previously studied (*24*). If we assume four different detectable oscillation

frequency as an outcome of different stirring rates and nearest neighbour interactions we obtain a theoretical total of 3.77 $x10^{22}$ different states in the BZ computation space whilst only consuming around 1.56 W of power. This could be compared to the state-of-the-art processors (e.g. core i9) which is capable of a teraflop (10^{12} operations) whilst expending 147 W of power. The challenge is now to extend the programmability of our system and go beyond 10^6 effective operations per second.

References

1. C. Rios, M. Stegmaier, P. Hosseini, D. Wang, T. Scherer, C. D. Wright, H. Bhaskaran, W. H. P. Pernice, Integrated all-photonic non-volatile multi-level memory. *Nat. Photonics*. **9**, 725–732 (2015).
2. T. Toffoli, Nothing makes sense in computing except in the light of evolution. *Int. J. Unconv. Comput.* **1**, 3–29 (2005).
3. A. Bérut, A. Arakelyan, A. Petrosyan, S. Ciliberto, R. Dillenschneider, E. Lutz, Experimental verification of Landauer's principle linking information and thermodynamics. *Nature*. **483**, 187–189 (2012).
4. V. V. Zhirnov, R. K. Cavin, J. A. Hutchby, G. I. Bourianoff, Limits to binary logic switch scaling - A Gedanken model. *Proc. IEEE*. **91**, 1934–1939 (2003).
5. T. D. Ladd, F. Jelezko, R. Laflamme, Y. Nakamura, C. Monroe, J. L. O'Brien, Quantum computers. *Nature*. **464**, 45–53 (2010).
6. S. L. Zhu, Z. D. Wang, Unconventional geometric quantum computation. *Phys. Rev. Lett.* **91** (2003), doi:10.1103/PhysRevLett.91.187902.
7. G. Deco, M. L. Kringelbach, Hierarchy of Information Processing in the Brain: A Novel 'Intrinsic Ignition' Framework. *Neuron*. **94**, 961–968 (2017).
8. V. Sourjik, Receptor clustering and signal processing in E. coli chemotaxis. *Trends Microbiol.* **12** (2004), pp. 569–576.
9. D. J. Watts, S. H. Strogatz, Collective dynamics of "small-world" networks. *Nature*. **393**, 440–442 (1998).
10. G. Deco, M. L. Kringelbach, Hierarchy of Information Processing in the Brain: A Novel 'Intrinsic Ignition' Framework. *Neuron*. **94** (2017), pp. 961–968.
11. L. Qian, E. Winfree, Scaling up digital circuit computation with DNA strand displacement cascades. *Science*. **332**, 1196–1201 (2011).
12. M. Conrad, On design principles for a molecular computer. *Commun. ACM*. **28**, 464–480 (1985).
13. A. Prokup, J. Hemphill, A. Deiters, DNA computation: A photochemically controlled and gate. *J. Am. Chem. Soc.* **134**, 3810–3815 (2012).
14. T. S. Gardner, C. R. Cantor, J. J. Collins, Construction of a genetic toggle switch in Escherichia coli. *Nature*. **403**, 339–342 (2000).
15. Y. Fang, V. V. Yashin, S. P. Levitan, A. C. Balazs, Pattern recognition with "materials that compute." *Sci. Adv.* **2**, e1601114–e1601114 (2016).
16. K. Gizynski, J. Gorecki, Chemical memory with states coded in light controlled oscillations of interacting Belousov–Zhabotinsky droplets. *Phys. Chem. Chem. Phys.*

19, 6519–6531 (2017).
17. A. Adamatzky, B. D. L. Costello, T. Asai, *Reaction-Diffusion computers* (Elsevier Inc., 2005).
18. Y. Gao, A. R. Cross, R. L. Armstrong, Magnetic resonance imaging of ruthenium-, cerium-, and ferroin-catalyzed Belousov-Zhabotinsky reactions. *J. Phys. Chem.* **100**, 10159–10164 (1996).
19. M. F. Crowley, I. R. Epstein, Experimental and theoretical studies of a coupled chemical oscillator: Phase death, multistability, and in-phase and out-of-phase entrainment. *J. Phys. Chem.* **93**, 2496–2502 (1989).
20. T. J. Hsu, C. Y. Mou, D. J. Lee, Effects of Macromixing on the oregonator model of the belousov — zhabotinsky reaction in a stirred reactor. *Chem. Eng. Sci.* **49**, 5291–5305 (1994).
21. B. Schrauwen, D. Verstraeten, J. Van Campenhout, An overview of reservoir computing: theory, applications and implementations. *Proc. 15th Eur. Symp. Artif. Neural Networks*, 471–82 (2007).
22. I. B. Yildiz, H. Jaeger, S. J. Kiebel, Re-visiting the echo state property. *Neural Networks*. **35**, 1–9 (2012).
23. F. Hoppensteadt, E. Izhikevich, Oscillatory Neurocomputers with Dynamic Connectivity. *Phys. Rev. Lett.* **82**, 2983–2986 (1999).
24. A. K. Dutt, S. C. Müller, Effect of stirring and temperature on the Belousov-Zhabotinskii reaction in a CSTR. *J. Phys. Chem.* **97**, 10059–10063 (1993).

Acknowledgements: The authors gratefully acknowledge financial support from the EPSRC (Grant Nos EP/H024107/1, EP/I033459/1, EP/J00135X/1, EP/J015156/1, EP/K021966/1, EP/K023004/1, EP/K038885/1, EP/L015668/1, EP/L023652/1), the ERC (project 670467 SMART-POM), and the DARPA molecular informatics project. We would like to thank Dario Caramelli for his help in producing some of the supplementary movies.

Author Contributions: L.C. conceived the original idea and J.M.P, S.T and L.C. together designed the project and the research plan; J.M.P, G.J.T.C and K.D designed and built the robotic platform, J.M.P and G.C. implemented the computer vision and the algorithms. J.M.P performed the experiments. S.T, A.S. and J.M.P did the data analysis. A. S. helped benchmark the system with L.C. and calculate the number of input and chemical states. J.M.P and L.C wrote the paper with help from the rest of the authors.

Data and materials availability: Due to the large total size of the experiment videos (above 500GB of data), the experimental data used in this work are available upon request to the

corresponding author at lee.cronin@glasgow.ac.uk. The code used to operate the platform is fully described in the Supplementary Information.

Competing interests: The authors declare no competing interests

Supplementary materials: The Supplementary Information document contains full information about how the platform was built, including the code used, information about all the experiments performed, and the relevant data produced. Finally, the SI also contains information about the data analysis, and in-depth details of the different Neural Networks used. There are four videos SM1-SM4.

Supplementary Information for

"A programmable chemical computer with memory and pattern recognition"

Juan M. Parrilla,[1] Soichiro Tsuda,[1] Abhishek Sharma,[1] Geoffrey J. T. Cooper,[1] Gerardo Aragon-Camarasa,[1] Kevin Donkers[1] and Leroy Cronin[1]*

[1] School of Chemistry, University of Glasgow, Glasgow, G12 8QQ, UK
**Corresponding author e-mail: lee.cronin@glasgow.ac.uk*

Contents

1 Overview of the automated platform

This section explains the different parts of the automated platform in detail. This platform is the one responsible for performing the physical experiments, and programming the inputs of the chemical computer processor which is housed in the reaction 'arena' containing the array of stirrer bars. These stirrer bars are housed in the fluidically interconnected grid. This section will cover the three main domains that make up the platform:

- The physical parts, which are a mixture of 3D-printed parts and hardware parts which are commercially available plus a set of DC motors and magnetic stirrers.
- The electronics, which are based on the Arduino microcontroller plus a custom-made PCB.
- The software to run the electronics which includes the firmware to run the Arduino board, and the Python script which drives the DC motors. This can be programmed so that complex input patterns can be used.

The fully integrated system also needs the chemical reaction details, artificial intelligence algorithms, and computer vision software to read out the outputs of the chemical computations. These are explained in later in sections 2, 3 and 5. This section will focus on how to build the automated platform. Figure S1 shows the three domains that will be covered in this section. The physical parts which are where the experiments are done, the electronics which actuate the DC motors, and the software, which is responsible for communication between the Arduino and the motors, as well as between the computer and the Arduino motor-programmer.

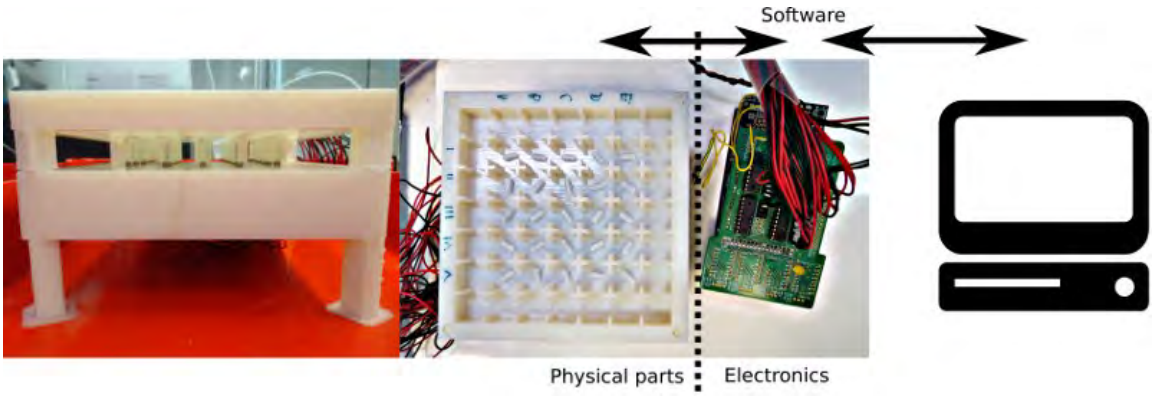

Figure S1: Outline of the platform showing the three main elements needed to build the physical parts, the electronics and the software.

1.1 Description of the physical parts required to build the platform

The construction of the physical setup is explained in this section. This involves producing 3D printed parts, and the DC motors and stirrer bars, as well as explaining how the DC motors are connected to the Arduino board.

3D printed parts

All the following 3D-printed parts were designed using the OpenScad software and printed with either a Stratasys Connex500 3D printer using the VeroWhitePlus material or using a RepRap i3 3D-printer, and using transparent polylactic acid (PLA). Figure S2 shows a photo of the final platform, showing all the different 3D-printed parts that will be discussed in this section: the stirrer bar array, spacers, motor magnet mount, motor holder array and stand or 'legs' that support the chemical processor or reaction 'arena'. The 3D printer files are available from the authors on request but screen shots of the source code to produce the files are given here.

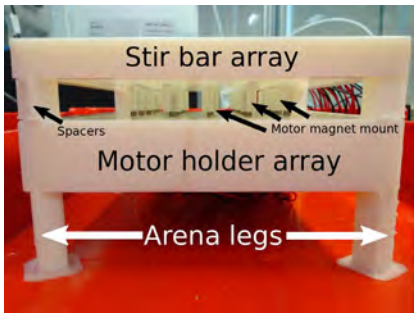

Figure S2: Photograph of the assembled platform, highlighting the different 3D printed parts that will be discussed in this section.

The main two 3D printed parts are the DC motor holder array, where the DC motors are inserted, and the stirrer bar array, which lays on top of the other one, and contains the chemical reaction arena. Figure S3 shows the design of the piece that will hold the motors. It contains an array of 7 by 7 cells, although only the central 5 by 5 array in the middle is used. The DC motors were inserted through the square cells, and their shaft would show through the holes. These squares and holes were designed to match the specification of the motors used (see Section 1.1).

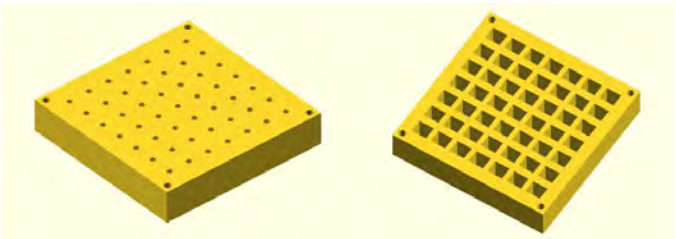

Figure S3: 3D design of the piece that holds the motors.

The following OpenScad source code (Source Code 1) shows all the variable definitions used in OpenScad in order to generate the motor holder matching our DC motors, as well as the stir bar array which will be discussed next. In this code, all the numbers given represent distances or sizes in millimetres. The following OpenScad source code (Source Code 2) can generate the designs shown in Figure S3 exactly.

The 3D designs shown in Figure S3 were 3D printed as described, and the results can be seen in Figure S4. The left part of this figure shows the bottom of the piece, where the motors were inserted. The right part of this figure shows the top of this piece, where it can be seen how the motor's shafts go through the 3D printed holes. The other 3D printed parts that can be seen in this figure will be discussed in this section.

Source Code 1: 3D designs specifications

```
//Cell dimensions
nx = 7;      //number of cells in x
ny = 7;      //number of cells in y
cx = 16;      //cell width
cy = 16;      //cell length
cz = 11;      //cell depth
//Arena total size is (nx*cx)x(ny*cy)
//Cells are (cx-0.5gw)x(cy-0.5gw)
//Base and edge thicknesses
base = 1.5;
edge = 15;
//Equidistant groove depth and width
gw = 2;      //width
gz = 0;      //depth
gh = 0;      //height above cell edge
shim = 0.0;      //narrowing wrt grooves
extend = 0;    //extension of grooves into sides
raise = -2;       //height of channels from bottom of cell [mm]
prop = 0.5;      //propoprtion of cell wall to have open as channel
//Stirrer motor parameters
md = 4;      //motor top sleeve diameter
mx = 12.05; //motor x width
my = 10.05; //motor y width
mz = 24;     //motor length
//Bolt hole paramters
boltd = 5.2;  //bolt diameter
bolte = 5;  //distance from edge
//Calculate arena dimensions
ax = nx*cx;
ay = ny*cy;
az = cz + gz;
//Calculate block dimensions
bd = sqrt((ax*ax+ay*ay))+edge;   //diameter
bz = az + base;      //depth
```

Source Code 2: Motor Holder OpenScad code

```
difference(){
  //Create block
  translate([-edge/2,-edge/2,bz*5])
  cube([ax+edge,ay+edge,mz],false);
  //Subtract bolt holes
  translate([-edge/2+bolte,-edge/2+bolte,bz*5-1])
  cylinder(h=mz+2,d=boltd,$fn=50);
  translate([ax+edge/2-bolte,-edge/2+bolte,bz*5-1])
  cylinder(h=mz+2,d=boltd,$fn=50);
  translate([-edge/2+bolte,ay+edge/2-bolte,bz*5-1])
  cylinder(h=mz+2,d=boltd,$fn=50);
  translate([ax+edge/2-bolte,ay+edge/2-bolte,bz*5-1])
  cylinder(h=mz+2,d=boltd,$fn=50);
  //Subtract motor holes
  for (i=[1:nx]){
    for (j=[1:ny]){
      translate([(i-0.5)*cx,(j-0.5)*cy,bz*6-1])
      cube([mx,my,mz],true);
    }
  }
  for (i=[1:nx]){
    for (j=[1:ny]){
      translate([(i-0.5)*cx,(j-0.5)*cy,bz*5-1])
      cylinder(h=mz+2,d=md,$fn=50);
    }
  }
}
```

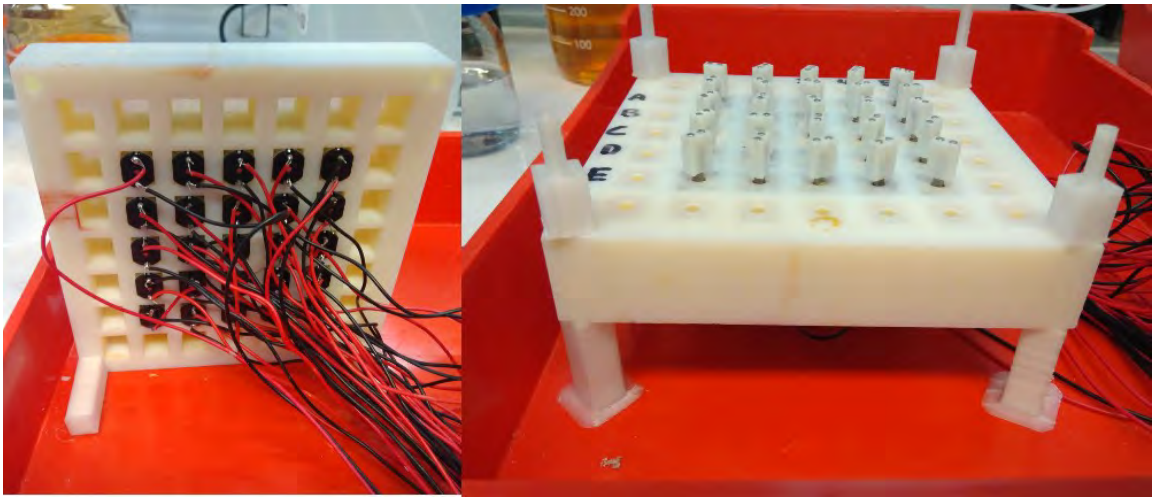

Figure S4: Photograph of the 3D printed motor holder. Left: The bottom of the piece, where the DC motors were inserted. Right: The top part of the piece, where the shafts coming through the holes can be seen.

To describe the stirrer bar array, we will first need to show the empty arena, which can be seen in Figure S5. The specifications of this design can be seen in the Source Code 1. This device was not used for the chemical computations described in the manuscript, but it was required for us to develop the final system. This is because some preliminary reaction-diffusion experiments were tested to develop the system, see Section 4.4.

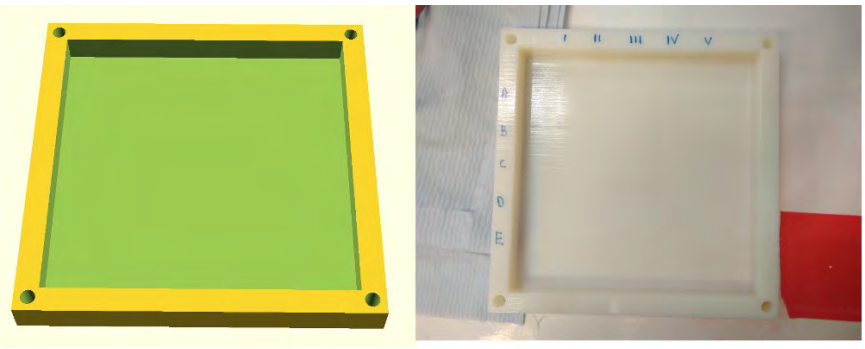

Figure S5: The 3D design of the stirrer bar array, in this case, only the empty arena is shown. The left image shows the 3D design, while the right image shows the 3D printed piece.

Source Code 3 details how to design this piece using OpenScad. The variables shown here were defined previously in Source Code 1. Figure S6 shows the 3D designs of the main stirrer bar arrays used during the experiments. As before, only the 5 by 5 cells in the middle were used. In these cells, a stirrer bar was placed as described in Figure S6. This figure shows the two main designs that we used in this research. In the left one, the gap between the cells is completely open, and the fluid is free to move throughout the array. In the right one, the gaps between the cells were narrowed restricting fluid flow. The specification of this design in terms of distances and sizes was described in the Source Code 1.

Source Code 4 details how to design a device like the one shown in the left part of Figure S6. This code uses the variables defined in Source Code 1 and the empty arena detailed in Source Code 3. To close the gap between cells, as shown for example on the right in Figure S6, the variable named “raise” in Source Code 1 was increased. Figure S7 shows the 3D printed device as described or shown on the left in Figure S6. This is the main device that was used to do the chemical computations described in the manuscript. Figure S8 shows other devices that were designed and 3D-printed, but have not been used during the research described in the main manuscript, but instead used to validate the approach. These are shown to show how easy it is to create different architectures, and hence create customised versions of the arena.

Figure S9 shows the 3D design of the magnet holders that were inserted into the shafts of the motors. The two holes in the top contained magnetic bars, while the bottom hole is the one where the motor shaft was inserted. The magnetic bars used were sourced from “First4Magnets”. They are described as “2mm dia x 2mm thick N42SH Neodymium Magnet - 0.15kg Pull”. Source Code 5 details how the magnet holders that were attached to the shafts of the motors was designed. As before, all the distances and sizes are represented in millimetres.

The last two pieces to detail are the “arena legs” which are responsible of holding up the whole chemical processor platform, and align the motor holder part, and the stirrer bar array as well as the 3D-printed “spacers”. These spaces are needed to create enough space between the motor holder part and the stirrer bar array part so that the shafts of the motors, with their magnetic holders, can be attached and can freely rotate. These need to be as close as possible to the stirrer bars placed in the stirrer bar array part, so that the rotation of the shafts will translate to efficient rotation of the stirrer bars above them. Figure S11 shows the 3D designs of these pieces. Source Code 6 shows the OpenScad code use to design these pieces, as well as their dimensions. Figure S12 shows the 3D-printed pieces. The “arena legs” and the “spacers” parts were 3D-printed using a RepRap i3 3D-printer, and using transparent polylactic acid (PLA). Once all the pieces are 3D-printed, it is very straightforward to assemble the final structure.

Source Code 3: Empty arena OpenScad code

```
difference() {
  //Create block
  union() {
    translate([-edge/2,-edge/2,0])
    cube([ax+edge,ay+edge,bz],false);
  }
  //Subtract arena
  translate([(0.5*gw),(0.5*gw),base])
  cube([(ax-gw),(ay-gw),(az+1)],false);
  //Subtract bolt holes
  translate([-edge/2+bolte,-edge/2+bolte,-1])
  cylinder(h=bz+2,d=boltd,$fn=50);
  translate([ax+edge/2-bolte,-edge/2+bolte,-1])
  cylinder(h=bz+2,d=boltd,$fn=50);
  translate([-edge/2+bolte,ay+edge/2-bolte,-1])
  cylinder(h=bz+2,d=boltd,$fn=50);
  translate([ax+edge/2-bolte,ay+edge/2-bolte,-1])
  cylinder(h=bz+2,d=boltd,$fn=50);
}
```

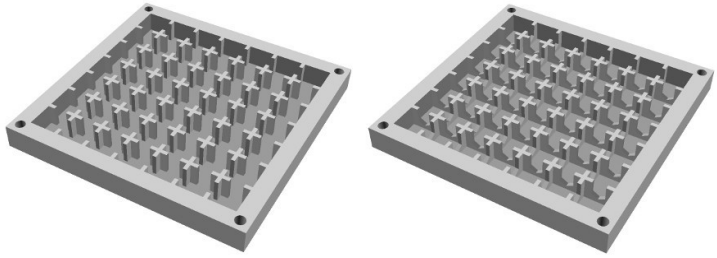

Figure S6: The 3D design of the stir bar array. These are the two main designs shown in the manuscript. In the left one, the gaps between the cells are completely open, and the fluid can go through. In the right one, the gaps have a barrier, limiting the fluid flow between the cells.

Source Code 4: Stir bar array OpenScad code

```
//Walls and Channels
difference() {
  //Walls
  union() {
    //Build X grid walls
    if (nx>1) {
      translate([cx-(gw*0.5)+shim,-(extend-shim),(base)])
      cube([gw-(2*shim),ay+((extend-shim)*2),(az+gh-(gz*2))]);
      for (i=[2:(nx-1)]) {
        if (i<nx) {
          translate([(i*cx)-(gw*0.5)+(shim),-(extend-shim),(base)])
          cube([gw-(2*shim),ay+((extend-shim)*2),(az+gh-(gz*2))]);
        }
      }
    };
    //Build Y grid walls
    if (ny>1) {
      translate([-(extend-shim),cy-(gw*0.5)+shim,(base)])
      cube([ax+((extend-shim)*2),gw-(2*shim),(az+gh-(gz*2))]);
      for (i=[2:(ny-1)]) {
        if (i<ny) {
          translate([-(extend-shim),(i*cy)-(gw*0.5)+(shim),(base)])
          cube([ax+((extend-shim)*2),gw-(2*shim),(az+gh-(gz*2))]);
        }
      }
    };
  }
  //Channels
  union() {
    //Cut X grid wall channels
    if (nx>1) {
      //subtracts a vertical stack of 4 hexagonal prisms half a diameter apart
      for (m=[1:(ceil(1/prop)*2)]){
        //channels (gaps) in x as single long triangular prisms
        for (l=[1:nx]){
          translate([(l-0.5)*cx,0,(m*prop*cx*0.5)+gz+base+raise-3])
          rotate([-90,90,0])
          cylinder(h=ay,d=(prop*cy),$fn=6);
        }
      }
    }
    if (ny>1) {
      //subtracts a vertical stack of 4 hexagonal prisms half a diameter apart
      for (m=[1:(ceil(1/prop)*2)]){
        //channels (gaps) in x as single long triangular prisms
        for (l=[1:ny]){
          translate([0,(l-0.5)*cy,(m*prop*cy*0.5)+gz+base+raise])
          rotate([0,90,0])
          cylinder(h=ax,d=(prop*cx),$fn=6);
        }
      }
    }
  }
}
```

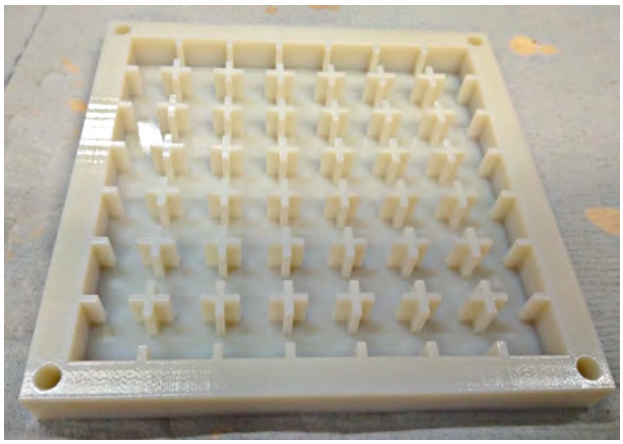

Figure S7: The 3D printed device as described in Source Code 4 and show as a schematic in Figure S6.

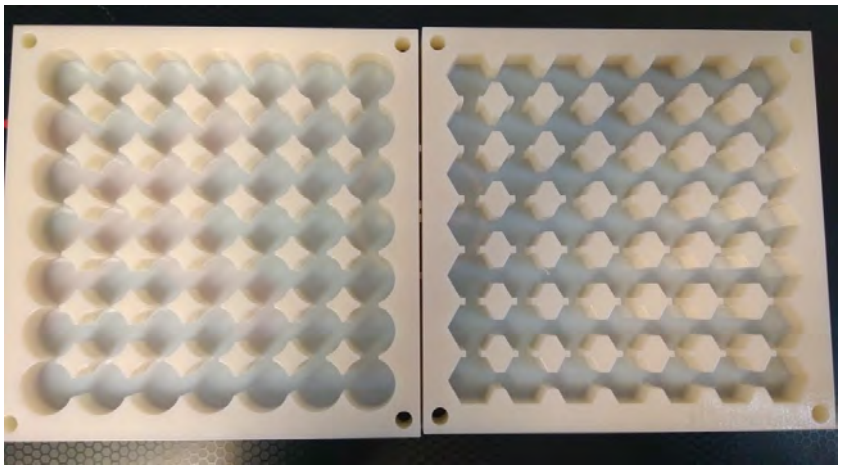

Figure S8: Examples of other devices that were designed and fabricated, but that were part of the research explained in the main manuscript.

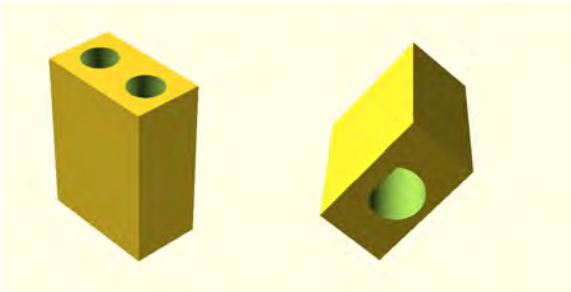

Figure S9: The 3D design of the magnet holder that is attached to the motor shaft. The two holes in the top contained small magnet bars, and the bottom hole was inserted into the motor shaft.

Source Code 5: Magnet holder OpenScad code

```
//Motor shaft paramters
shtd=3;       //shaft diameter
shtl=7;       //shaft length

//Magnet parameters
magd = 2.06;       //magnet diameter (cylinder)
magh = 2;        //magnet height (cylinder)
magx = 1;        //magnet width (cube)
magy = 1;        //magnet length (cube)
magz = 1;        //magnet depth (cube)
mags = 1.5;       //magnet spacing

//Holder parameters
hldd = 7;           //holder diameter (cylinder)
hldh = 2.5;           //holder height (cylinder)
hldx = 4;           //holder width (cube)
hldy = 7;           //holder length (cube)
hldz = 10;           //holder depth (cube)

//Construct
difference(){
  //Holder
  translate([hldd/2,hldd/2,0])
  cylinder(h=hldh,d=hldd,center=false,$fn=150);
  //Magnets
  translate([x/2,y/2-magd/2-mags/2,z-magh+0.1])
  cylinder(h=magh,d=magd,center=false,$fn=50);
  translate([x/2,y/2+magd/2+mags/2,z-magh+0.1])
  cylinder(h=magh,d=magd,center=false,$fn=50);
  //Shaft
  translate([x/2,y/2,-0.1])
  cylinder(h=shtl,d=shtd,center=false,$fn=150);
}
//shaft catch
cube([(hldx-shtd)/2+0.55,hldy,shtl],center=false);
```

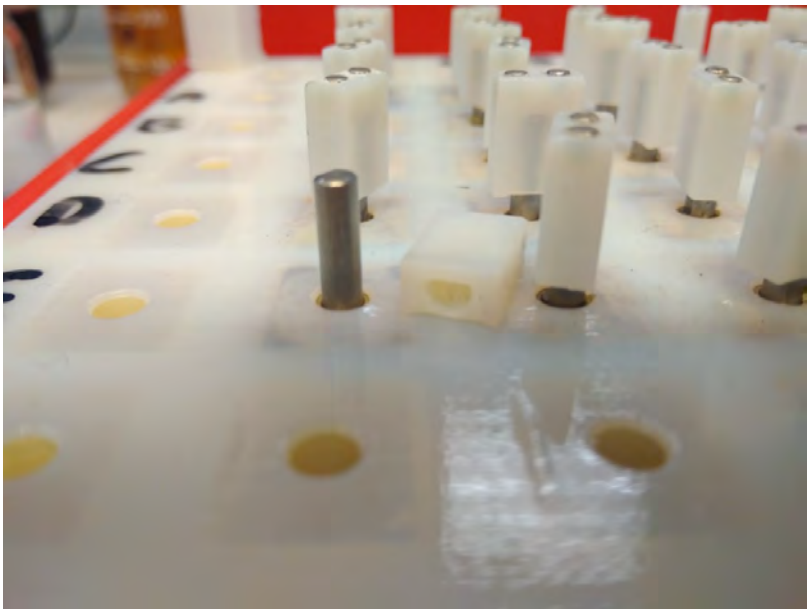

Figure S10: The 3D printed device as shown in Figure S9. In this figure it can be seen how the final design looked, and how it was attached to the motors.

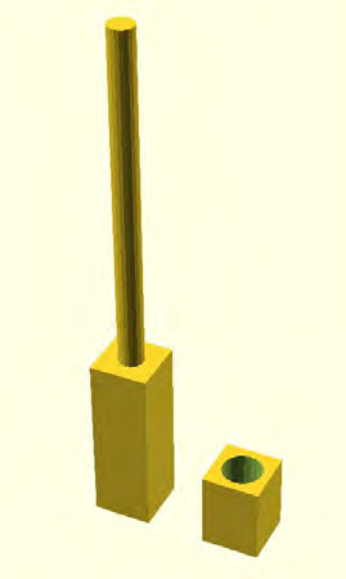

Figure S11: The 3D designs of the arena legs (left) and spacer (right).

Source Code 6: Arena legs and spacers OpenScad code

```
// Arena legs
cube([10,10,30]);
translate([5,5,30])cylinder(h=60, d=4.5, $fn=20);
// Spacers
difference() {
  cube([10,10,13.5]);
  translate([5,5,-1])cylinder(h=20, d=7, $fn=20);
}
```

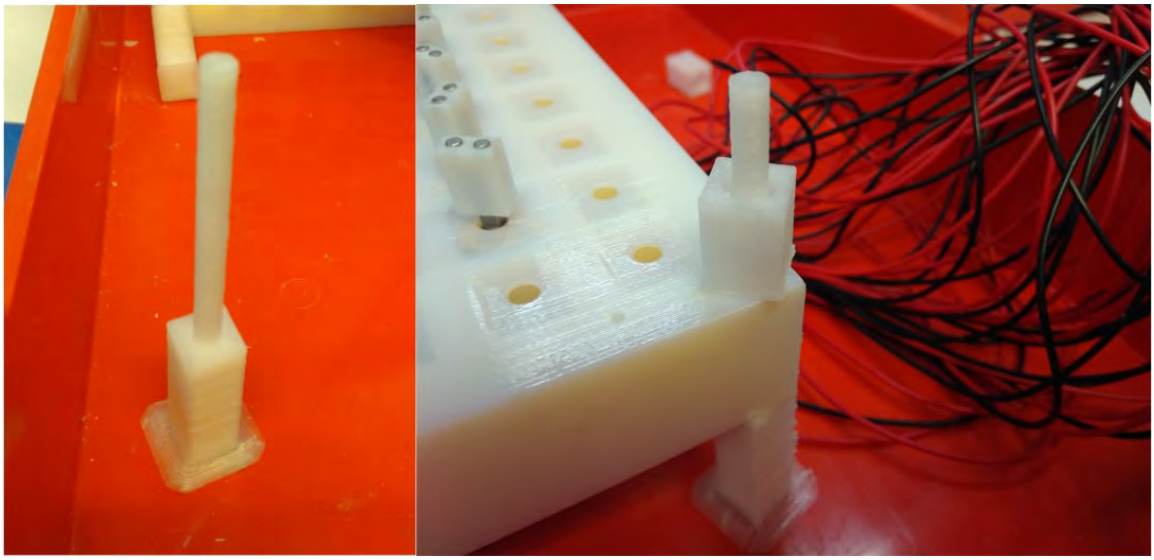

Figure S12: The 3D printed pieces of the arena legs (left) and spacer (right).

So in summary, the overall platform shown in Figure S2 has:

- 1x Stir bar array
- 1x Motor holder array
- 4x Arena legs
- 4x Spacers
- 25x Motor magnet mount
- 50x Magnet bars

DC motors

The DC motors used were bought from “AliExpress” under the following description: “DC 6V 200RPM Mini Metal Gear Motor With Gearwheel Model:N20 3mm Shaft Diameter”. Figure S13 shows the motor specifications from the seller’s website. All the 3D printed pieces which used the motors (motors holder array and magnet mounts) were designed based on these specifications. Figure S14 shows a photo of the actual motors. These motors were inserted into the motor holder array as can be seen in Figure S4, and the magnet mounts were attached to their shafts as can be seen in Figure S10. As their specifications show, when supplied with 6V they are expected to rotate at 200 RPM. We visually calibrated them to rotate at 90 RPM by modulating the PWM signal generated by the electronics (see Section 1.2). This motor speed was chosen because it generated stable BZ oscillations in the array (see Section 4.7) that could be easily tracked visually.

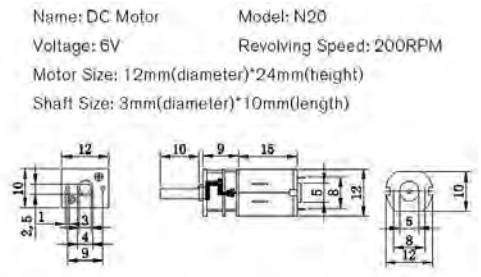

Figure S13: DC motor specifications from the seller’s website.

Stirrer bars

The stirrer bars used in our platform were sourced from “Fisherbrand”. They are described as “magnetic follower, micro” with a size of 8 by 3 mm. Our objective was to get the largest possible stirrer bars so that the quantity of fluid transferred would be maximized, while at the same time being small enough so that their magnetic fields don’t interfere with each other. Figure S15 shows these stirrer bars placed in the “stirrer bar array”.

Figure S14: Photo of one of the DC motors used in this platform.

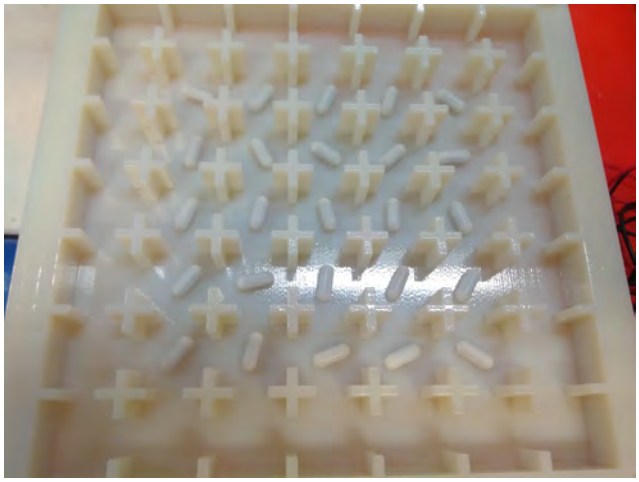

Figure S15: Photo showing the stirrer bars placed in the “stirrer bar array”.

1.2 Electronics

In order to turn the motors, we based the electronics on the Arduino microprocessor boards. In this platform we used the Arduino Mega board. To achieve precise motor control we opted to use pulse width modulation (PWM) signals that can be generated in an Arduino in order to control the voltage received by the motors. As shown in Section 1.1, when these motors receive 6 volts they rotate at 200 RPM, but they can be rotated at lower speeds by supplying a lower voltage. Because we needed to actuate 25 motors, and this is more than an Arduino can control via its default pins, we used the Arduino compatible shield “Adafruit 16-Channel 12-bit PWM/Servo Shield - I2C interface”. This shield expands Arduino’s functionality to 16 different PWM signals, which is still not enough, but these shields can be connected and stacked to increase the number of PWM signals available. In our case, we used two shields in total, generating a total of 32 different PWM signals, which exceeds the 25 we need for the platform. Finally, in order to transform these PWM signals into voltages, we designed a shield (Figure S16). This shield used four “ULN2803A Darlington Transistor Arrays”, which were used to transform the PWM signals into voltages. Figure S17

outlines our set-up. Figure S18 shows a picture of the actual electronics. The connection between our purpose designed PCB and the DC motors was achieved via a wiring loom see Figure S4.

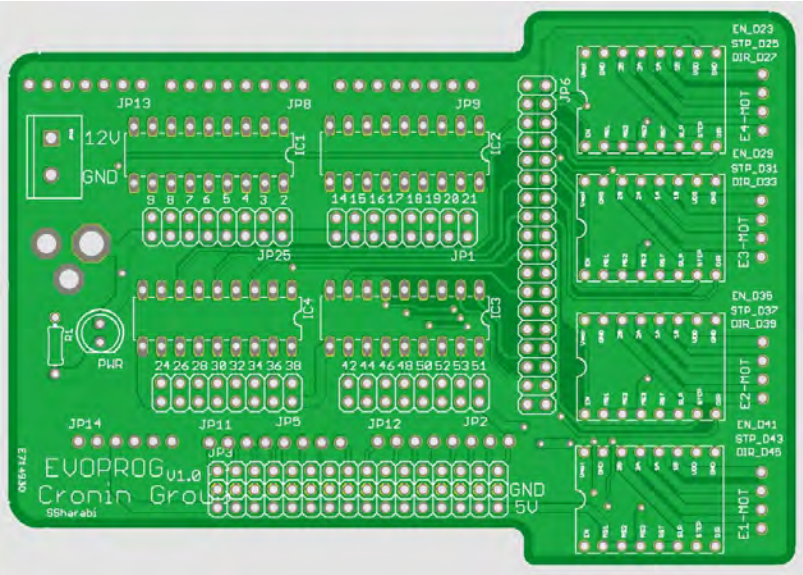

Figure S16: The PCB shield designed by us to transform the PWM signals into voltages using ULN2803A Darlington transistor arrays. Further schematics to aid reproduction of this are available from the authors on request.

The power supply used in this platform was a “80W Switched Mode DC Multi Voltage Slim Bench Power Supply”. In particular, the model “N27GG”. It was set to “6.09V”, and the range was set to “16V 5A”.

1.3 Software

The software layer responsible for controlling the described platform can be divided into two parts:

- The firmware that runs in the Arduino board. It is responsible for generating the electronic pulses that actuate the motors.
- A Python script that runs on a computer connected through USB to the Arduino board. This Python script aims to provide a more user-friendly level abstraction to the actuation of the platform.

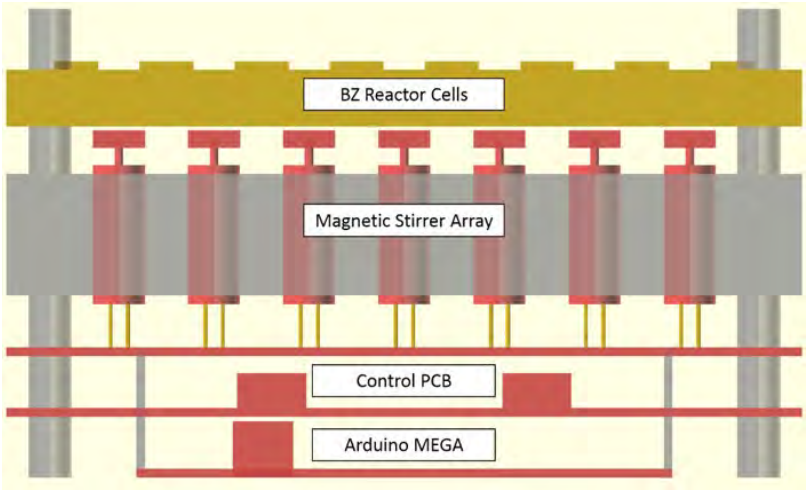

Figure S17: Outline of the electronics setup used.

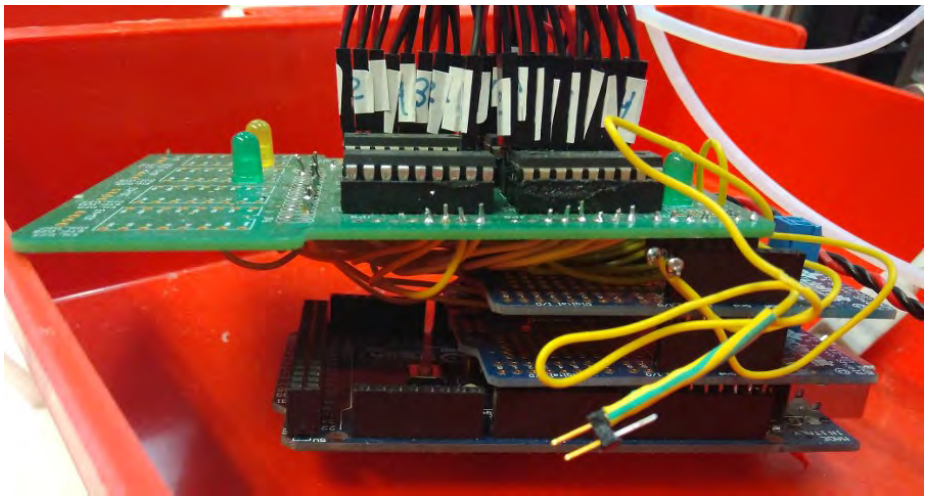

Figure S18: Picture of the electronic system used, which is based on the Arduino platform. From top to bottom: Arduino Mega, Adafruit 6-Channel 12-bit PWM/Servo Shields, Adafruit 6-Channel 12-bit PWM/Servo Shields and our purpose designed PCB.

Firmware

The main objective of the Firmware is to generate the different signals that will actuate the motors and it is based on the standard Arduino syntax and libraries. Also, because we are offering a higherlevel interface in Python to the user, the firmware is also responsible for reading the commands generated by the user, decode them, and generate the relevant electronic signals. In this way the chemical computer can be programmed at a high level away from the Arduino using a purpose built system.

As described during the Electronics section (Section 1.2), in order to generate PWM signals that would actuate the motors, we used an “Adafruit 16-Channel 12-bit PWM/Servo Shield - I2C interface”. Thus, in order to send commands to this PWM Shield, we used its corresponding Arduino library: https://github.com/adafruit/Adafruit-PWM-Servo-Driver-Library. With this library loaded, in order to send different commands for PWM signals, we will need to use the function “setPWM(pin, 0, speed)” where pin refers to the particular motor we want to actuate, “0” should always be zero, and speed is the factor that will generate the PWM signal. In our case, speeds lower than 500 would not be able to actuate all motors, and the maximum available value is 4000. Because our platform is using two of this Adafruit boards, our firmware contains two Adafruit objects, which we called “pwm0” and “pwm1”.

To get all the motors to rotate at a similar speed, we aimed for all of them to require a PMW signal of around 500, and this translates to around 90 revolutions per minute. Because all the motors are slightly different, the actual value was calibrated individually, on a motor by motor basis. The speed of 90 revolutions per minute was the standard speed used throughout all the experimentation, except when described otherwise and hence can be considered to be our standard base speed.

Finally, the firmware is also responsible for decoding messages from the user which would specify which motor to actuate and at which speed. The syntax of these commands is similar to GCode and it is detailed in Table S1. In the case of the pin number, Adafruit shield 0 accepts values from 0 to 15, while Adafruit shield 1 accepts values from 0 to 8, because there are 25 motors in total. In the case of the PWM signal, the Adafruit library accepts any value between 0 and 4000, but our experience with the particular DC motors used is that any value lower than 500 might not achieve actuation.

Code	**Description**
AX	Selects Adafruit shield X. $X \epsilon [0, 1]$
PY	Selects pin Y. $Y \epsilon [0, 15]$
SZ	Selects PWM signal. $Z \epsilon [0, 4000]$

Table S1: “AX PY SZ” Example of G-code operations decoded by the firmware layer.

Following this syntax, the Arduino board would receive a command like “A1 P8 S600” through the USB serial connection. Then, the firmware decodes this command and generates the corresponding PWM signals using the Adafruit software library as explained. In this case, for example, it will use the software object “pwm1” (because the parameter “A” is given a “1”), and then execute the command “pwm1.setPWM(8, 0, 600)”.

Python user interface

The objective of this layer is to offer to the user a higher-level interface in order to actuate the platform. It offers an API to the user with commands like “actuate motor” or “disable motor”, and then transforms these commands into a G-Code command as explained in the previous section. Table S2 describes the API of the Python user interface used to control the platform. This user interface will either be used by a user, or by any other higher-level decision-making layer.

A user would for example execute the function “activate motor(”A1”, 600)”. The first thing this Python interface does is to translate from ”A1” to Adafruit board and pin number, which in this case refers to board number 1, and pin number 8. Therefore, a command like “A1 P8 S600” is sent to the Arduino through the USB serial connection.

Code	**Description**
init__(port)	Connects to the serial port “port” and loads a dictionary which relates from motor codes such as “A1” or “E5” to its corresponding Adafruit shield and pin
del__	Disables all the motors and closes the serial connection
close()	Same as del__
Activate_motor(code, speed)	Activates motor “code” at speed “speed”
Disable_motor(code)	Disables motor “code”
Activate_all(speed)	Activate all the motors at speed “speed”
Disable_all()	Disable all the motors
Pattern_from_file(file)	Loads the JSON “file” which should specify a pattern. Returns a pattern object
Activate_pattern(pattern, speed)	Activates the motors following the pattern “pattern” at the speed “speed”

Table S2: bzboard.py API.

1.4 Bill of materials

- 25x Fisherbrand magnetic follower, micro. 8 by 3 mm.
- 25x DC 6V 200RPM Mini Metal Gear Motor With Gearwheel Model:N20 3mm Shaft Diameter.
- 1x Motor array (3D-printed)
- 1x Stir bar array (3D-printed)
- 4x Arena legs (3D-printed)
- 4x Legs spacers (3D-printed)
- 25x Motor shaft magnet holder (3D-printed)
- 50x First4Magnets 2mm dia x 2mm thick N42SH Neodymium Magnet - 0.15kg Pull.
- 1x Arduino Mega 2560
- 2x Adafruit 16-Channel 12-bit PWM/Servo Shield - I2C interface.
- 1x PCB shield designed by ourselves which was used to transform the PWM signals into voltages. It used ULN2803A Darlington Transistor Arrays.
- 1x Computer running Python 3 and OpenCV 3.
- 1x Microsoft LifeCam Cinema Web camera.

2 Chemistry

2.1 Preparation of the reagent solutions for the BZ reaction

The solutions were prepared the following way:

- Ferroin Indicator: 0.025M solution was prepared by dissolving 0.70g of ferrous sulfate heptahydrate and 1.5g of 1,10-phenanthroline in 100mL of water. Finally, 15mL of this product was dissolved in 110mL of water.
- Potassium Bromate: 1M solution was prepared by dissolving 16.7g $KBrO_3$ in 100mL of 1M H_2SO_4.
- Sulfuric Acid: 1M H_2SO_4 was prepared by taking 5.6mL conc. H_2SO_4 (96%, 18M) and adding water to reach a total volume of 100mL.

- Malonic Acid: 1M solution was prepared by dissolving 10.4g malonic acid in 100mL 1M of water.

1M H_2SO_4 was sourced from Fisher Scientific, >95% analytical reagent grade. Malonic acid was sourced from Sigma Aldrich, Reagent Plus 99%. Ferrous sulfate heptahydrate was sourced from Sigma Aldrich, >=98%. 1,10-phenanthroline was sourced from Sigma Aldrich, >=99%. Potassium bromate was sourced from different sources. The main body of work of this research used the one sourced from Lancaster, 99%. Eventually all of it was used, and we could not source more from the same company. We then sourced it from different suppliers: Scientific Laboratory Supplies, 99% Alfa Aesar, 99.8% Alfa Aesar and Millipore Ensure.

2.2 Experimental protocol

The first step required was to define the working recipe that would be used in the experiments unless stated otherwise. In order to do so, different experiments with different ratios of the components described above were performed. The objective was to obtain a recipe that would output a constant colour through the time of 1 hour, as well as well-defined oscillations. The results of this search can be seen on Section 4.3. The recipe chosen contained 2.5mL of the ferroin solution, 20mL of water, 12.5mL of the Sulfuric acid solution, 18mL of the malonic acid solution, and finally 19mL of the Potassium bromate solution. Based on this recipe, the experimental protocol is as follows:

1. Prepare the described recipe, in the described order, in a 100mL glass beaker. This glass beaker must contain a stir bar.
2. Place the beaker in a magnetic stirrer. In our case, we used a “IKA big-squid ocean” set to around 33% of speed.
3. Eventually the BZ medium will start to flash or oscillate. Once it flashes clearly twice, transfer it to the arena (motors disabled).
4. Wait for 10 minutes and let the BZ medium rest. The objective is to stop the possible oscillations that were started when the liquid was transferred.
5. Activate the motors in the desired pattern.
6. Record the experiment for 30 minutes (or any other desired length, in our case most of the experiments were 30 minutes).
7. Remove the contents of the arena and clean the arena with water. Wait until all remains of water are gone before starting a new experiment.

The different volumes were transferred using a “SciPette Autoclaveable Variable Pipettor” with a range from 2mL to 10mL, and 0.1mL precision.

3 Image processing

The image processing software layer is responsible for:

- Detecting the BZ oscillations with image processing. In the case of this project, the objective was to assign the state of the cells as being either “red” or “blue”.
- Using the oscillation data from a whole experiment, we generated a “time-map” plot, which is a very common visualization technique in BZ experiments where the oscillations are plotted against time.

3.1 Camera and configuration used

A Microsoft LifeCam Cinema Web camera was situated 12.5 cm above the arena in order to record the experiment. While the experiment proceeded, the video stream from the camera was fed into a computer running a Python (3.6.5) OpenCV (3.4.1) script, which generated a video file for the experiment. In the majority of the experiments the video was recorded first, and then the oscillation detection and data analysis were performed later, but it was possible to operate the system in real time for closed loop experiments. The video was configured to 800 by 600 pixels, and 30 frames per second (FPS) and XVID compression was used. Figure S19 shows the positioning of the camera with respect to the platform 12.5 cm above the centroid of the arena. The camera was configured using the software Guvcview and Figure S20 shows the configuration parameters used.

A Microsoft LifeCam Cinema Web camera was situated 12.5 cm above the arena in order to record the experiment. While the experiment happened, the camera stream was fed into a running Python (3.6.5) OpenCV (3.4.1) script, which generated a video file of the experiment. In the majority of the experiments the video was recorded first, and then the oscillation detection and data analysis were performed later. The video was configured to 800 by 600 pixels, and 30 frames per second (FPS). XVID compression was used. Figure 19 shows the positioning of the camera respect to the platform.

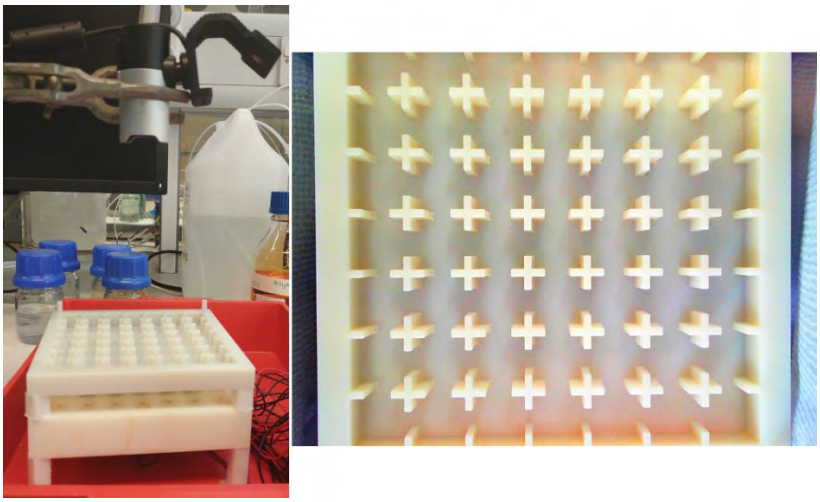

Figure S19: Left: Picture of the platform and positioning of the camera, which is 12.5 cm above the arena. Right: Picture of the arena as seen from the camera.

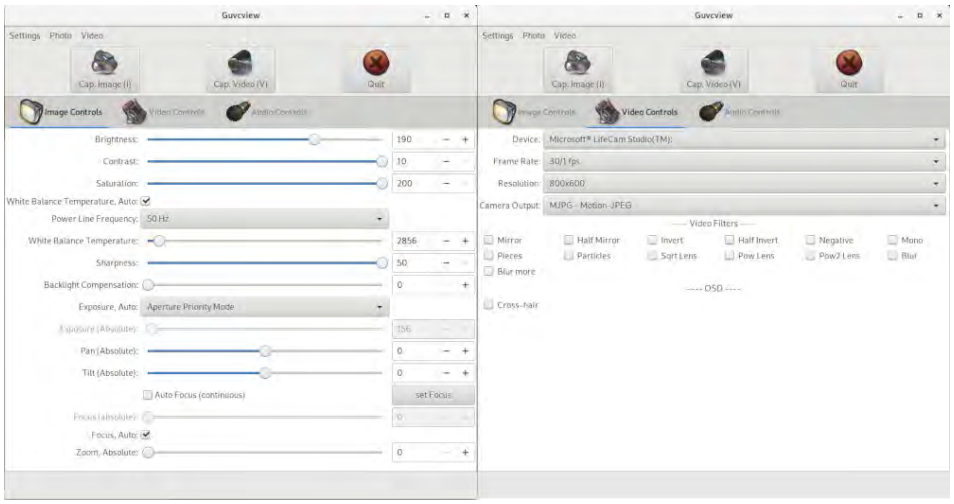

Figure S20: Camera configuration using the software Guvcview.

3.2 Detection of oscillations

This section focuses on how computer vision algorithms were used in order to detect the BZ oscillations. These BZ oscillations were labelled as red or blue. The objective of this software layer is to, given a camera frame like the one shown in Figure S21 – left, output the classification of the cells between red and blue, as shown in Figure S21 – right.

Initially, the problem of segmenting between red and blue might look simple, but if we look at Figure S22, for example, we can see that very often just based on the colour it is difficult to say if a cell is blue or red. The cause of this is that the BZ reaction colour changes over time (see Section 4.3). This change depend on many factors, among them, the number of motors enabled, and their

respective speeds. It would be possible to model all these variables and obtain for any given configuration its expected colour, but in this type of scenarios, it is often easier to use machine learning. In this case, we used a support vector machines (SVM) to help us assign / classify the states of the cells. The reason for choosing an SVM is because they are able to classify such states, they are very well integrated within the OpenCV library, they work very small for small datasets, and once trained they can be used extremely quickly. This last point is important because in some of our experiments we will need to classify the cells at a rate of 30 FPS.

In order to train the SVM a dataset was built. This dataset was built by a human researcher who labelled different cells, in different videos, at different points of the BZ reaction. In total, 1541 samples of “red” were labelled, and 888 of “blues”. These samples looked like the square cells shown in Figure S22. In order to provide more information to help the training step, the average colour of the whole BZ medium during the previous 3000 frames for each of the cells was also recorded and used. In particular, the blue and red channel average values were stored as part of the file name, with values between 0 and 255.

In order to train the SVM, firstly the samples as shown on Figure S22 were equalised using CLAHE (as implemented in OpenCV). The clip limit was set to 1, and the tile Grid Size was set to 4 by 4. The next step consisted of transforming the RGB data from an image into the input data that could be used with the SVM. Several different transformations were tested, such as only taking the blue channels, or a PCA, but ultimately we obtained the best results using a 3D histogram in the HSV colour scheme; 8 bins were used in the histogram for each of the channels. This histogram was then input to the SVM, with the average colour of the previous 3000 frames in the red and blue channel, as explained before.

The SVM library used was the one included in OpenCV. An RBF kernel was used, and the type was set to “C SVC”. The C parameter was set to 5, and the gamma parameter was also set to 5. An exploration was done to find these two parameters, and these two values were the ones that resulted in a better model. The results could be seen in Figure S21. Although here only images are shown, the code was designed to work specifically with the video data.

3.3 Generation of time-maps

The generation of time-maps is a very common and powerful way of representing the behaviour of the BZ reaction oscillations as a function of time. The objective is to take a given video and generate a plot that shows how the system oscillates through time, see Figure S23.

In order to achieve the generation of the time maps for a given video, an algorithm was used that would take five columns of pixels for every frame. Each of these columns was centered around one of the columns of the 5 by 5 arena. Then these five columns would be stitched together in a single column. Then the algorithm would take the next frame, and repeat the process. The new columns generated would be placed next to the previous one, see Figure S24. This algorithm can

be applied to raw videos, like the one shown in Figure S23, or to already segmented videos, like the example shown in Figure S25.

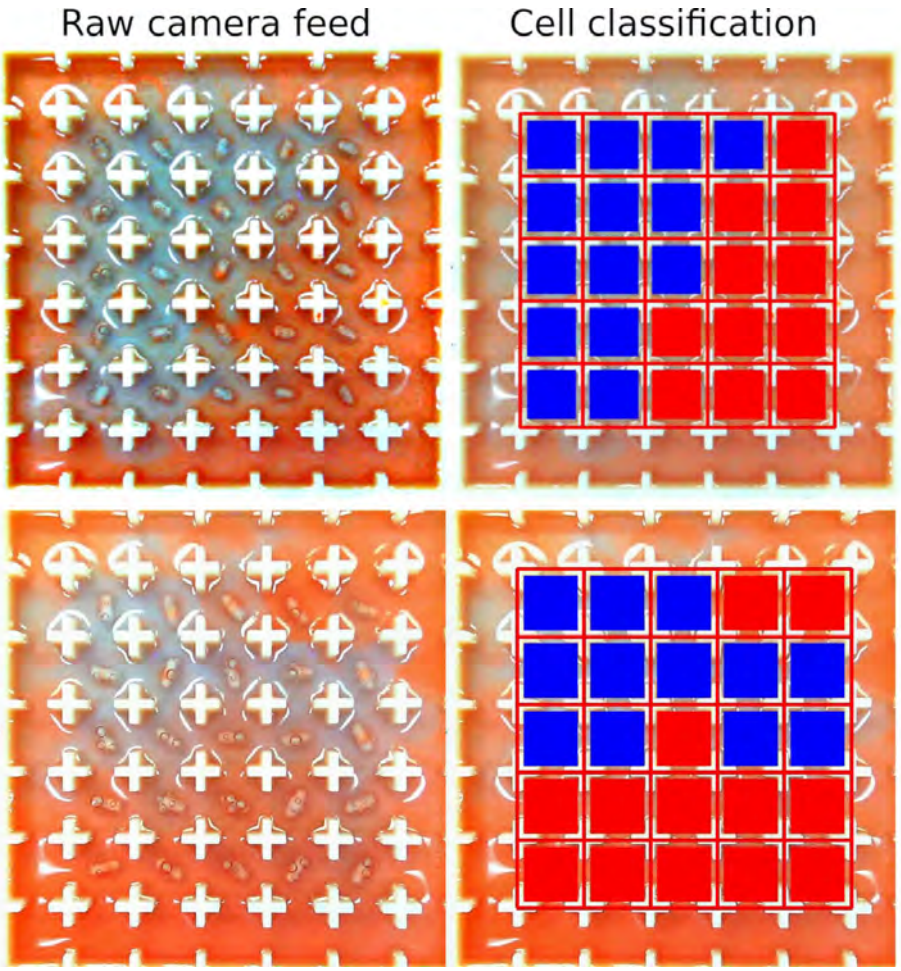

Figure S21: Left: Raw camera frame as received by the software. Right: Same frame with the oscillations detected.

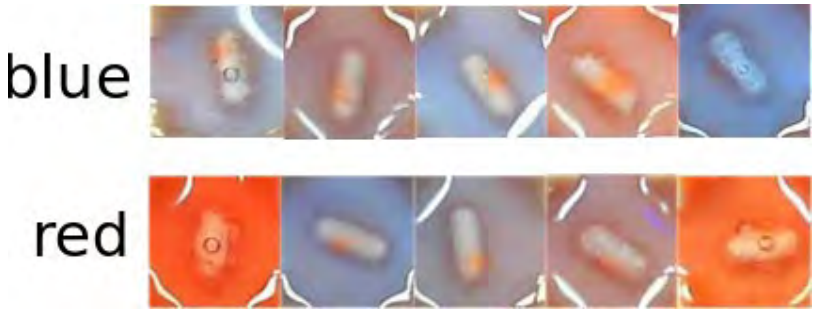

Figure S22: Examples of red and blue BZ oscillations as labelled by a human researcher.

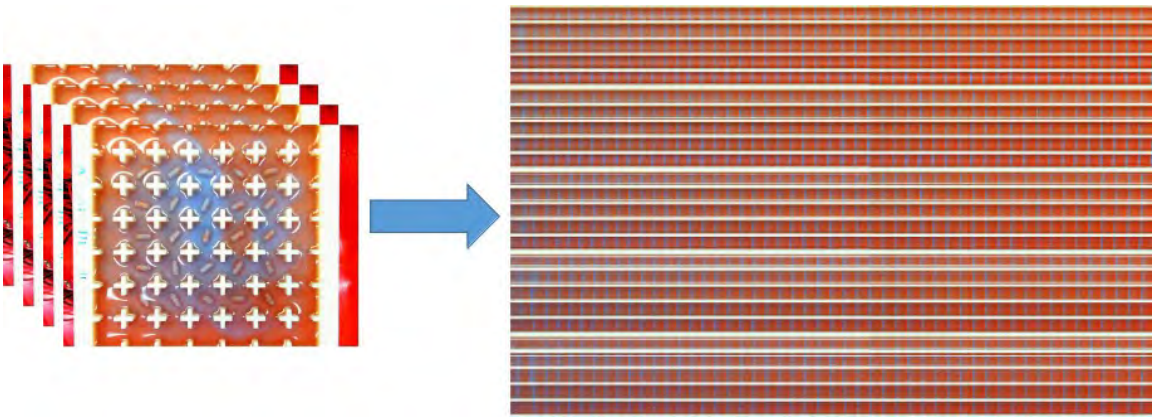

Figure S23: Left: A video sequence of BZ reaction. Right: The time map generated, where the blue lines show when the BZ reaction oscillated between states. The ‘y’ axis is the stack of columns from the array lined one above on each other, and the ‘x’ axis is time with each different image showing a different time state for the entire arena.

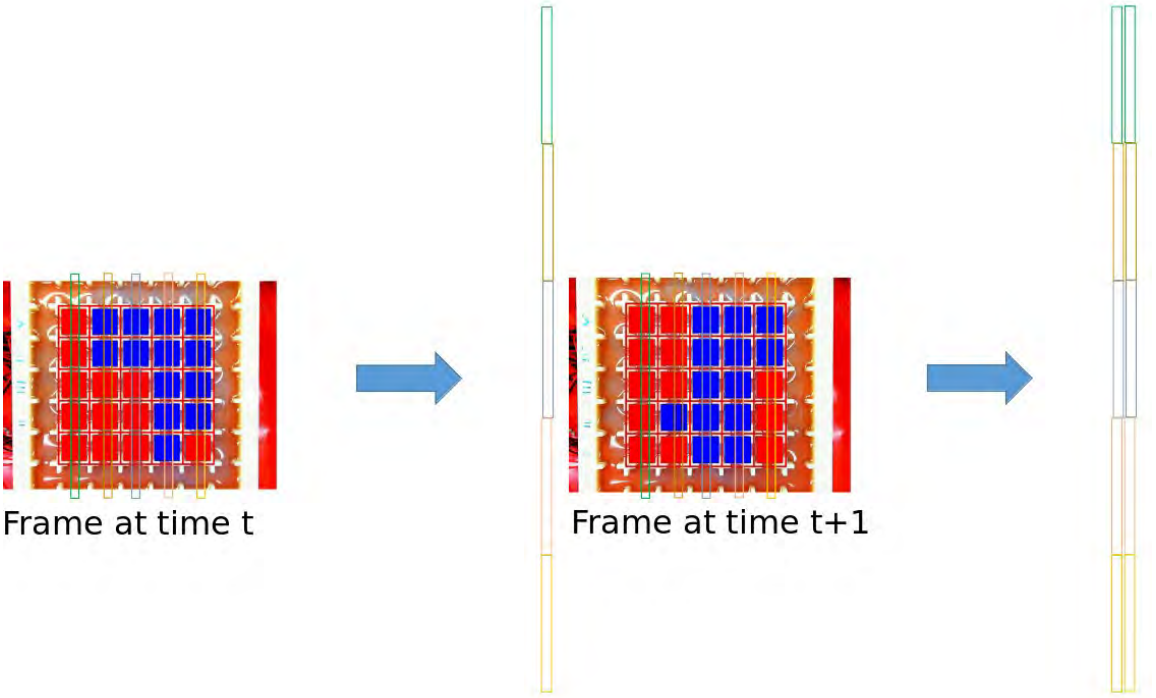

Figure S24: Example of how the time-maps were built. The columns used were of 1 pixel width.

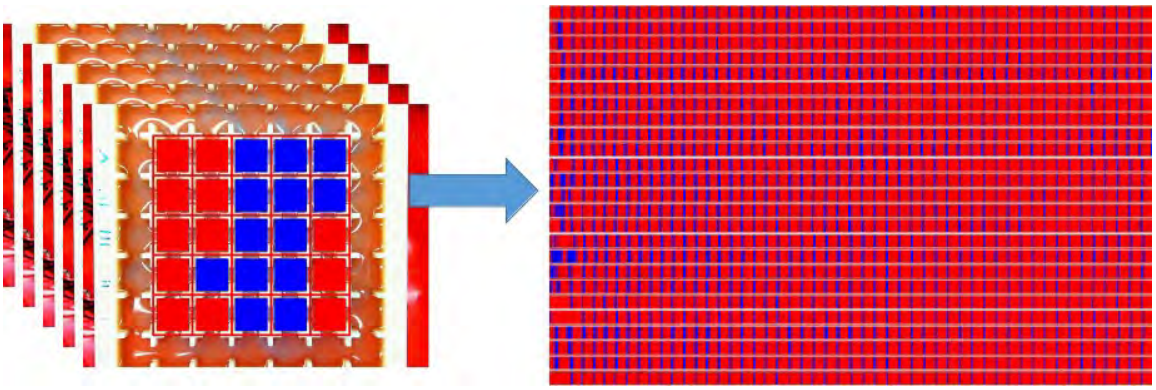

Figure S25: Left: A video sequence of BZ reaction. Right: The time map generated, where the blue flashes show when the BZ reaction oscillated. In this case, the video input is a segmented one, and therefore the output also shows a segmented time-map.

4 Experimental data

This section will cover all the experimental data generated using our BZ platform. The main data structure used to show the data will be the time-map plots described on Section 3.3.

4.1 Studying the relation between arena architecture and oscillations

By using 3D printing to construct grids of discrete but fluidically-connected cells, we were able to control the propagation of wave patterns from a cell to a neighbouring cell. The designs were manufactured in a chemically resistant white plastic to allow the colour of each cell to be easily monitored. The basic starting design for the reactionware comprised a monolithic rectangular block into which a square arena was inset. This was then divided into equal sized cells by printing walls at equal spacings, with cut-outs in each wall to allow fluidic connection.

We first performed several pilot experiments to determine a suitable cell design that would produce sustained bulk BZ oscillation waves over the whole cell, while being sufficiently large to be imaged consistently. The best results were obtained using a 7 by 7 grid of 16 by 16 by 5 mm cells where the cut-out accounted for a third of each connecting wall. Of the 7 by 7 grid, only the middle 5 by 5 cells were used for experiments in order to avoid cells on the edges (with fewer neighbours) which might be expected to oscillate differently.

To control the interaction between cells, we first designed a prototype array of BZ cell grid which had a “v” shape opening between cells (Figure S26C left) and the BZ reaction volume used was 70 ml, which filled the arena to three quarters of its height, well above the “v” opening. With this design, it was found that oscillations did not propagate to neighbouring cells and the platform acted similarly to a display screen, where only the cells that were enabled flashed in blue, while the other ones remained red (Figure S26A-B). This demonstrated that our platform can act as a “display

screen". In order to test it, we used a static activation pattern of cells to flash a "smiley emoji" pattern (Figure S26A) and also a sequenced pattern where columns were activated one after the other, left to right (Figure S26B).

To facilitate improved interaction between cells, we completely removed the "v" shaped part of the opening, leaving only the corners of each cell to define it (Figure S26C right) as fluid dynamics simulations showed that the removal of the barriers allowed the fluid from a stirred cell propagate to neighbouring cells upon stirring. This way, as can be seen in the 4-way neighbourhood test, the fluid from an activated cell would propagate to its neighbours when stirred, and we could, for example, activate a cell that was disabled by stirring (and therefore activating) its neighbours.

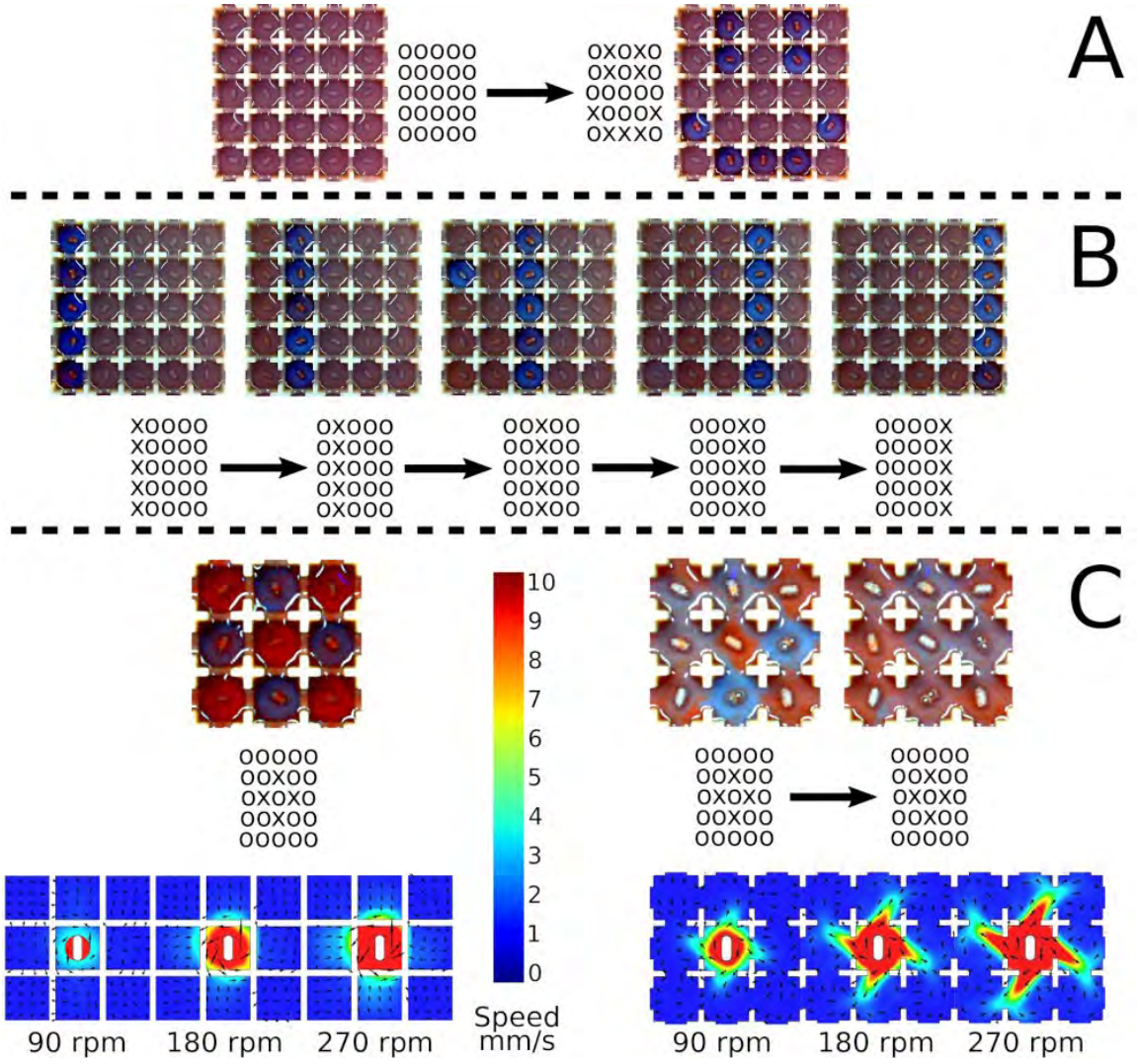

Figure S26: Addressing the oscillating cells. In this figure, every video frame is accompanied by a matrix of "x" and "o". This matrix indicates if in that given frame a motor was enabled (marked with a "x") or disabled (marked with a "o"). In the first experiments, a grid design with 16mm by 16mm cells with 5 mm of depth, in a grid with 7 by 7 cells, and containing 70 ml of BZ reaction was used.

Out of those 49 cells, only the 5 by 5 in the centre contained a stir bar and were placed above a motor, thus the outer 24 ones were always disabled. With a v-shape opening between cells, we could flash images like in a display screen. In (a) for example, it was flashed a smiley emoji, while in (b) it was flashed a sequence of patterns were initially only the left most column was enabled, followed by the adjacent columns in successive steps, until arriving to the right most column. The main drawback of this v-shape opening between cells is that very little fluid was transferred between them, as can be seen in C-left. Thus, we decided to completely open the gap, see C-right, and this allowed for bigger quantities of fluid to move between cells, and in this way we achieved the objective of enabling a cell which was disabled just by enabling its surrounding cells.

4.2 Input patterns used for pattern recognition

In all the following figures white square means disabled, while red square means enabled. In some of the experiments, “disabled” meant that the motor was completely off, and “enabled” meant that the motor was on at double speed of the default speed explained during the Firmware section (Section 1.3). This was for example the case of the AND/OR experiments explained during the main manuscript. In some other cases, “disabled” meant that the motor was actuated at the default speed, while “enabled” meant that the motor was actuated at five times the default speed. This was the case of the XOR experiment in the main manuscript. All the pattern recognition experiments used this protocol. The reason behind this was about generating global BZ waves, while in the case of “disabled” meaning completely off, the waves were not necessarily global. Finally, when here we mean “twice the speed” or “five times the speed”, we mean in terms of the PWM signal generated, not in terms of the actual speed of the motors in terms of revolutions per minute.

Figure S27 shows the input patterns used for 0 to 9. Number “1” used two different shapes, one was a straight line, while the other had more shape. Figure 28 shows the input patterns used for the letters A, B, C, E, G, L, M, N and R. Figure 29 shows three input random patterns that were used with five, seven and nine enabled motors.

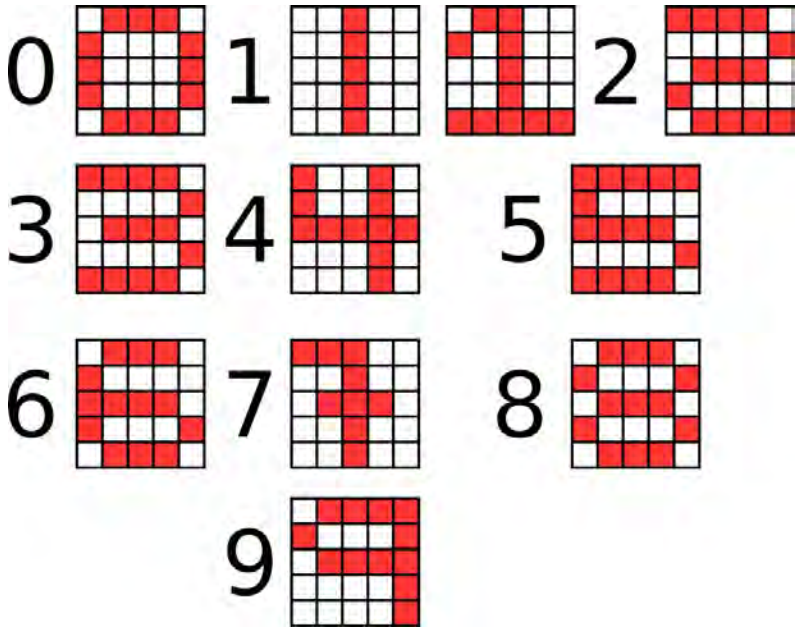

Figure S 27: Input patterns used for pattern recognition in the BZ platform. White means disabled, red means enabled. These patters represent the numbers from 0 to 9.

4.3 Studying the colour changes based on the input recipe

The BZ system used during this research, as explained in Section 2, oscillates between two states, which for simplicity we named “red” and “blue”. The BZ medium changes colour as the BZ reaction goes on. Initially it has an almost purple colour, with the oscillations being blue, while after one hour it has a dark red colour, with the oscillations being dark blue. Eventually, the medium is dark red, and no oscillations can be seen. In order to help detecting the oscillations as explained in the image processing section (Section 3), we tried to utilize a BZ recipe in which the colour changed the least in a 1 hour long experimental window. This section will show the different recipes used and the colour variation they produced. The one chosen was: 2.5 mL Ferroin, 20 mL water, 12.5 mL sulfuric acid, 18 mL malonic acid and 19 mL potassium bromate. The only reason this recipe was chosen is because it produced the most constant colour scheme. It is also worth noting that different recipes will produce different regimes of oscillations, and when choosing between different recipes that looked potentially good (from a colour scheme perspective) we settled for the one with the highest frequency of oscillations.

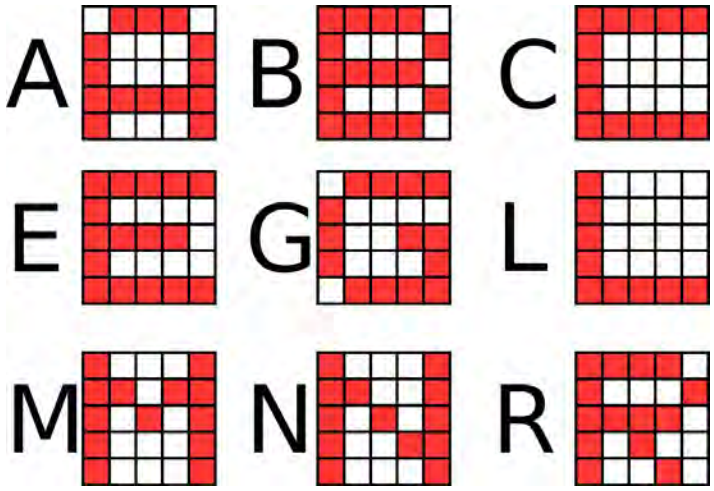

Figure S 28: Input patterns used for pattern recognition in the BZ platform. White means disabled, red means enabled. These patterns represent the letters A, B, C, E, G, L, M, N and R.

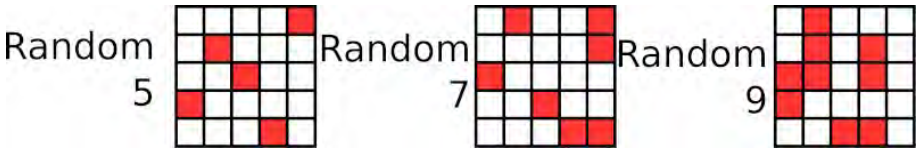

Figure S29: Input patterns used for pattern recognition in the BZ platform. White means disabled, red means enabled. These patterns represent three different patterns that were randomly chosen with 5, 7 and 9 enabled motors.

In all the following figures, the BZ medium was prepared and placed using the protocol described in Section 2, and then all the motors were switched on at the default speed for 1 hour. Figures 30 to 40 show the results.

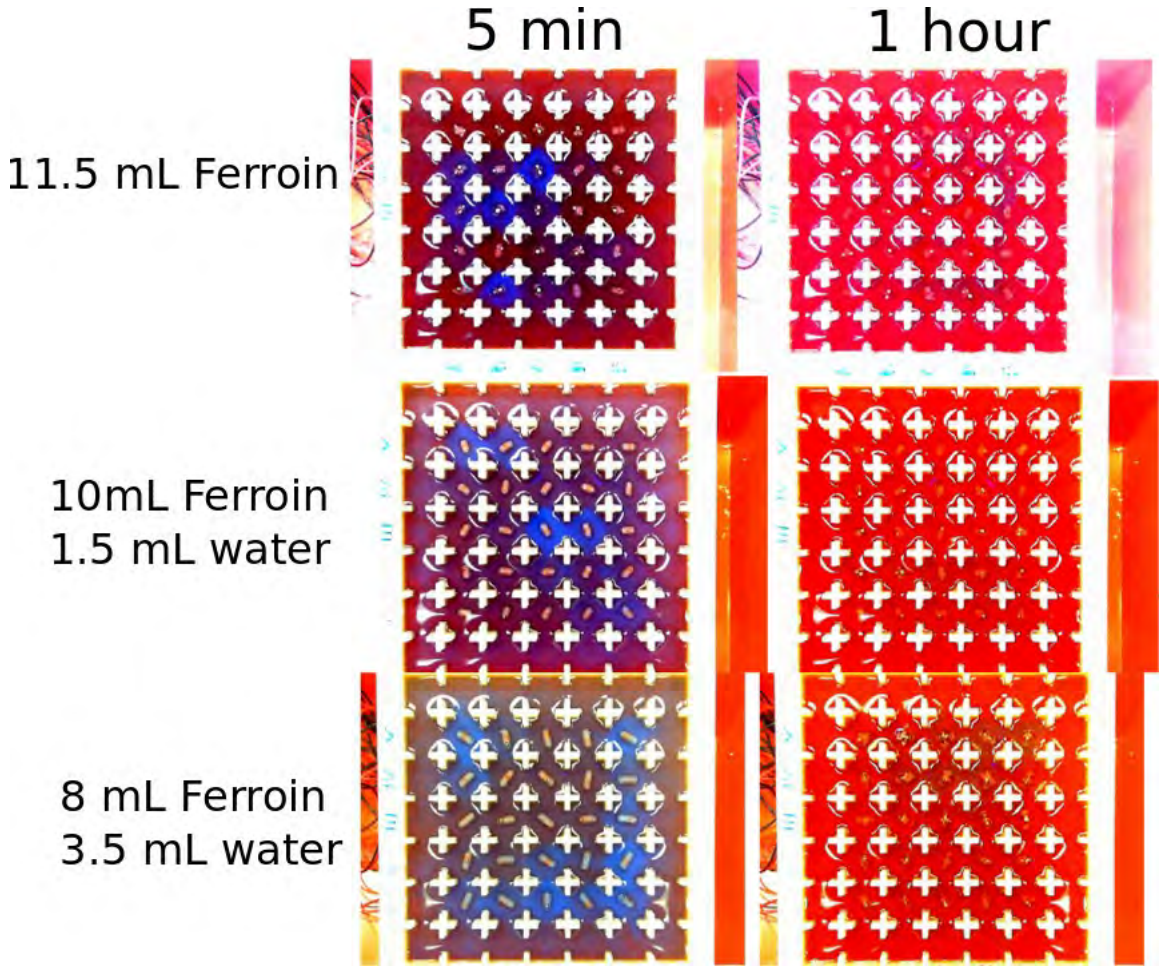

Figure S30: Testing for the BZ recipe with the best colour scheme. In this case, none of these recipes produced flashes after 1 hour. The recipe here used contains 15 mL sulfuric acid, 21.5 mL malonic acid and 22.5 mL potassium bromate. First row of the image then contains 11.5 mL of Ferroin, the second one 10 mL of Ferroin and 1.5 mL of water, and the last row 8 mL of Ferroin and 3.5 mL of water.

The objective was to obtain the least possible change in colour. Good candidates were identified, and for each of them a time-map (as explained in Section 3.3) was generated. As an example of a experimental recipe with a big change of colour, Figure S41 is shown. Figures S41 to S46 show the time-map of the main candidates. It can be seen that some of them were not able of producing oscillations through the whole experimentation time. The last one in particular: 2.5mL ferroin,12.5mL sulfuric acid, 18mL malonic acid, 19mL potassium bromate and 20mL of water; was the main recipe used during this research.

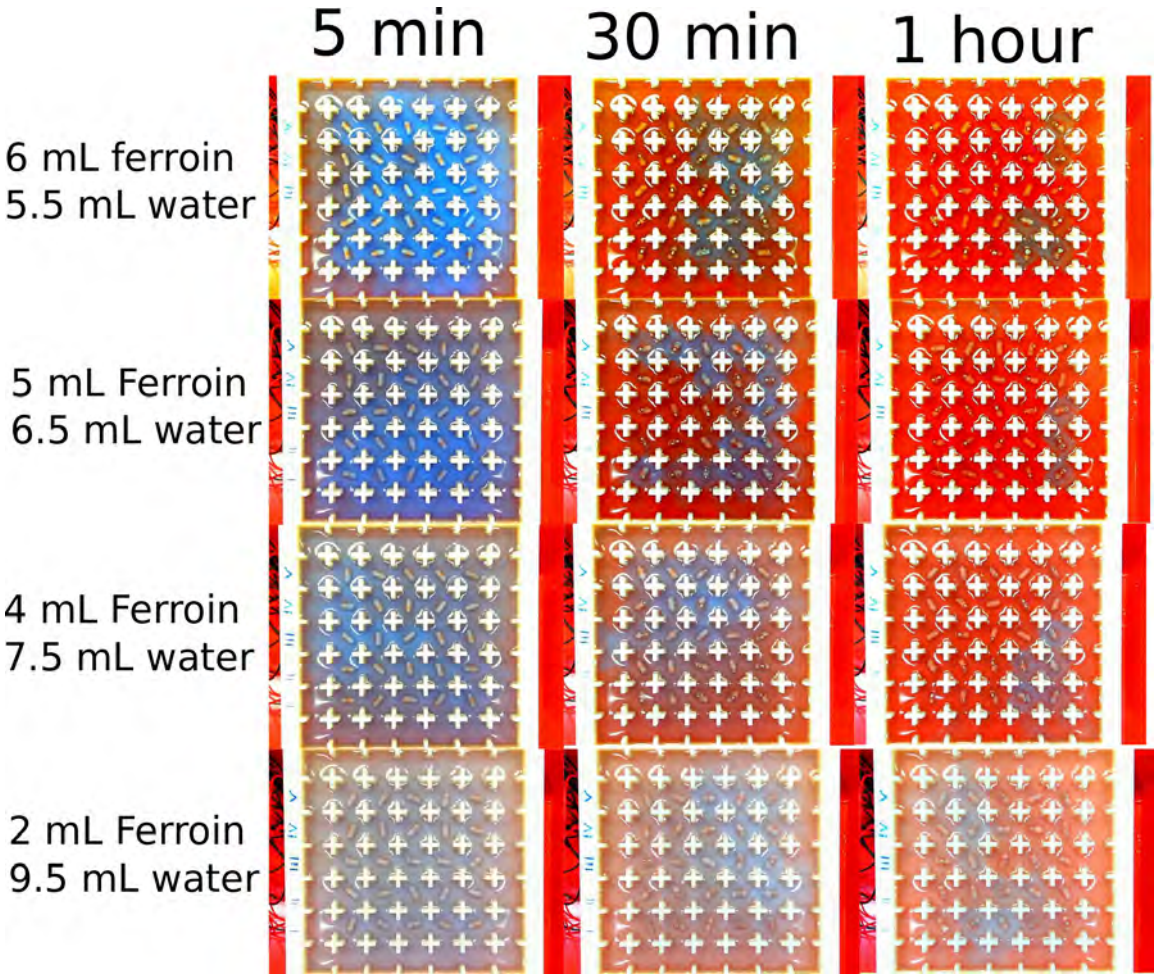

Figure S31: Testing for the BZ recipe with the best colour scheme. The recipe here used contains 15 mL sulfuric acid, 21.5 mL malonic acid and 22.5 mL potassium bromate. First row of the image then contains 6 mL of Ferroin and 5.5 mL of water, the second 5 mL of Ferroin and 6.5 mL of water, the third one 4 mL Ferroin and 7.5 mL water, and the last row 2 mL of Ferroin and 9.5 mL of water.

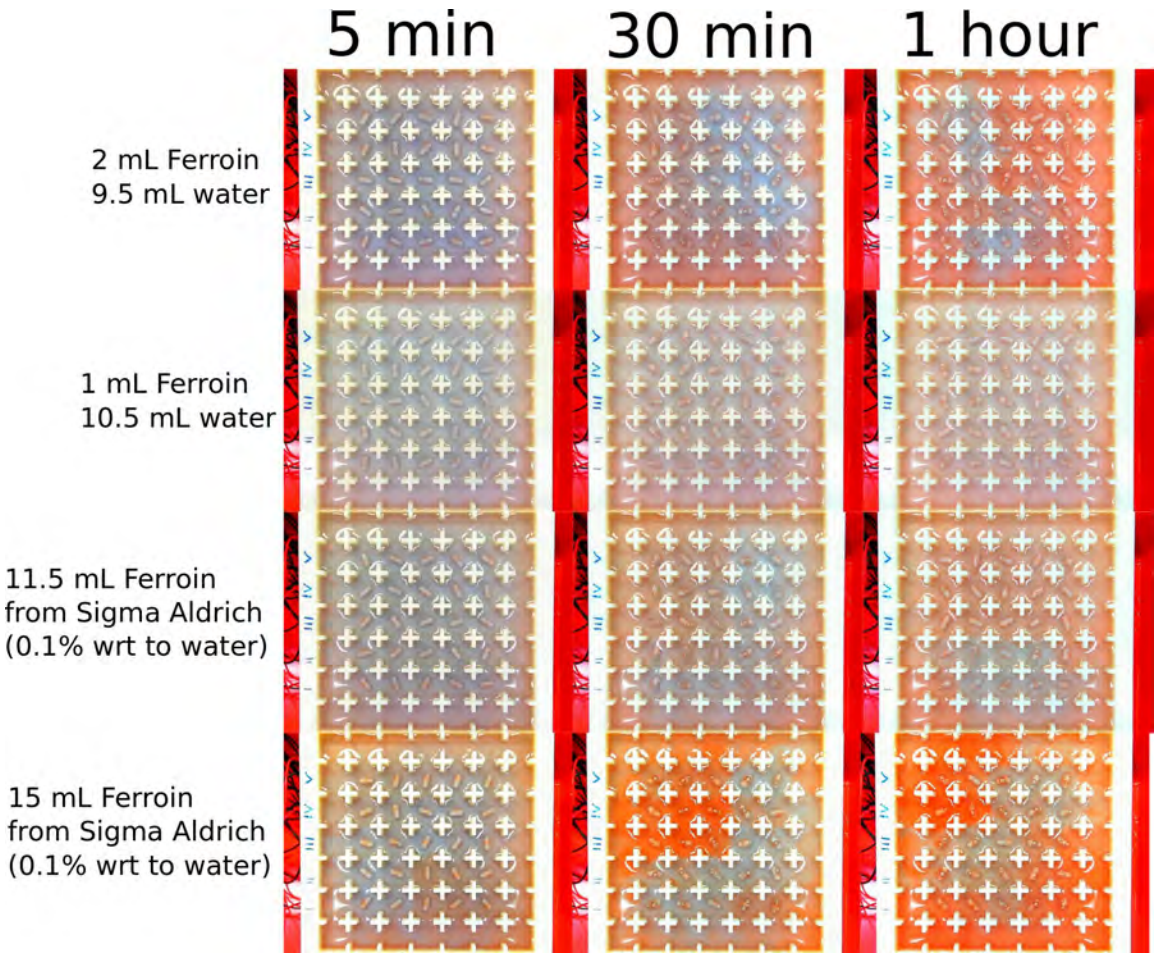

Figure S32: Testing for the BZ recipe with the best colour scheme. The recipe here used contains 15 mL sulfuric acid, 21.5 mL malonic acid and 22.5 mL potassium bromate. First row of the image then contains 2 mL of Ferroin and 9.5 mL of water, the second 1 mL of Ferroin and 10.5 mL of water, the third one 11.5 mL Ferroin sourced from Sigma (0.1% wrt to Water), and the last row 15 mL Ferroin sourced from Sigma (0.1% wrt to Water).

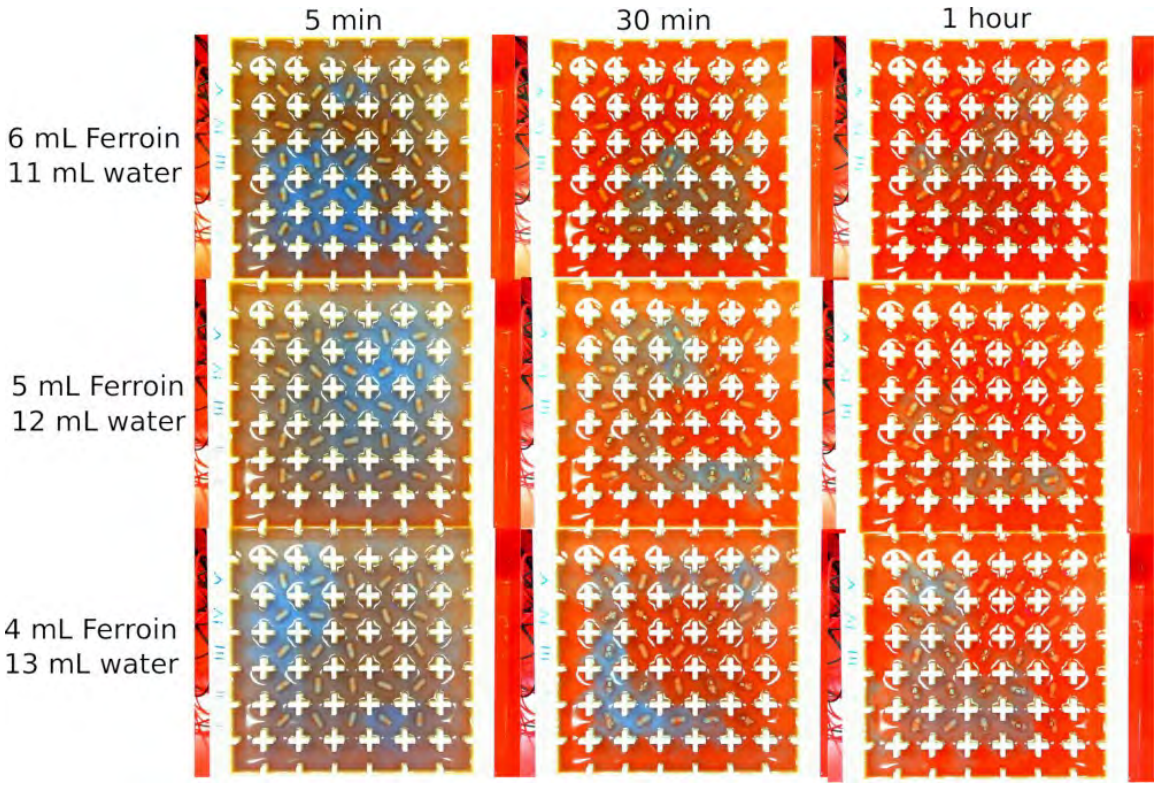

Figure S33: Testing for the BZ recipe with the best colour scheme. The recipe here used contains 13.5 mL sulfuric acid, 19.5 mL malonic acid and 20.5 mL potassium bromate. First row of the image then contains 6 mL of Ferroin and 11 mL of water, the second 5 mL of Ferroin and 12 mL of water, and the last row 4 mL of Ferroin and 13 mL of water.

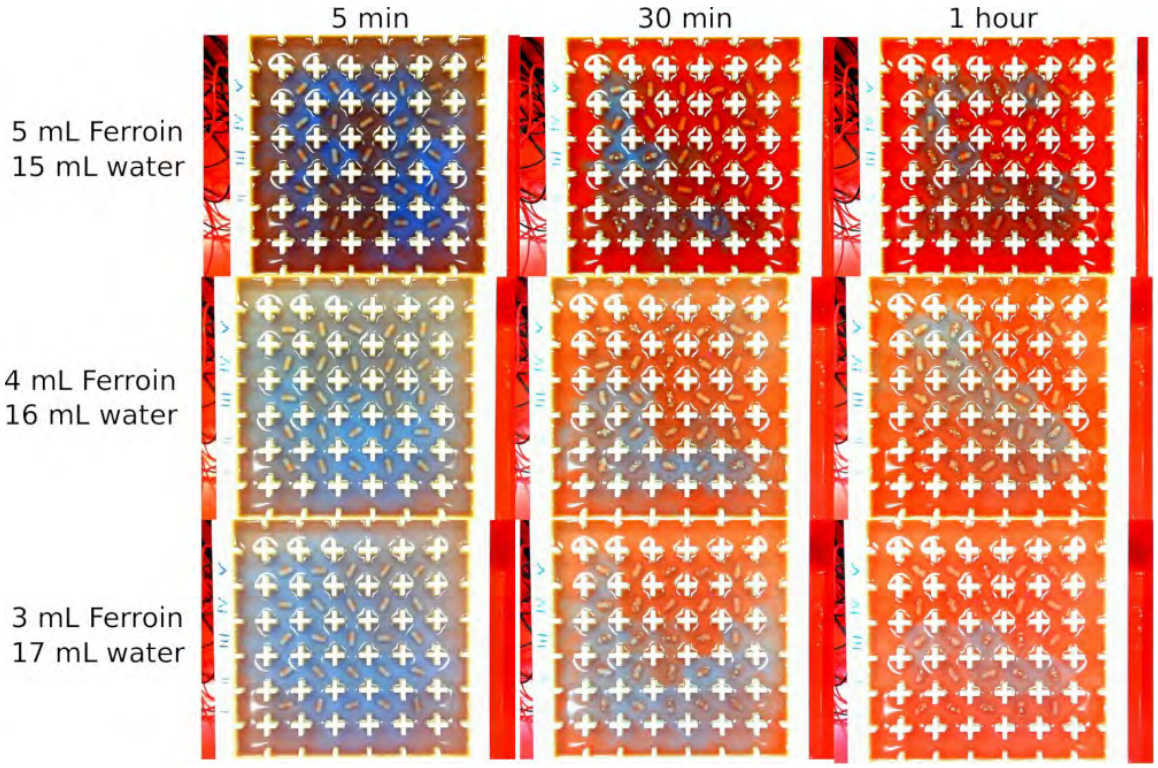

Figure S34: Testing for the BZ recipe with the best colour scheme. The recipe here used contains 12.5 mL sulfuric acid, 18.5 mL malonic acid and 19.5 mL potassium bromate. First row of the image then contains 5 mL of Ferroin and 15 mL of water, the second 4 mL of Ferroin and 16 mL of water, and the last row 3 mL of Ferroin and 17 mL of water.

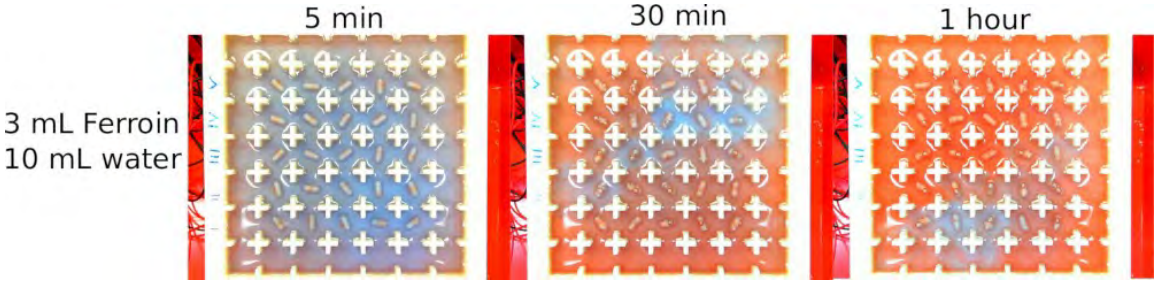

Figure S35: Testing for the BZ recipe with the best colour scheme. The recipe here used contains 15.5 mL sulfuric acid, 21.5 mL malonic acid and 23.5 mL potassium bromate. The only row contains 3 mL Ferroin and 10 mL of water.

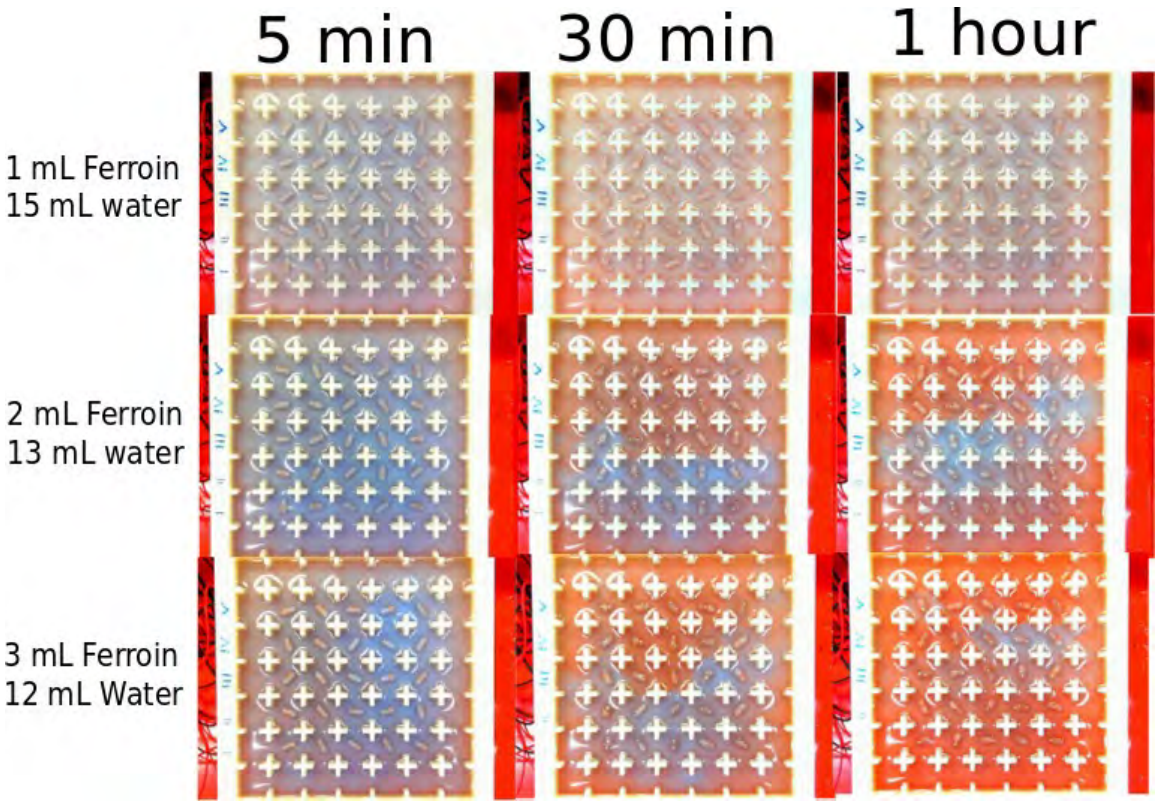

Figure S36: Testing for the BZ recipe with the best colour scheme. The recipe here used contains 15 mL sulfuric acid, 21.5 mL malonic acid and 22.5 mL potassium bromate. The first row contains 1 mL Ferroin and 14 mL of water, the second row contains 2 mL Ferroin and 13 mL water, the third row contains 3 mL Ferroin, 12 mL water.

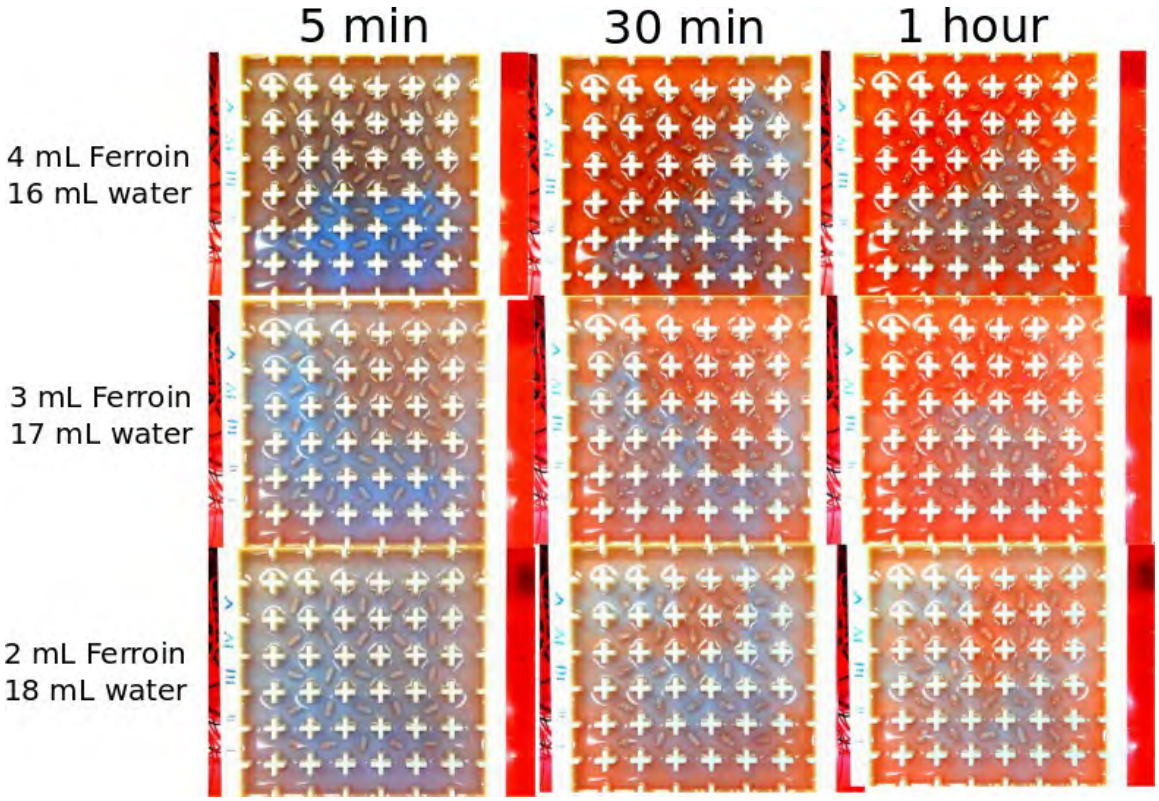

Figure S37: Testing for the BZ recipe with the best colour scheme. The recipe here used contains 15 mL sulfuric acid, 21.5 mL malonic acid and 22.5 mL potassium bromate. The first row contains 4 mL Ferroin and 16 mL of water, the second row contains 3 mL Ferroin and 17 mL water, the third row contains 2 mL Ferroin, 18 mL water.

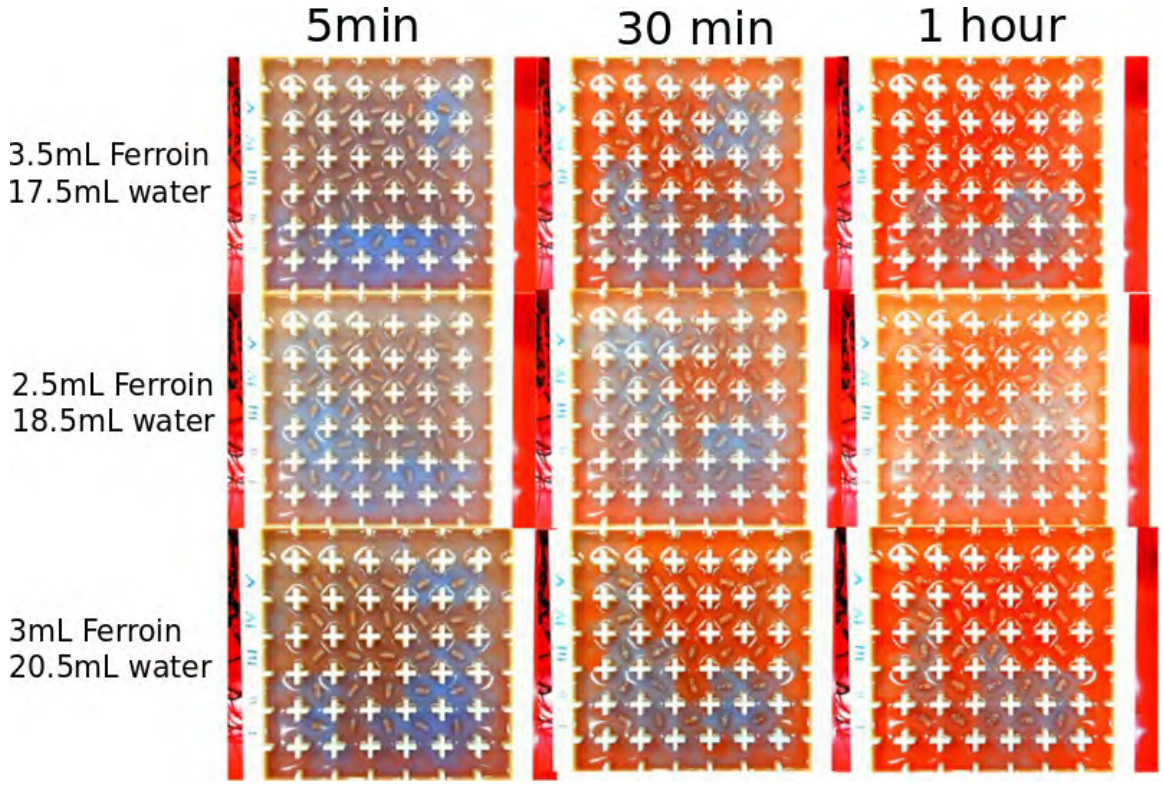

Figure S38: Testing for the BZ recipe with the best colour scheme. The recipe here used contains 12.5 mL sulfuric acid, 18 mL malonic acid and 19 mL potassium bromate. The first row contains 3.5 mL Ferroin and 17.5 mL of water, the second row contains 2.5 mL Ferroin and 18.5 mL water, the third row contains 3 mL Ferroin, 20.5 mL water.

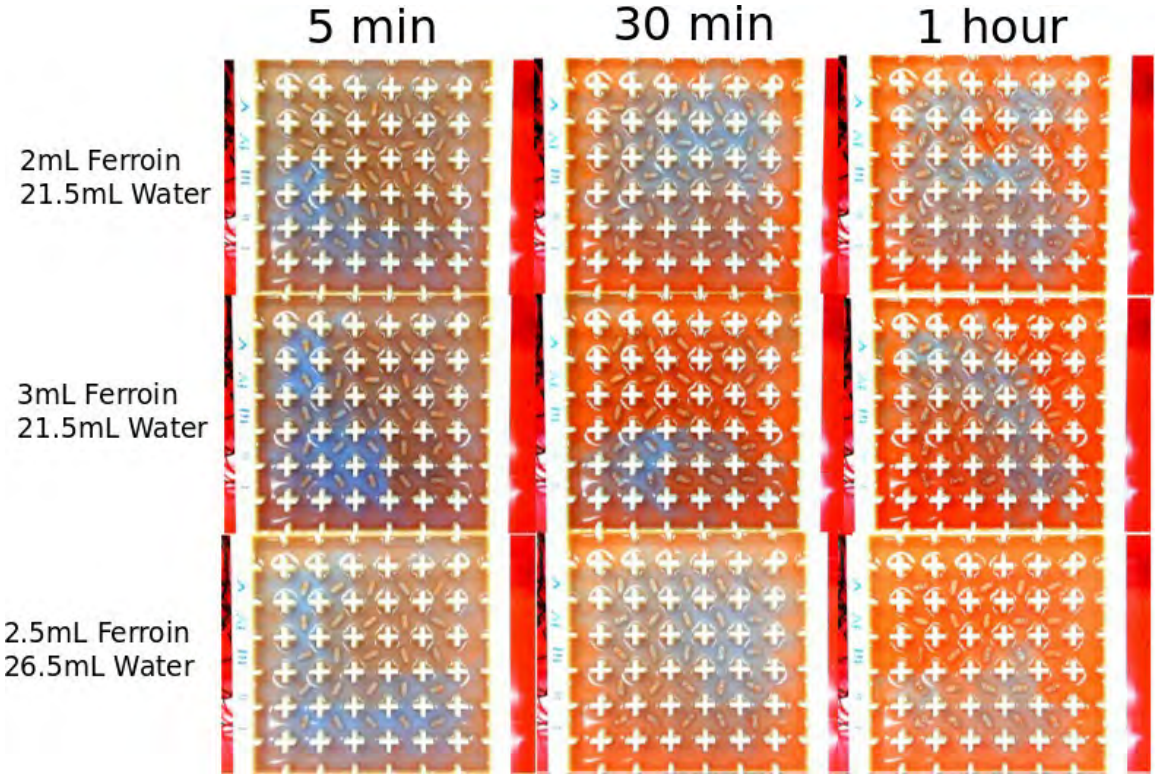

Figure S39: Testing for the BZ recipe with the best colour scheme. The recipe here used contains 12.5 mL sulfuric acid, 18 mL malonic acid and 19 mL potassium bromate. The first row contains 2 mL Ferroin and 21.5 mL of water, the second row contains 3 mL Ferroin and 21.5 mL water, the third row contains 2.5 mL Ferroin, 26.5 mL water.

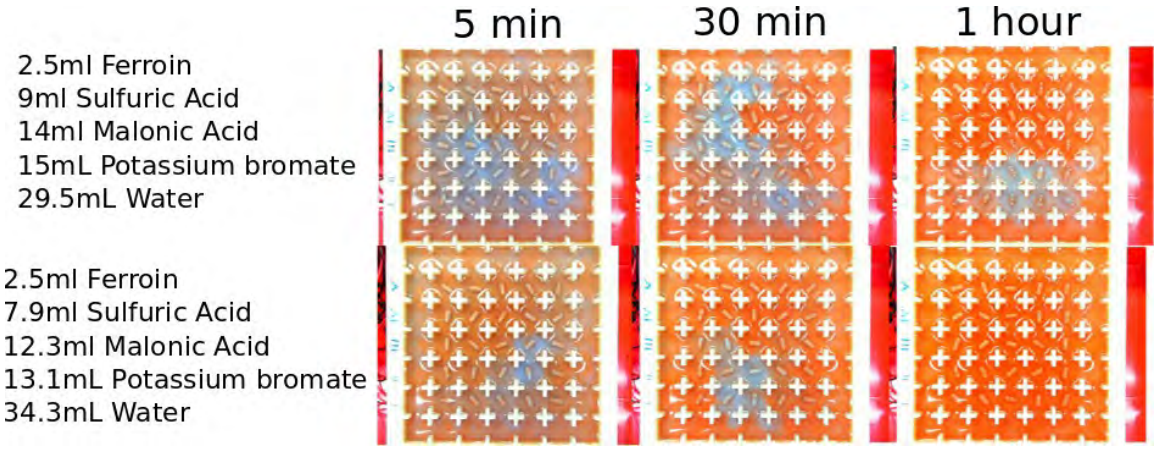

Figure S40: Testing for the BZ recipe with the best colour scheme. The two rows have different recipes, as shown by the legend.

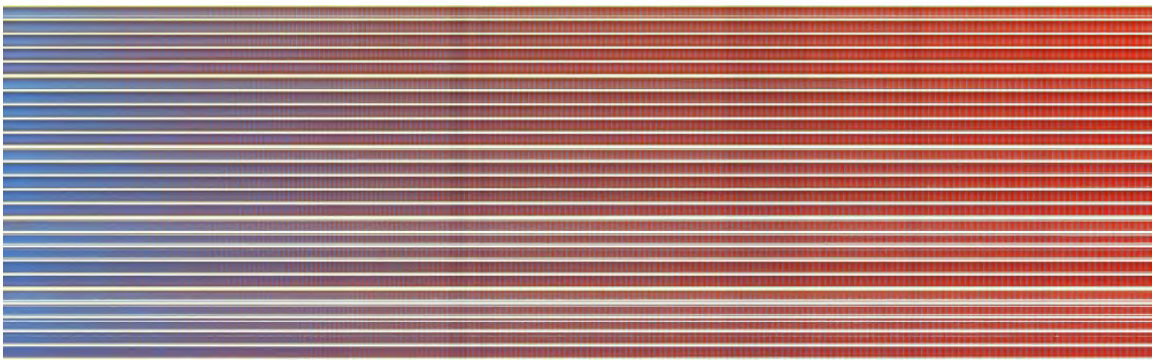

Figure S41: One hour time-map for the recipe containing 4mL of Ferroin, 10mL of sulfuric acid, 15mL of malonic acid, 21.5mL of potassium bromate and 22.5mL of water.

4.4 Reaction-diffusion experiments in a device without walls

An experimental arena like the one shown on Figure S5 was tested. This arena did not contain walls or corners. The results can be seen on Figure S47. In this experiment, all the stirrers were “on” at the default speed (90 RPM). The experiment lasted 2 minutes and 36 seconds.

4.5 Testing for how long the BZ system can oscillate

Three-hour long experiments were performed to test for how long the BZ reaction would oscillate. All the motors were set to “on” to the default speed, and the BZ medium continued to oscillate until the three-hour mark, see Figure S48.

4.6 Studying the memory effect of the BZ medium

A very interesting phenomena of the BZ medium is that it has memory. That is, if a pattern of motors is enabled and therefore their stir bars rotate, a global wave will emerge in the system. If these motors then are disabled, this global wave will continue in the system for a series of oscillations, until it finally disappears.

This was tested in a series of experiments, where all the motors were first enabled, and then disabled, in continuous cycles. The total length of these experiments was 1 hour. First, the motors were enabled and disabled in cycles of 5 minutes (5 minutes on, followed by 5 minutes off), see Figure S49. Therefore, in 1 hour there were 6 of these on/off cycles. The oscillations seemed to perfectly persist after 5 minutes of all the motors being disabled. Secondly, a similar experiment was done, but in this case the motors were on for 5 minutes, followed by 10 minutes of them being disabled, see Figure S50.

Therefore, in one hour there were four of these on/off cycles. In this experiment it can be seen that after 5 minutes of all the motors being off, the signal starts to weaken, and around the 10 minutes mark, when the motors are re-started, the signal was almost completely gone. This indicates that the system can keep a memory for around 5 minutes, although more experiments would be needed in order to certify the exact time the memory can keep a signal. One very interesting thing about this phenomena, is that each BZ cell can be considered like a cell in a recurrent neural network (RNN). Following the RNN model, we outlined the BZ process on Figure S51, where it can be seen how the state depends on the inputs, the state of the neighboring cells, and the previous global state of the BZ medium.

In order to quantify the relation between the BZ chemical recipe and the “memory” of the oscillations, it was decided to perform a series of experiment using the default BZ recipe but changing the quantity of $KBrO_3$ from 12 to 22 ml in steps of 1ml. In this particular experiment, as soon as it starts all the stirrers are enabled for 7.5 minutes. Then all of them are disabled for 7.5 minutes. Then all of them are enabled for 7.5 minutes. Finally, all of them are disabled for 7.5 minutes. The results can be seen on Figure S52. These results seem to indicate that the number of oscillations once the stirrers are stopped (the “memory”) increase with the quantity of $KBrO_3$. This might be perhaps related with the fact that a higher concentration of $KBrO_3$ generates oscillations with a higher frequency.

4mL ferroin, 13.5mL H2SO4, 19.5mL malonic acid, 20.5mL KBrO3, 13mL water

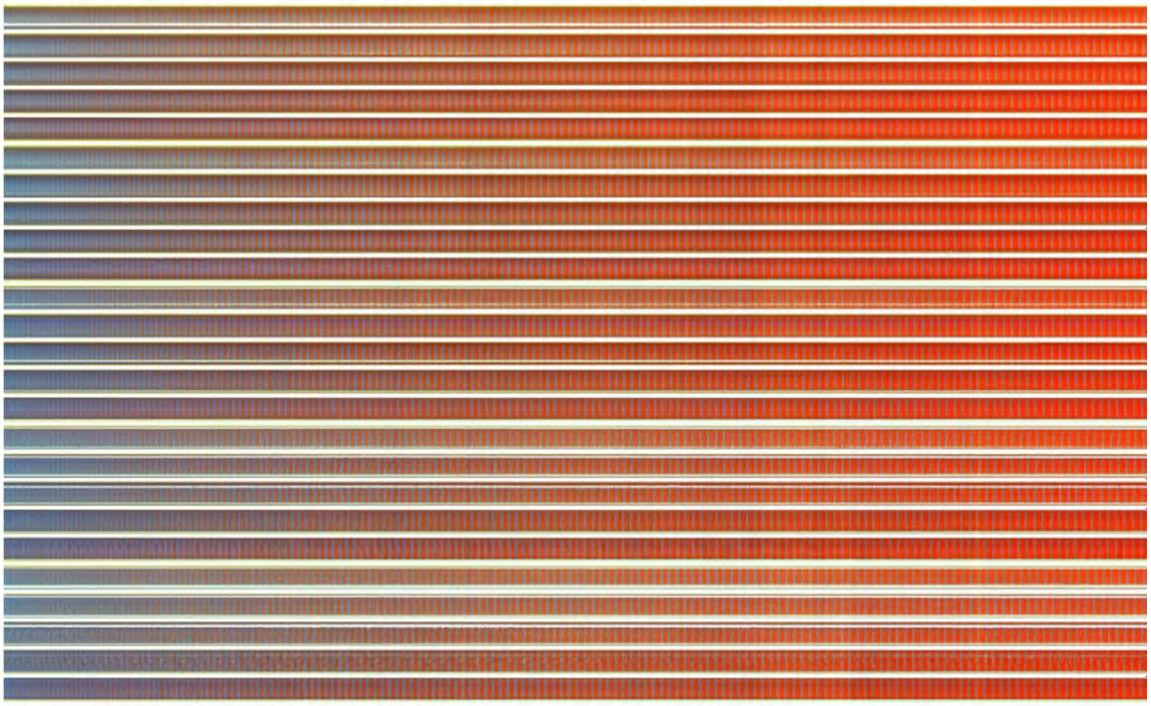

3.5mL ferroin, 12.5mL H2SO4, 18mL malonic acid, 19mL KBrO3, 17.5mL water

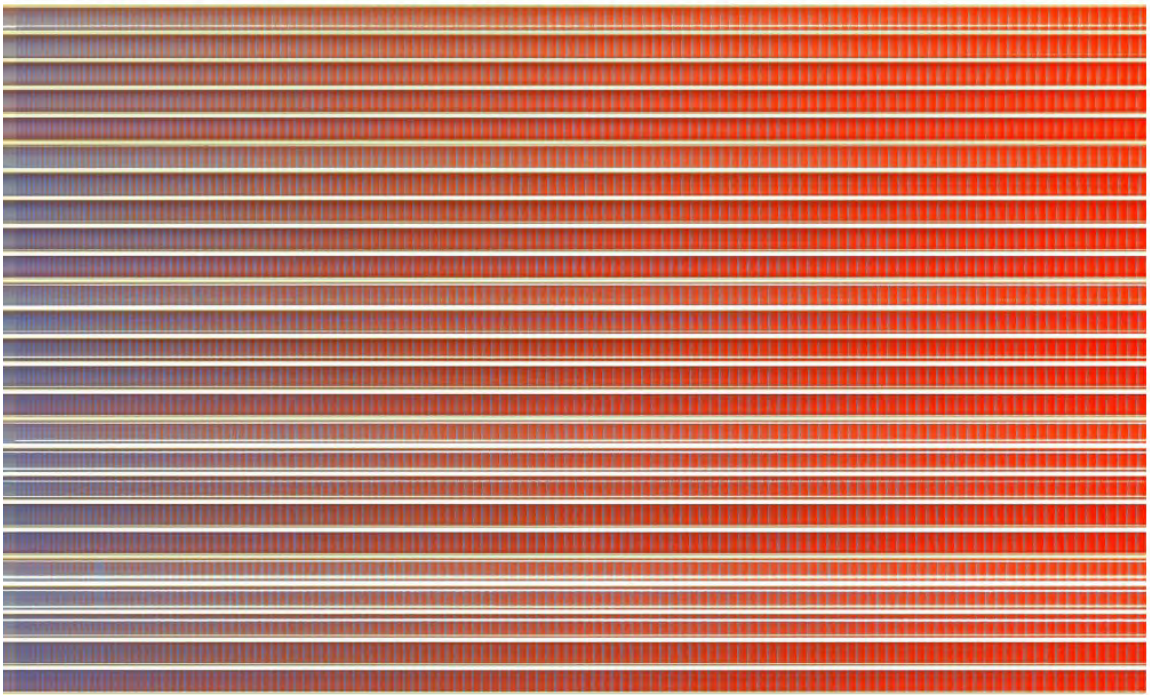

Figure S42: One hour time-map for two of the best colour-scheme candidates. In this case the focus was in the oscillations.

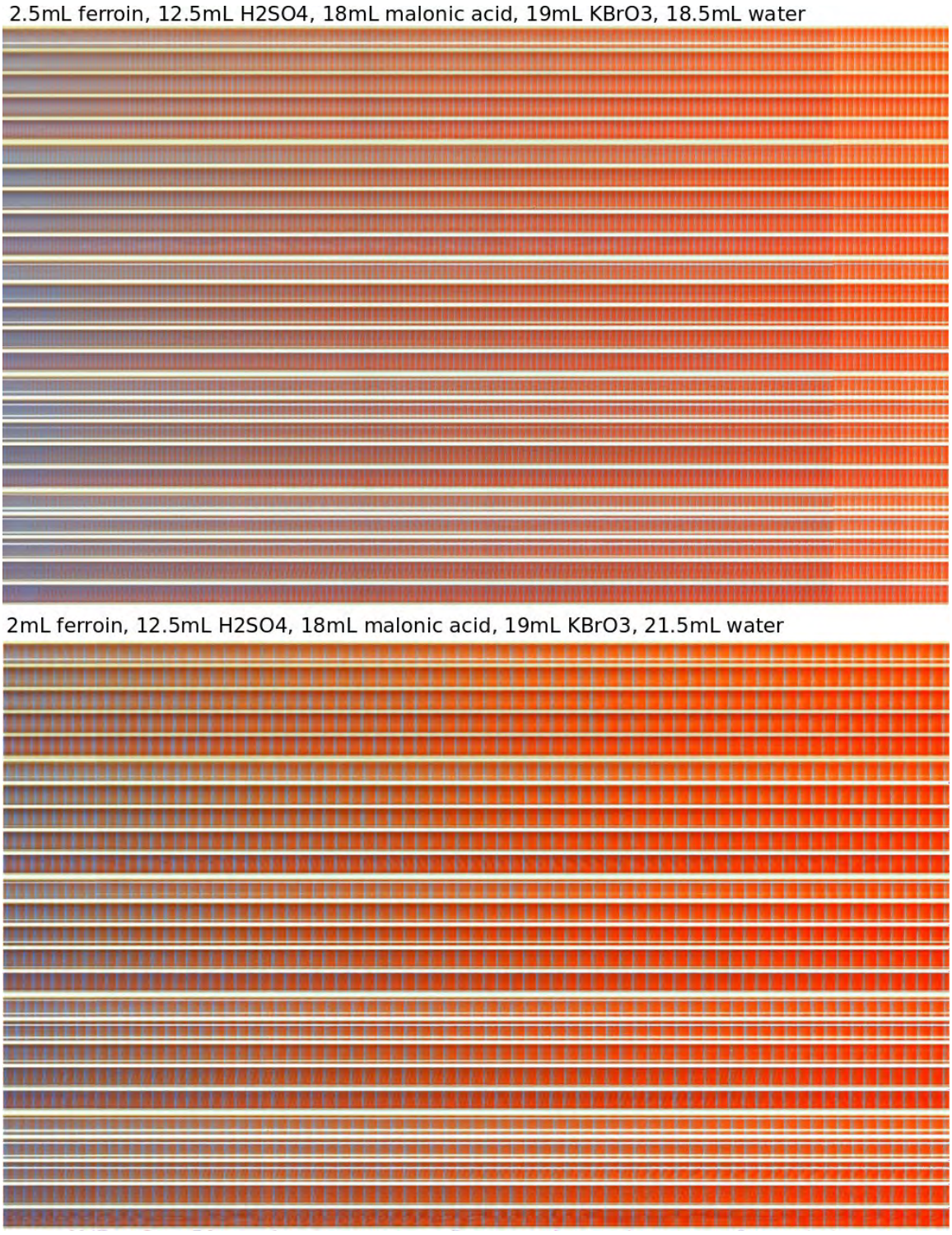

Figure S43: One hour time-map for two of the best colour-scheme candidates. In this case the focus was in the oscillations.

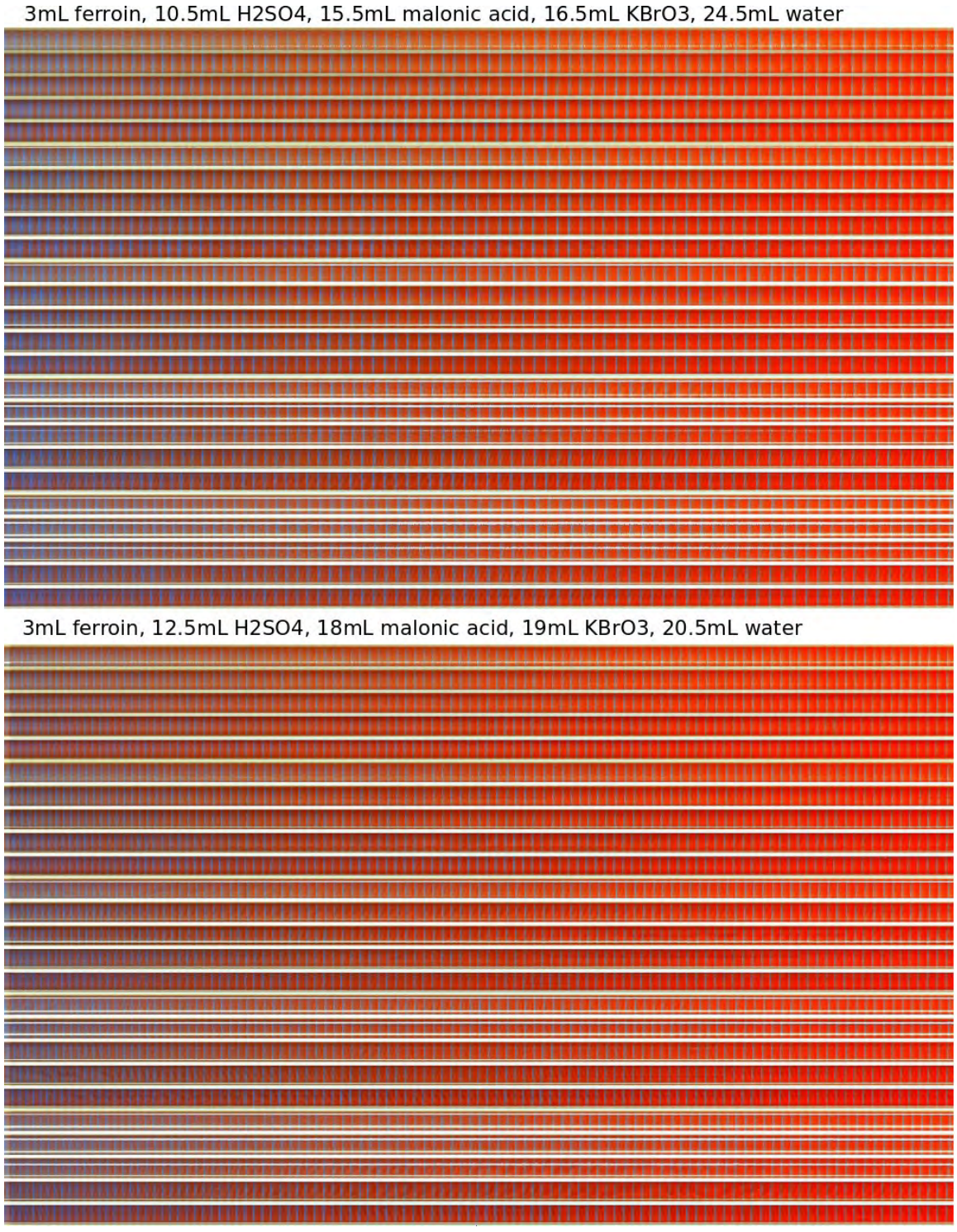

Figure S44: One hour time-map for two of the best colour-scheme candidates. In this case the focus was in the oscillations.

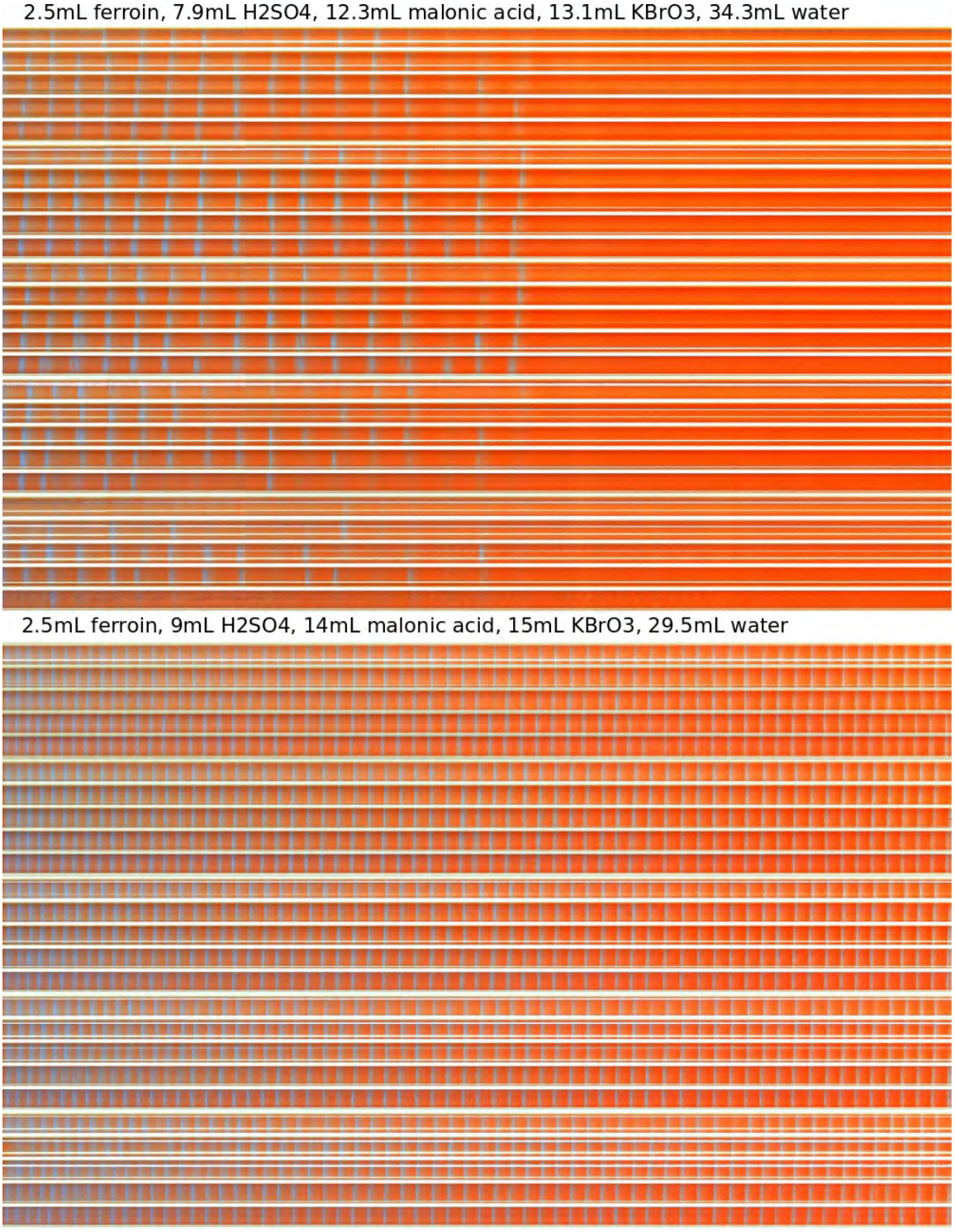

Figure S45: One hour time-map for two of the best colour-scheme candidates. In this case the focus was in the oscillations.

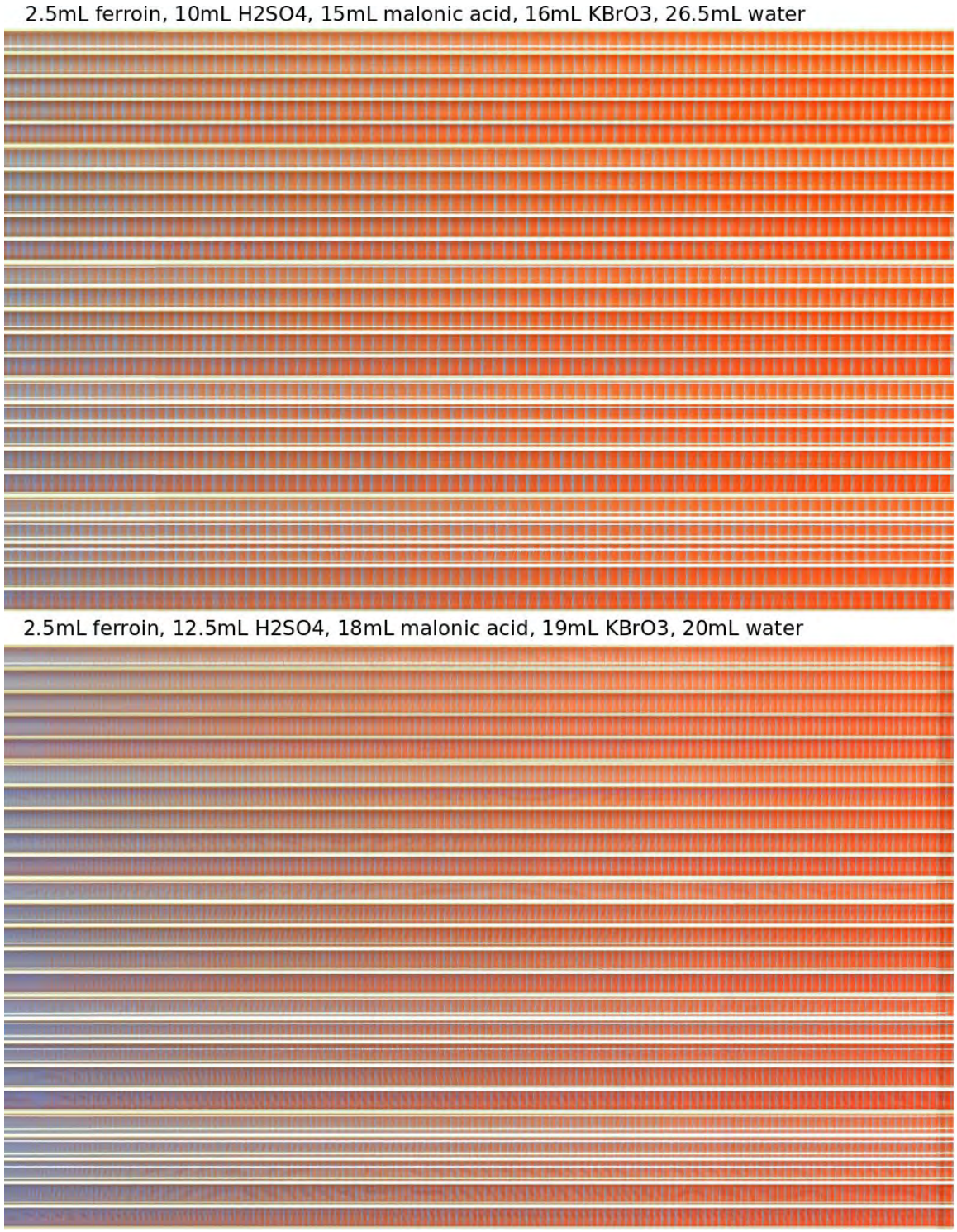

Figure S46: One hour time-map for two of the best colour-scheme candidates. In this case the focus was in the oscillations. The second recipe here is the main recipe used during this research: 2.5mL ferroin, 14mL of sulfuric acid, 19mL of potassium bromate, 18mL of malonic acid and 20mL of water.

Figure S 47: Experiment using a experimental arena without walls (see Figure 5). Here the timemap is shown. In total this experiment lasted 2 minutes and 36 seconds. At 30 FPS every row of pixels in this image represents a frame.

4.7 Studying the speed of stir rotation and its relation to BZ oscillations

It was also tested how different stirrer speeds impact the frequency of oscillations. In order to do so, the pattern flashed was “10001” meaning the first column of stirrers were enabled, the following three were completely off (not moving) and the last column was also enabled. The speeds tested were: default speed, two times the default speed, and five times the default speed. Figure 53 shows the time-map for the three speeds. In this case we took the first five rows of the time-maps instead of the 25 as in the previous ones. We also only focused on the last 15 minutes of the experiment. We did it this way because it was considered that they would be easier to compare. It can be seen in the results how higher stirring speeds actually decrease the frequency of the oscillations. In these results, the default speed generated 26 oscillations in 15 minutes, double the speed generated 24 oscillations, and five times the speed generated 23 oscillations. These numbers seem very similar, but in the figure described it can better be seen. Another side-effect of high speeds is that they sometimes failed to generate oscillations. This can be seen in the figure described, in the last two rows within the last row: near the end, it fails to oscillate.

Setting each stirrer at a random speed

A series of experiments were performed were the speed of each motor was set randomly. We used Python Random library to choose a number between 0 and 4000 for each motor. As described before, PWM signals under 500 did not produce motor rotations, therefore, some of the motors were disabled. Our expectation was that the system would struggle to arrive to a coherent state pattern, and it did take more than that usual, but it did manage to arrive to a coherent pattern. See

Figure 54. There it can be seen, for example, that the 21st row (fifth from the bottom) took a third of time to oscillate, but eventually it did oscillate. The total time of this experiment was 30 minutes.

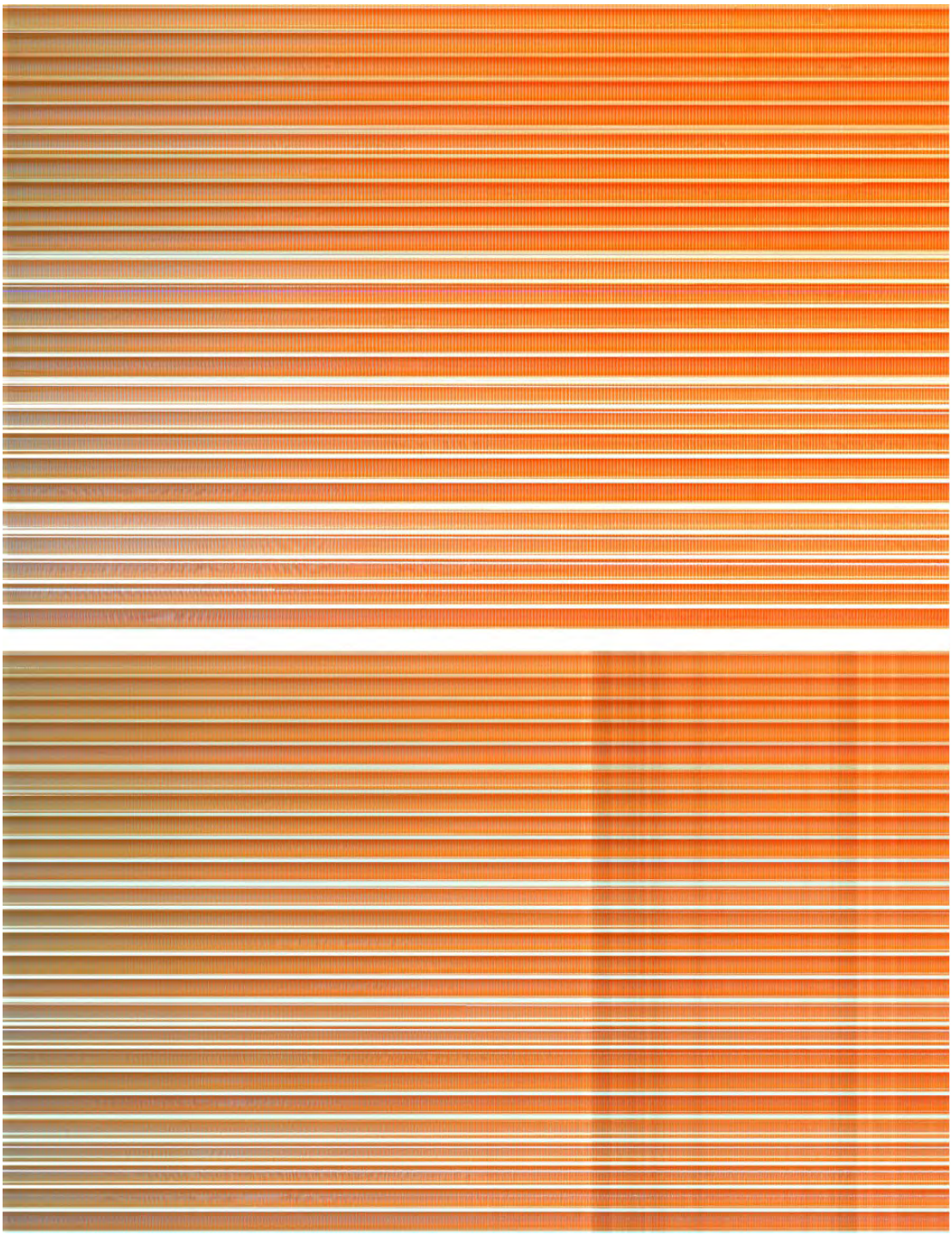

Figure S48: Two executions of 3 hour long experiments. All the motors were set to the default speed.

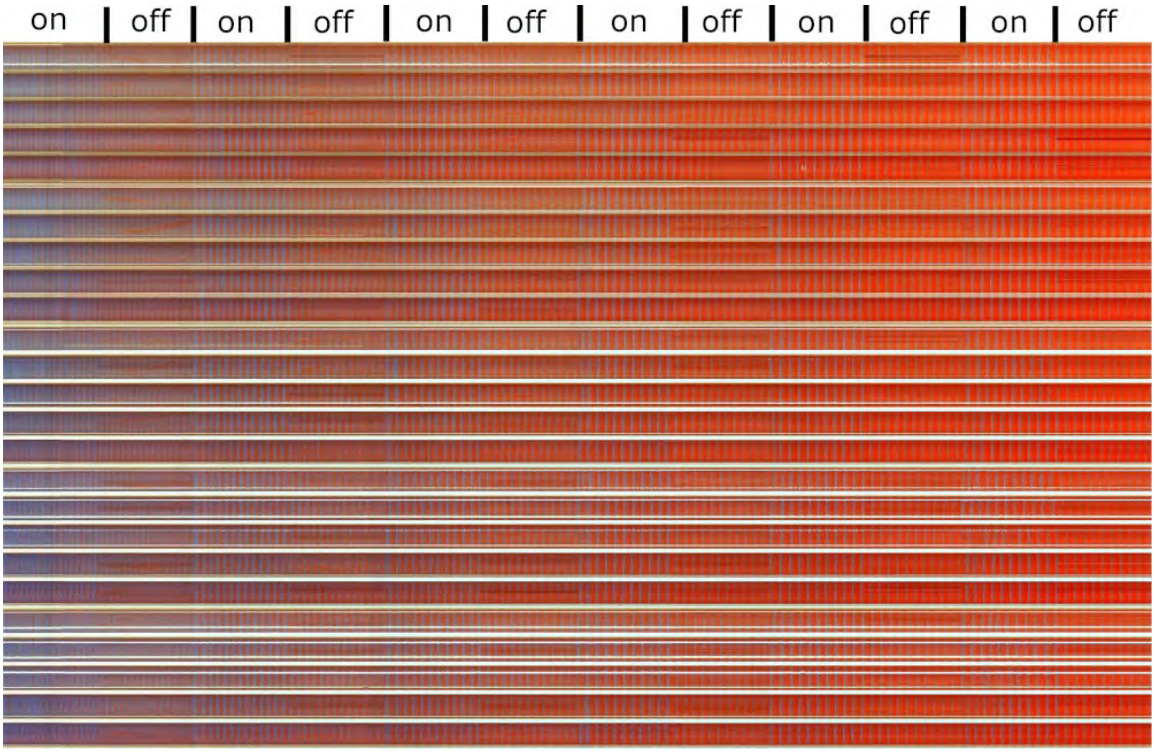

Figure S49: Enabling and disabling all the motors in 5 minute cycles. Total experiment was 1 hour.

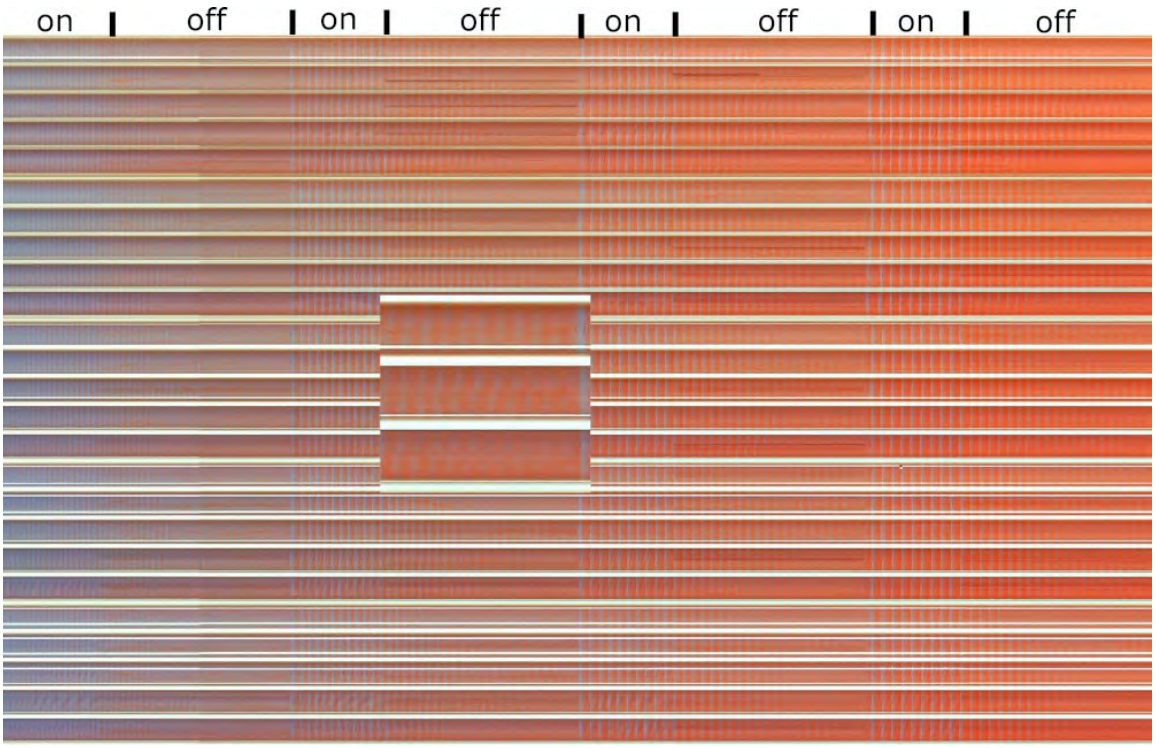

Figure S50: Enabling all the motors for 5 minutes, and then disabling them for 10. Total experiment was 1 hour. Centre image zooms into the end of a 10 minutes off period.

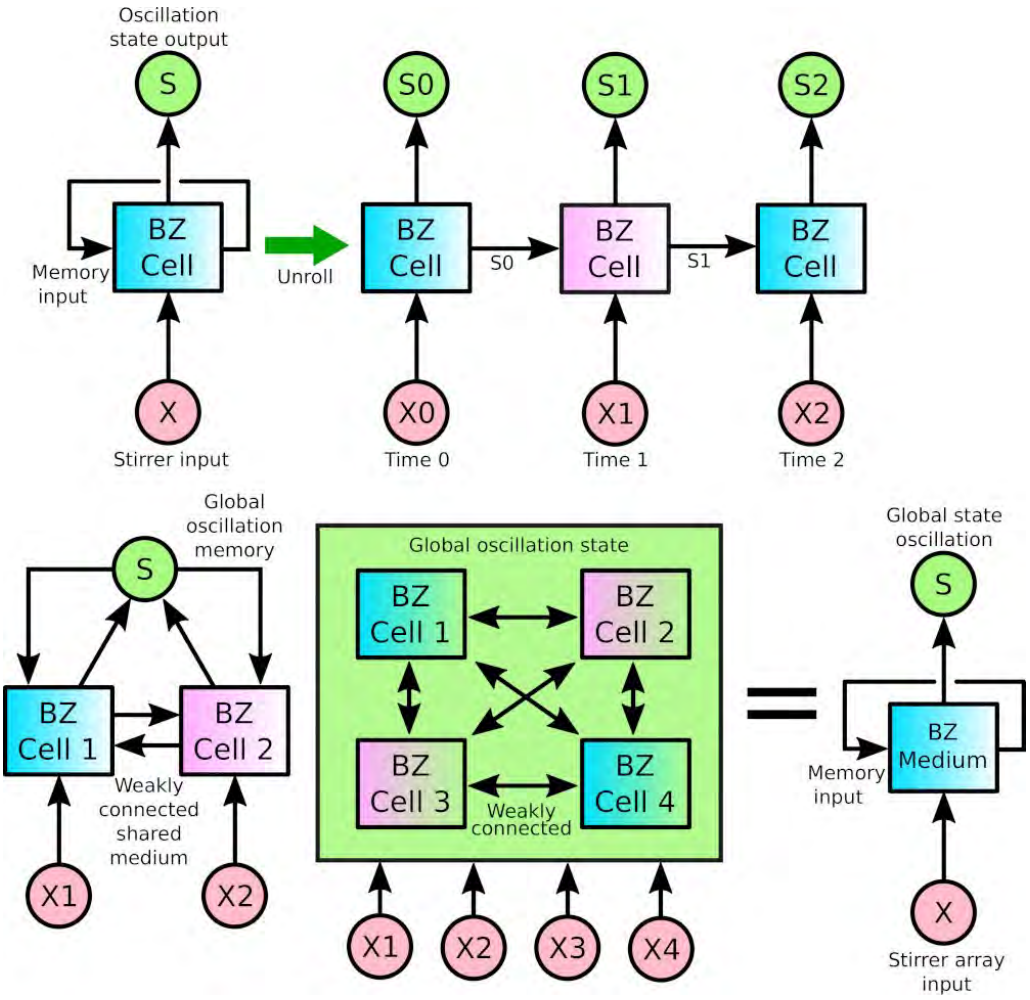

Figure S51: In systems with multiple cells weakly connected, not only the state depends on the inputs plus the memory of the system, but also depends on the weakly connections between cells. The top row in this figure represents a system with only one cell. Bottom-left image represents a system with two cells, and bottom-right represent a system with multiple cells. This multiplecell system can be “encapsulated” and seen like the system with only one cell in terms of inputs, memory, and output.

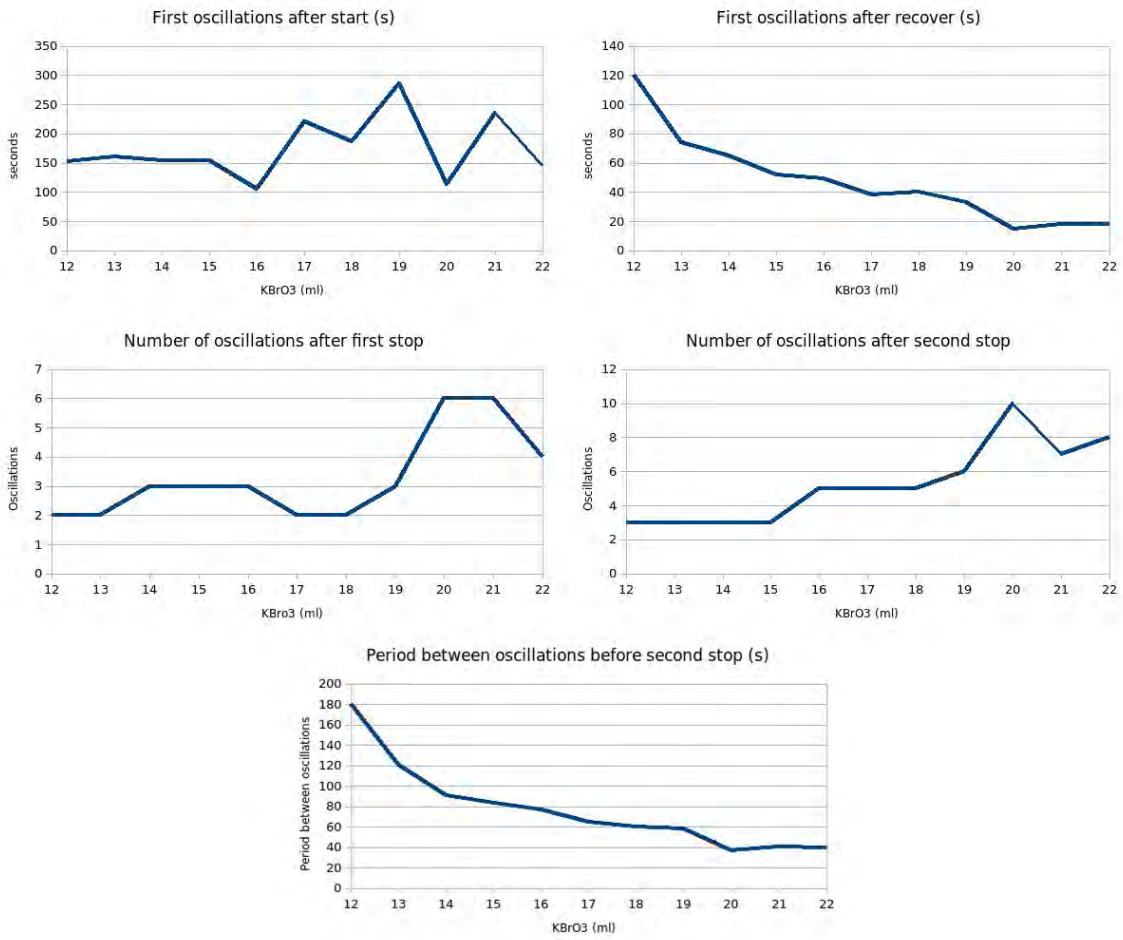

Figure S52: Studying the number of oscillations that appear in the system once all the stirrers are disabled. Our results seem to indicate that a higher concentration of $KBrO_3$ generates a bigger "memory".

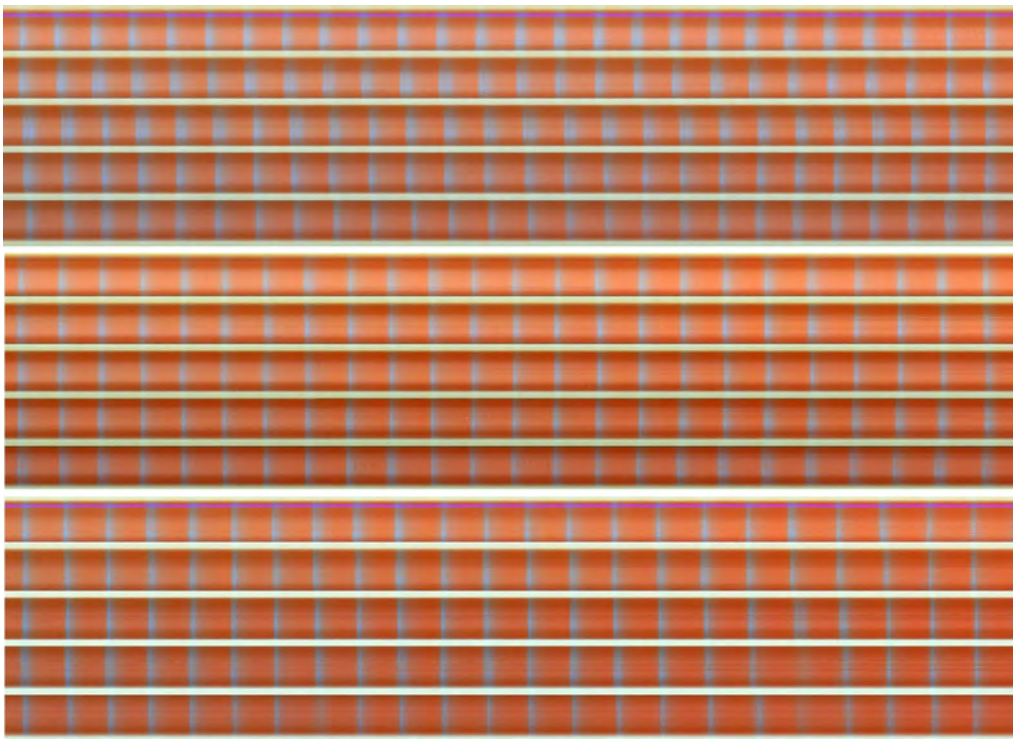

Figure S53: Top row: default speed. Middle row: Two times default speed. Bottom row: Five times default row.

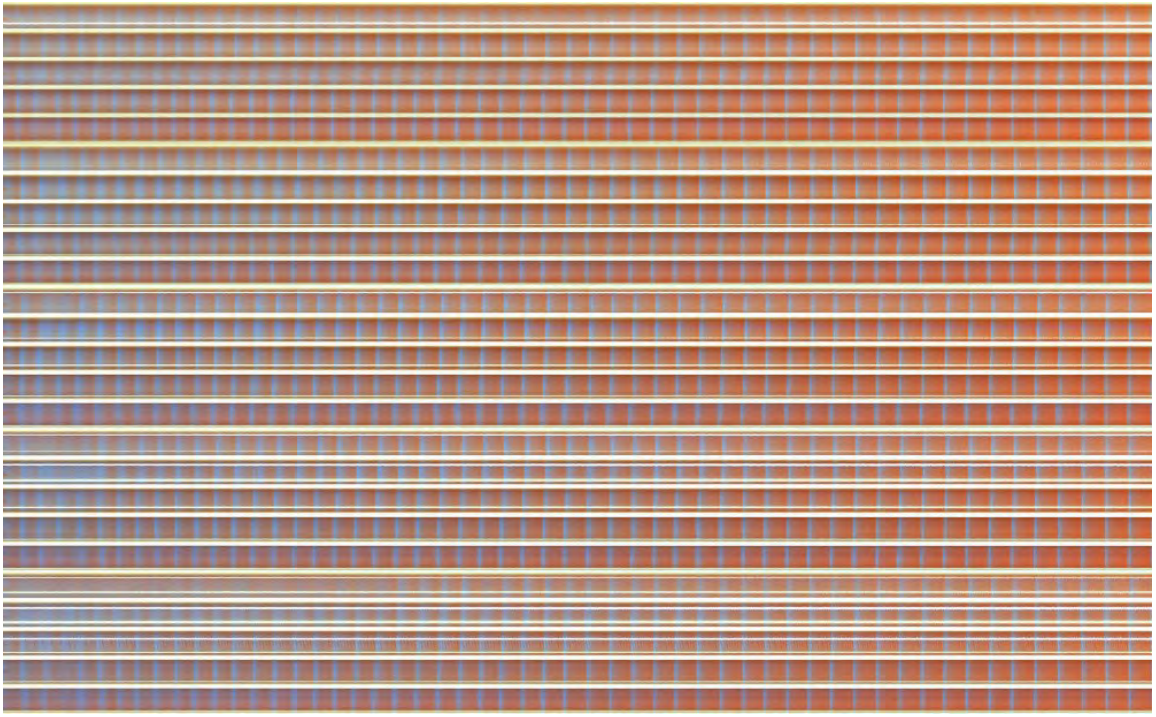

Figure S54: In this experiment all the stirrers were set to different random speed. From completely disabled to full speed.

Setting different parts of the grid at different defined speeds

Based on these results, it was decided to test how the system would behave if within the same arena a set of stirrers was stirred at a slow speed, and a set of stirrers was stirred at a faster one, see Figure S55. In order to do so, an experiment was designed where the first two columns rotated at the default speed (a PWM signal of 500), the third column was completely disabled, and the fourth and fifth column rotated at four times the default speed (a PWM signal of 2000).

In Figure S55, we focused on column 2, 3 and 4. Column 2 was set a default speed (500), column 3 was completely disabled, and column 4 was at four times default speed (2000). This experiment showed that the when using this sort of pattern, the system did not arrive to a global coherent pattern, and that the part rotating at 500, and the part rotating at 2000, generated BZ oscillations at different frequencies. What was very interesting, as can be seen on this figure, is that only when the two systems of oscillations were in phase, then and only then would the column 3, which was disabled, oscillate. In this figure, this phenomena is marked with arrows.

4.8 Programming a pattern sequence into the BZ medium

The next objective was to study if by flashing different patterns in a sequence we could modify the global oscillation generated by the BZ medium. This idea is supported by the fact that the BZ medium has memory, as shown before (Section 4.6). Therefore, the hypothesis is, if we have a pattern A that generates a global oscillation A', and we also have a pattern B that generates a global oscillation B'; if, for example, we flash first A, and then B, we can assume that the first global oscillation generated will be A', but once it switches to B, will it be B' or something different?

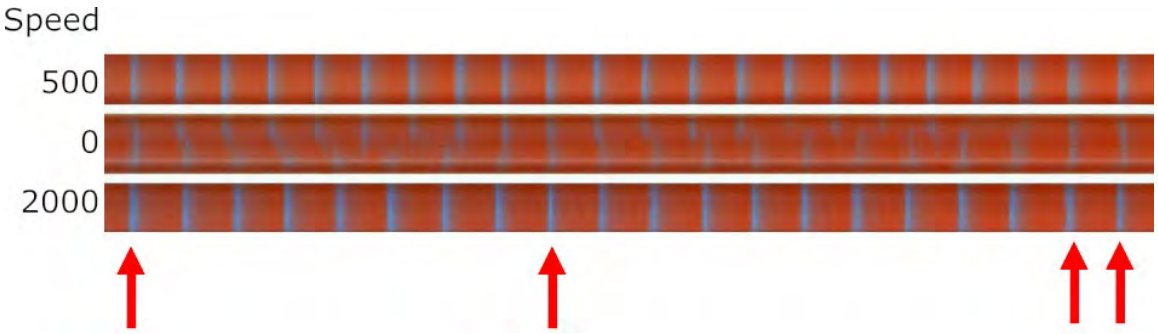

Figure S55: Column 2 rotated at the default speed (around 80rpm, which was generated with a 500 PWM signal). Column 3 was disabled. Column 4 rotated at four times the default speed (2000 PWM). Only when the two systems were in phase would then column 3 oscillated.

To test this hypothesis, we tested it using two different experimental pipelines, shown on Figure S56. In the first one, which is the top half sequence of this figure, initially we flashed a base pattern for 10 minutes, in our case, the one related to "0" (see Section 4.2). Then it followed by a period of

5 minutes were nothing was flashed. Then, there it was flashed a sequence of 3 patterns, each of them for 5 minutes. We tested for pattern 1, then pattern 2 and then pattern 3, and also for pattern 4, then pattern 5 and then pattern 6. The bottom half of this figure shows the other sequence of patterns we tested. In this case, patterns 0, 1, 2 and 3 looped in a 1 minute period (therefore, 30 iterations in total) where each of these patterns was flashed for 15 seconds.

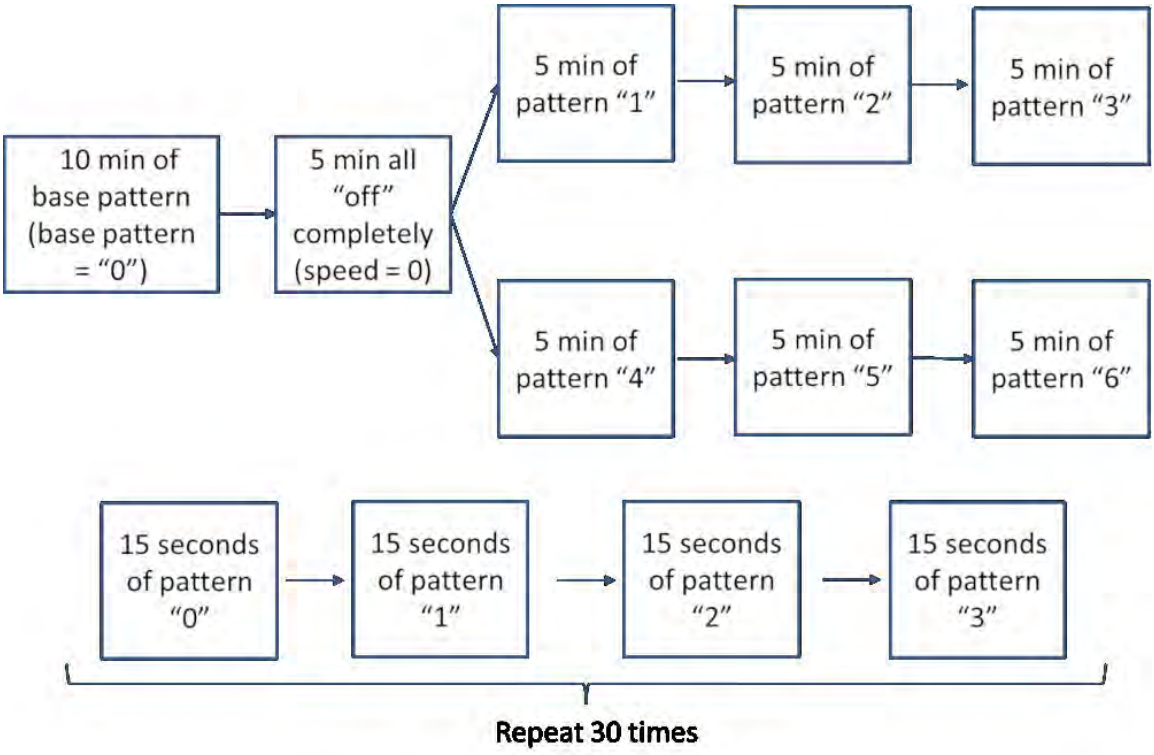

Figure S56: In order to test the programmability of the system, we tested two different experimental pipelines. In one of them, four different patterns were flashed in a sequence, each pattern only appearing once for 5 or 10 minutes, for a total of 30 minutes. In the other one, we had 4 pattern iterating continuously in 1 minute cycles.

The results of these experimental pipelines are shown on Figure S57. These figures contains a series of linear plots. In each of these plots, the lines represent the direction of the BZ global wave. For example, in the bottom left linear plot, with lines going in a diagonal from bottom left to top right, the global wave was moving in the direction suggested by these lines. In order to obtain these plots, for each frame of a experiment, we extracted the blue channel, and calculated its moment and the centre of mass. We then concatenated these centres of masses between plots, and the way the centre of mass varies between frames is what is represented in these linear plots.

In this figure, initially we show the waves described by the patterns 0, 1, 2 and 3 when they are the only ones flashed during 30 minutes. These plots contain red lines. Then we show the case in

which these four different patterns are flashed in a continuous loop, where each pattern is flashed for 15 seconds. These plots contain green lines. Finally, we show the case where initially a pattern 0 is flashed for 10 minutes, followed by 5 minutes of nothing, and then pattern 1, then 2 and then 3, five minutes each, in a sequence. These plots contain blue lines.

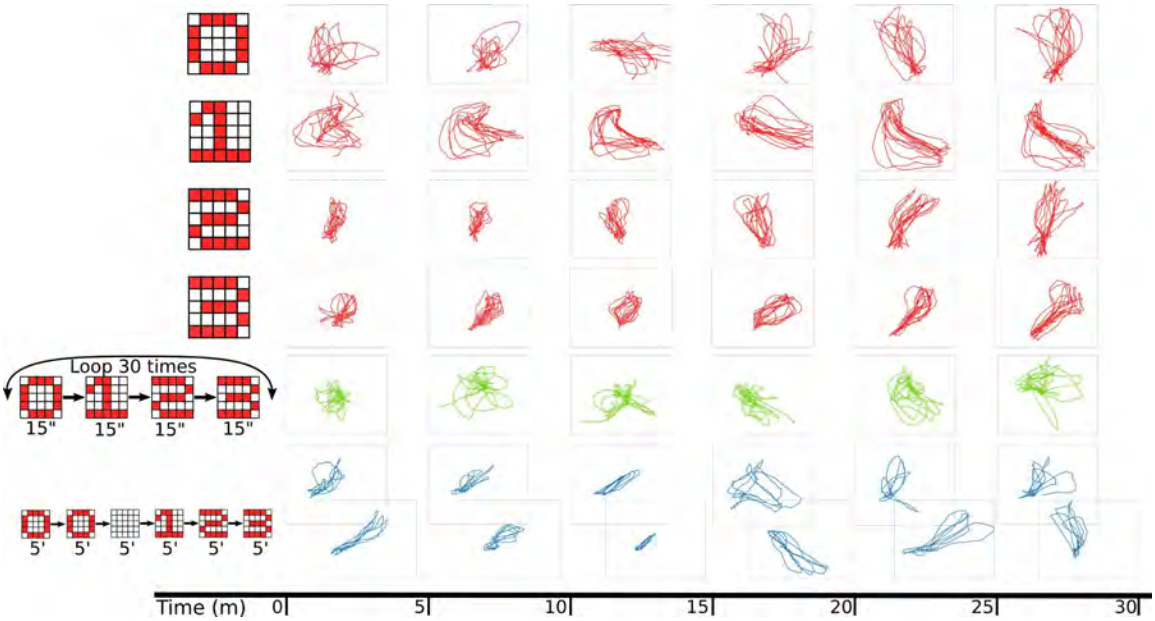

Figure S57: Plot lines in red: patterns flashed in isolation for 30 minutes. Plot lines in green: Patterns 0, 1, 2 and 3 looped in 1 minute cycles, where every pattern was flashed for 15 seconds. Plot lines in blue: experimental pipeline where 4 different patterns were flashed in a sequence, each pattern was only flashed once for 5 or 10 minutes. While previously (red or green line plots) each plot represents 5 minutes of experiment, in this case (blue line plots) each plot represents 2.5 minutes of experiments.

In the case of the continuous loop pattern, it seems that the system never arrived to a coherent global wave. In the case of the sequence of the four different patterns, it seems that it arrived to a global wave for every pattern, and each of these global waves were different. In particular, if we compare for example the wave described by pattern 1, 2 or 3 when they are flashed in isolation, or the wave described when they were flashed in a sequence, there it can be seen that the global waves were different. This might mean that we were able of “programming” the system by flashing a sequence of patterns, but we were never able of proving if this was actually being caused by our experimental pipeline, or if it was cause by the stochasticity of the system.

4.9 Experimenting with water medium instead of BZ medium

In order to test if the BZ medium was necessary in the system in order to perform the described computations, we executed a series of experiments where instead of BZ medium we used water. As it is shown in the main manuscript, and also described in Section 5, the platform described using BZ medium was able of encoding input patterns, such as the ones shown in Section 4.2, and then decoding them with the aid of machine learning.

In these experiments with water, the objective was to see if the water medium was also able of encoding input patterns, that later on were decoded with the aid of machine learning. In this case, the patterns for “0” and “4” were flashed into the system by stirring those motors with the defined pattern. Then a 30 minute video was recorded of the arena (see Figure S58 A). For each of the 25 cells, we extracted its RGB value through time, and transformed it into the HSL colour scheme. Figure S58 B shows the brightness level of the 25 cells during the experiment. The scale goes from 0 to 255, but here we are focusing on values between 150 and 185. In this Figure, there it can be seen that the brightness variation through the experiment is minimal because the system was not oscillating. With this data, we input it to our machine learning model, in order to decode it, but our test performance was around 50%, therefore the decoding phase was completely random. These results then show that a chemical oscillating system is necessary in order to compute.

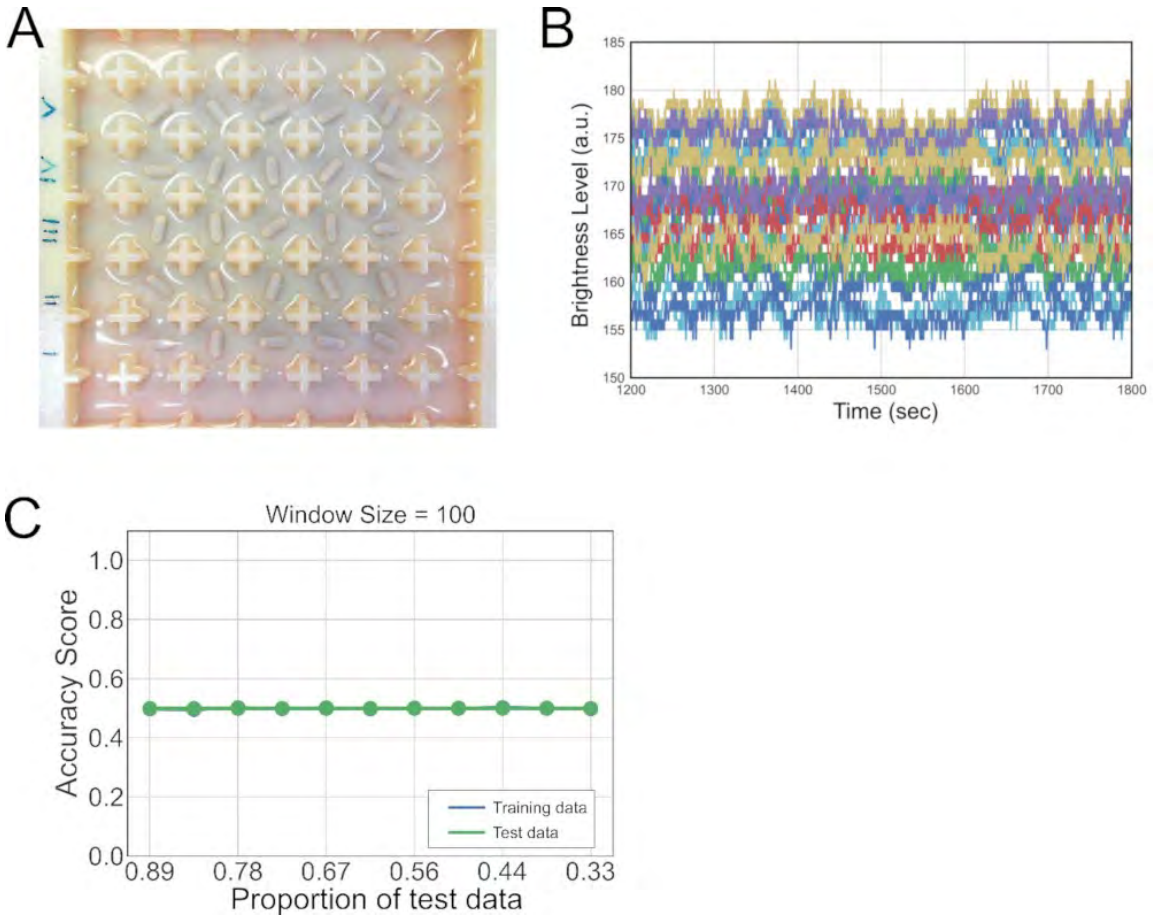

Figure S58: Water experiment. (A) A raw camera image of the experiment. Pure water was added in the grid instead of BZ reaction medium. (B) Example time-series data from the experiment. (C) Results of prediction for two input patterns (“0” and “4” as shown in Section 4.2). Note that the training data and test data were overlapped each other, thus only the test data (green line) was visible.

4.10 Emulation of AND and OR gates

Logic gates form the basis of modern digital computers, and from a theoretical perspective they are the unit of computation because they are the fundamental discrete logic element. By creating circuits of interconnected logic gates, computers can calculate more complex operations, such as adders, multiplexers, flips-flops, and eventually processing and control units. Therefore, the first objective of our physiochemical computer was to emulate the behaviours of the simplest binary logic gates. In order to build linearly separable binary logic gates, such as the “AND” and “OR” gates, we focused on the fact that BZ excitation waves generated at an activated cell easily propagate to direct neighbours (i.e. distance = 1), but very rarely propagate to cells further away (i.e. distance ¿ 1). By exploiting this feature, we designed 2-bit logic gates using the distance between inputs in order to implement “AND” and “OR” gates (Figure S59). Depending on the

distance between the inputs and the position of the output, our system can emulate “AND” and “OR” logic gates. When the distance between the two inputs (denoted as X and Y, respectively) is set to 3 (column 1 as X and 5 as Y) and the output is set as the middle column between them (column 3), our platform behaves like an “AND” gate, because oscillations in the output column are only observed when both inputs are activated. On the other hand, when the distance between the inputs is set to 2 (column 1 and X and 3 as Y) and column 2 is defined as output, then the system behaves like an “OR” gate, because whenever any of the inputs is enabled, the oscillations propagate to the output column.

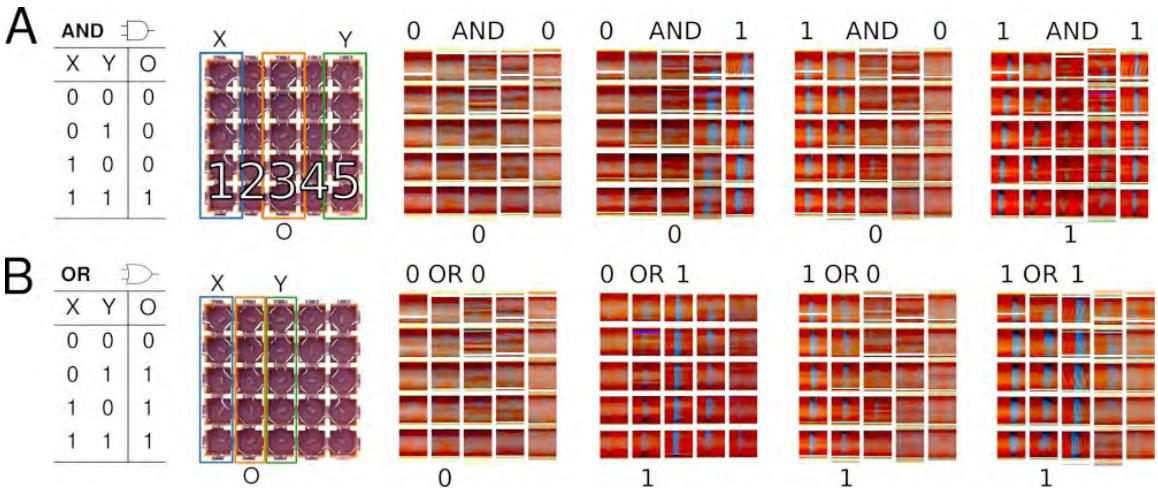

Figure S59: Designing “AND” and “OR” logic gates using the distance between the BZ input oscillations. The leftmost part of this section describes the truth tables for both the “AND” and “OR” gates. “X” and “Y” are the input bits, while “O” is the output bit. Next to the truth tables, there it can be seen how using the distance between inputs the platform can emulate said logic gates. If X and Y are separated by 4 cells, then it behaves like an “and” gate (X=column 1, Y=5, O=3), while if they are separated by 2 cells, then it behaves like an “or” gate (X=1, Y=3, O=2). The following eight pictures are different snapshots of our platform where it can be seen how the platform actually emulates these logic gates. The base colour (no oscillation) is orange, and a blue line represents an oscillation. The top row represents the “AND” gate, and there it can be seen that the output column only oscillates when both inputs oscillate. The bottom row represents the “OR” gate, and in this case the output column oscillates whenever any of the inputs oscillate.

AND gate data

Figure S60 shows the case where both inputs were set to 0. In this case, no stirrers were activated, therefore, no oscillations appeared. Three repetitions were done of this case, but here we only show one, because all of them looked the same. Figures S61 to S63 show the 0-1 case for the

AND gate. In this case, only the left-most column was enabled, while all the other motors were disabled. Here it can be seen that the left-most column oscillates, and also the nearest column to it (column 4) but the oscillations are not able to arrive to the middle column, which in the case of the AND gate was considered as the output. Therefore, this was a 0, which is the expected output for the 0-1 case in an AND gate. Figures S64 to S66 show the 1-0 case. Figures S67 to S69 show the 1-1 case.

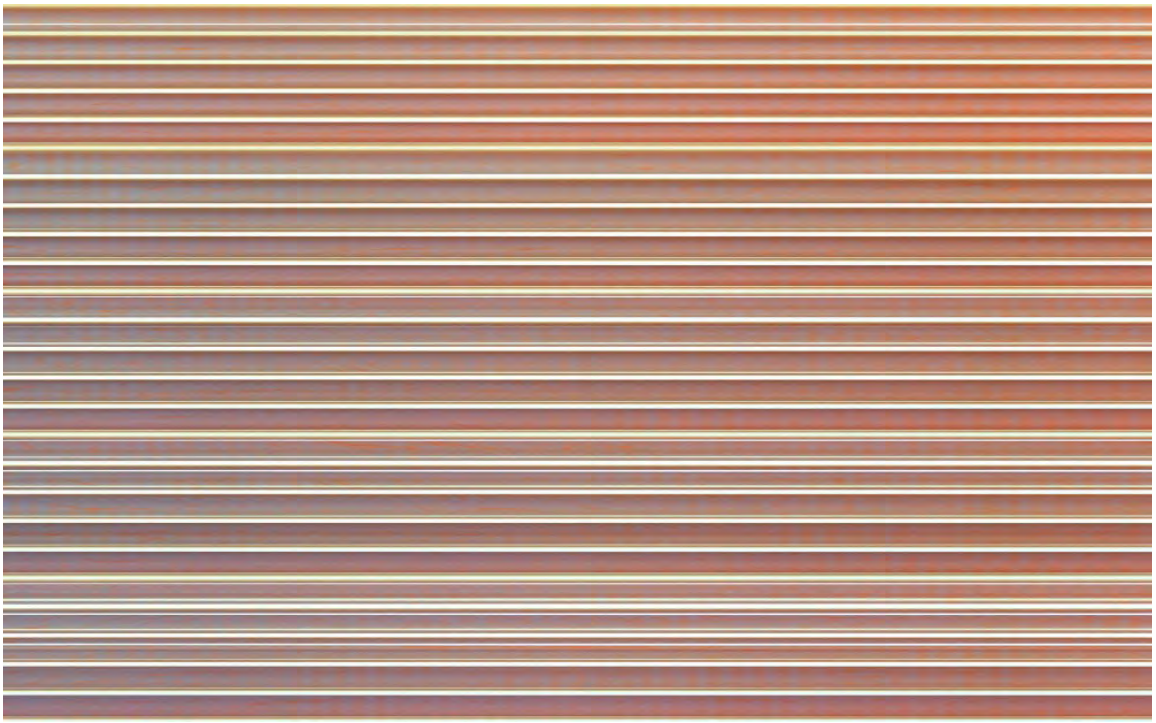

Figure S60: BZ experiments were all the stirrers were off. This is the case 0-0 for the AND and OR logic gates.

OR gate data

In the case of the OR gate, the 0-0 case and the 1-0 are the same as before. 0-0 is again everything disabled, and this was shown on Figure 60. 1-0 is again only the left-most column enabled, while everything is disabled. This was shown on Figures S61 to S63. Figures 70 to 72 show the 0-1 case for the OR gate. Figures S73 to S75 show the 1-1 case for the OR gate.

4.11 Analysis procedure for XOR gate emulation

To implement a non-linearly separable logic gate, such as “XOR”, we exploited the fact that when all of the stirrers were activated, globally synchronized wave patterns emerged from the system. In this case, the ON/OFF binary state of inputs employs two different stirrer speeds (ON for the full

speed and OFF for the slowest rotation speed possible), instead of fully activating or disabling stirrers as we did before. The global wave patterns were consistent, i.e. similar patterns were observed between experiments when the stirrer input patterns were the same. However, when sufficiently different stirrer input patterns were given, the corresponding global wave patterns were different. We speculate that the emergence of globally synchronized patterns comes from two properties of the BZ reaction: (1) Sustained oscillation: once activated, a BZ reaction tends to sustain its oscillation even after the stirrer is off. Thus, each cell can be considered as an oscillator. (2) Signal

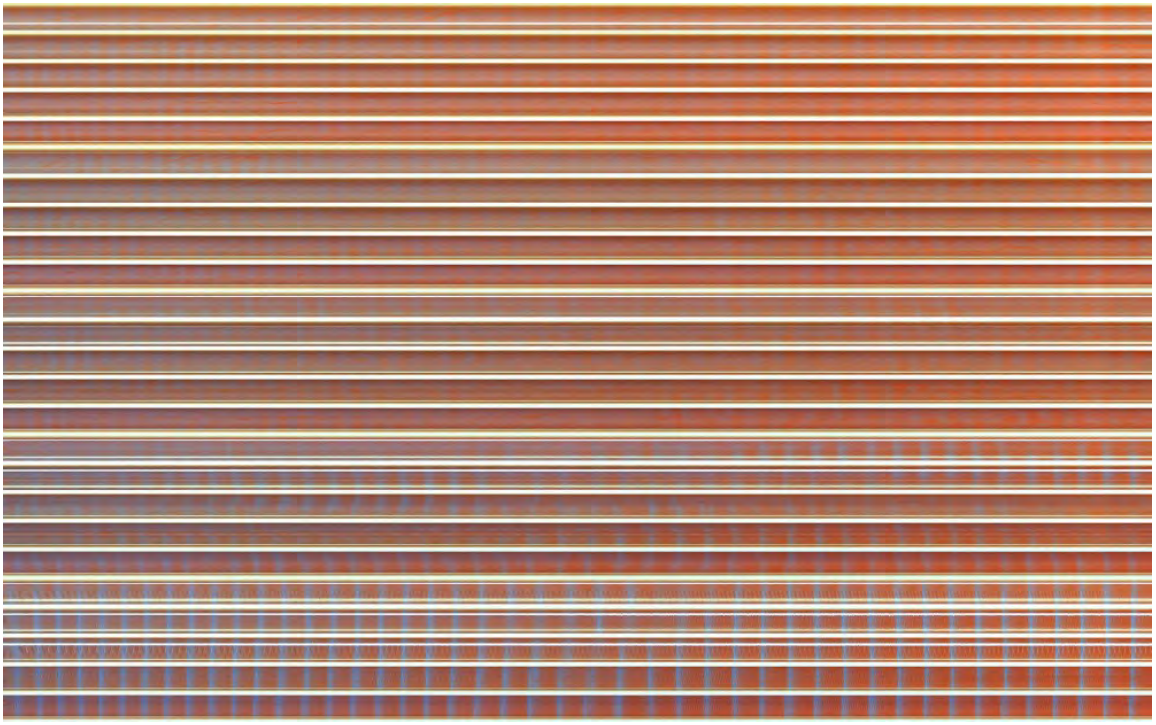

Figure S61: BZ experiments were only the left-most column was on, while all the other motors were off. This is the case 0-1 for the AND gate. First repetition.

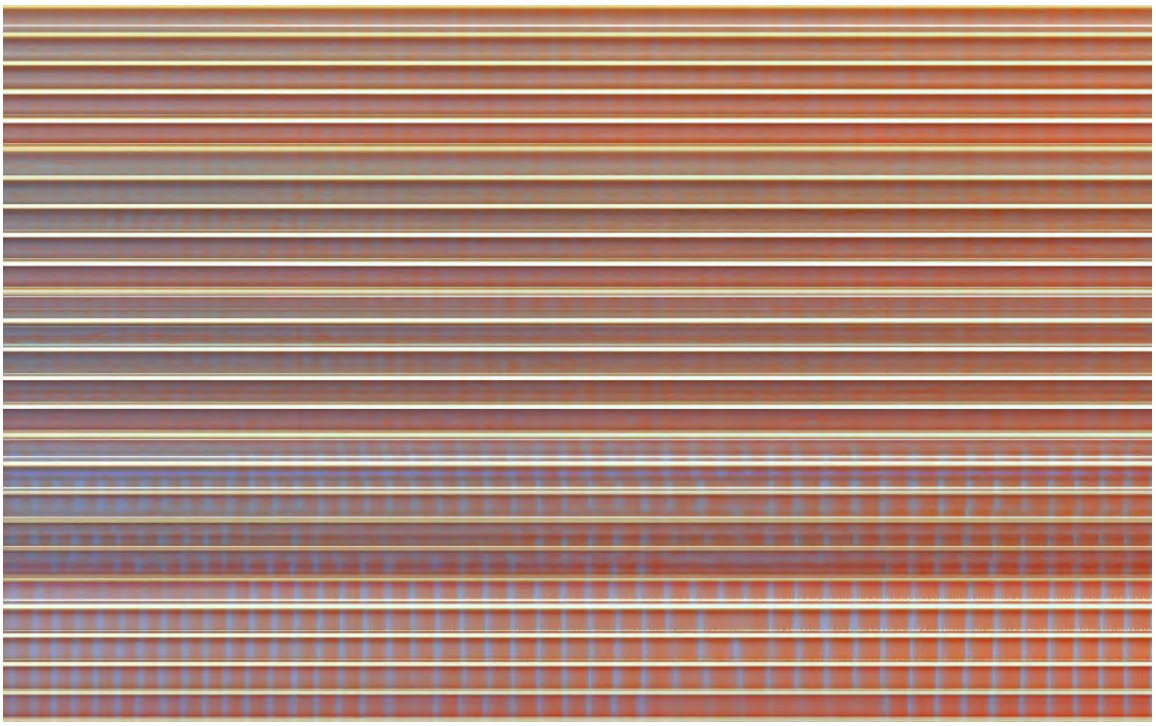

Figure S62: BZ experiments were only the left-most column was on, while all the other motors were off. This is the case 0-1 for the AND gate. Second repetition.

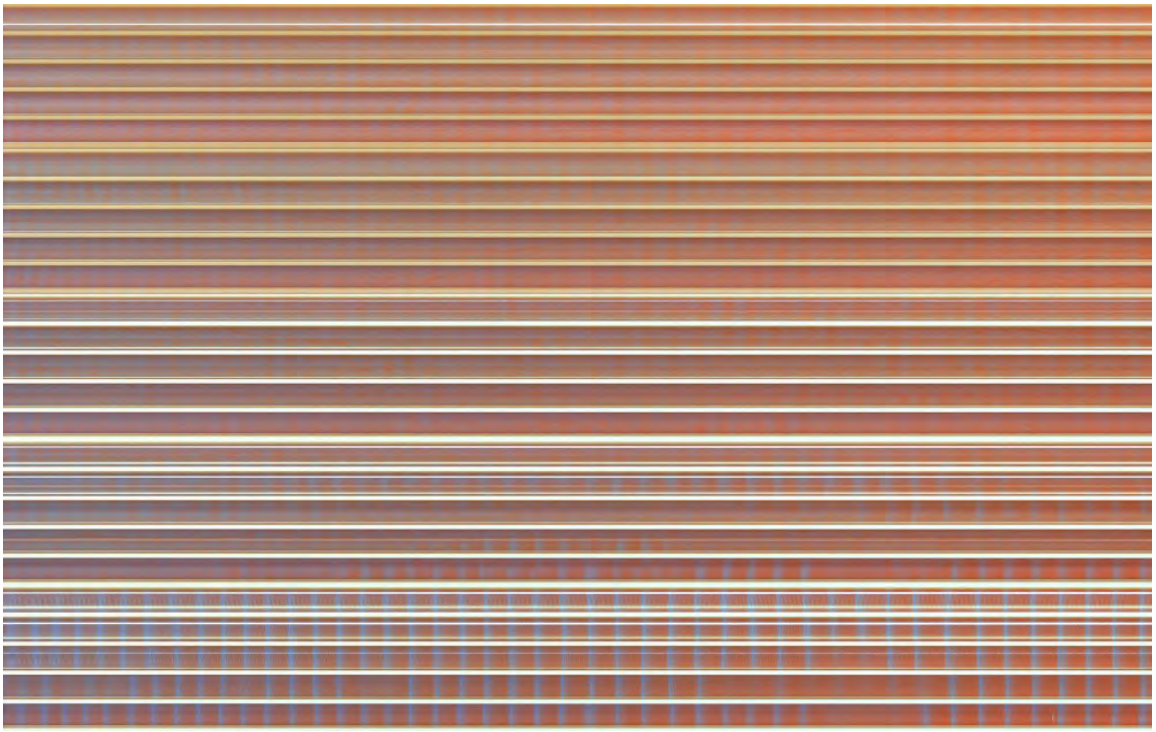

Figure S63: BZ experiments were only the left-most column was on, while all the other motors were off. This is the case 0-1 for the AND gate. Third repetition.

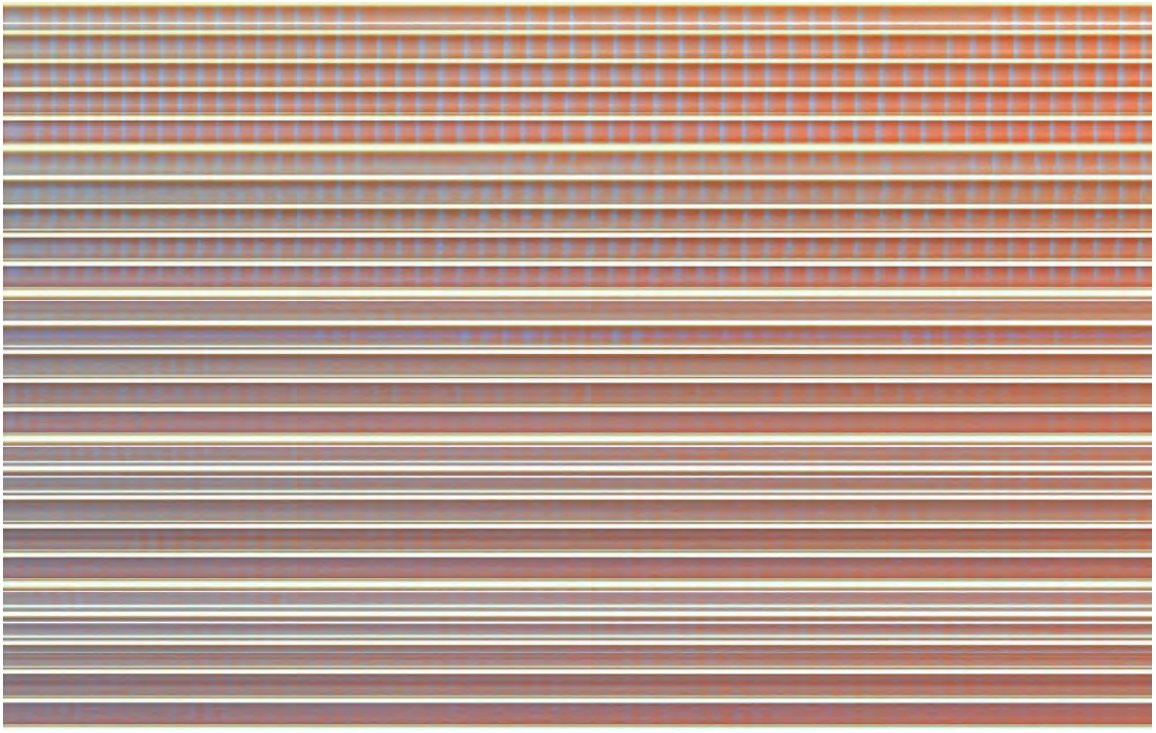

Figure S64: BZ experiments were only the right-most column was on, while all the other motors were off. This is the case 1-0 for the AND gate. First repetition.

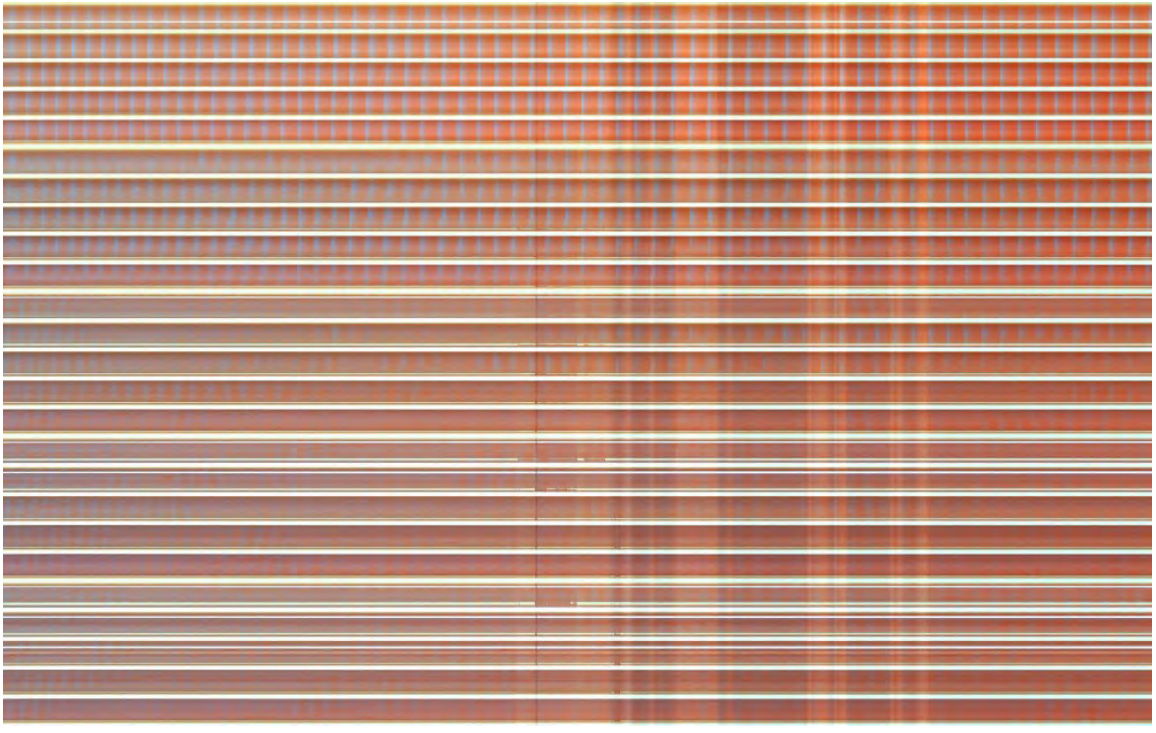

Figure S65: BZ experiments were only the right-most column was on, while all the other motors were off. This is the case 1-0 for the AND gate. Second repetition.

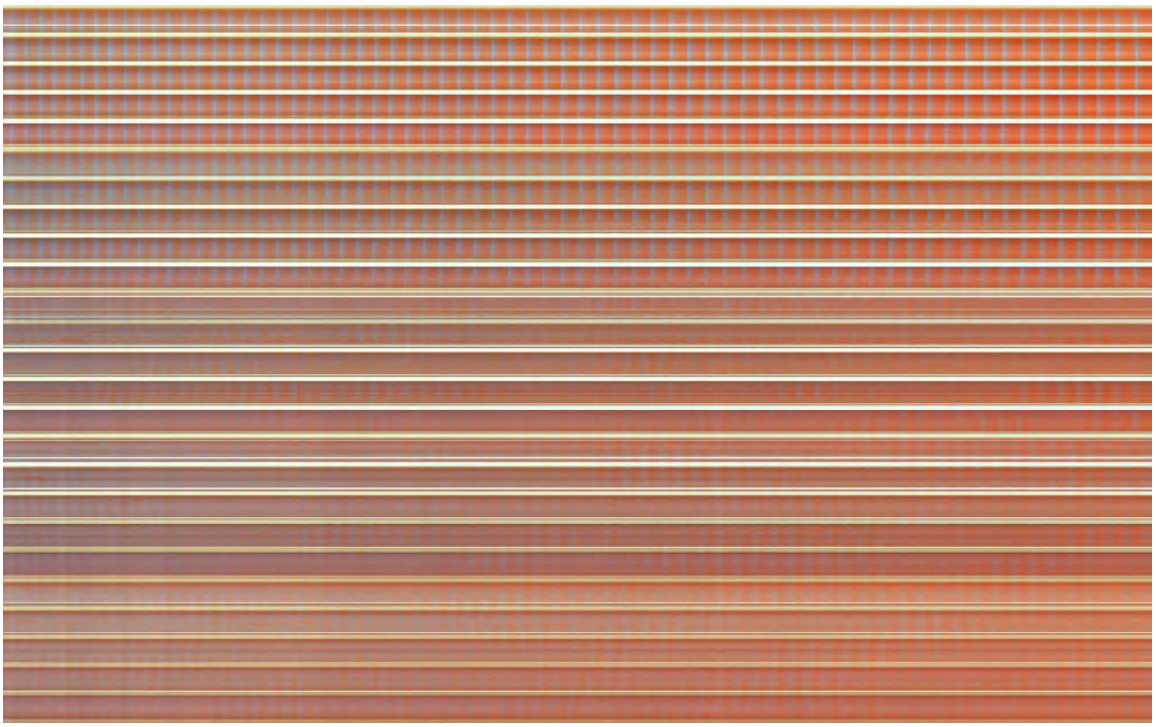

Figure S66: BZ experiments were only the right-most column was on, while all the other motors were off. This is the case 1-0 for the AND gate. Third repetition.

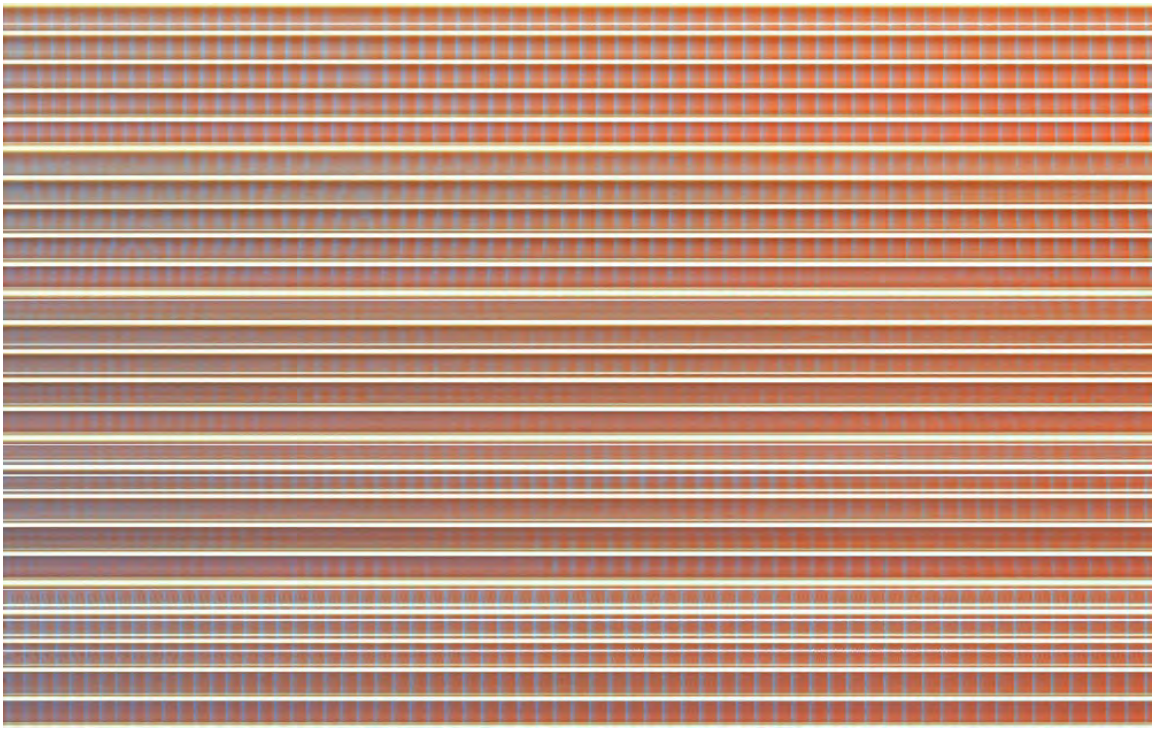

Figure S67: BZ experiments were only the left-most and right-most column were on, while all the other motors were off. This is the case 1-1 for the AND gate. First repetition.

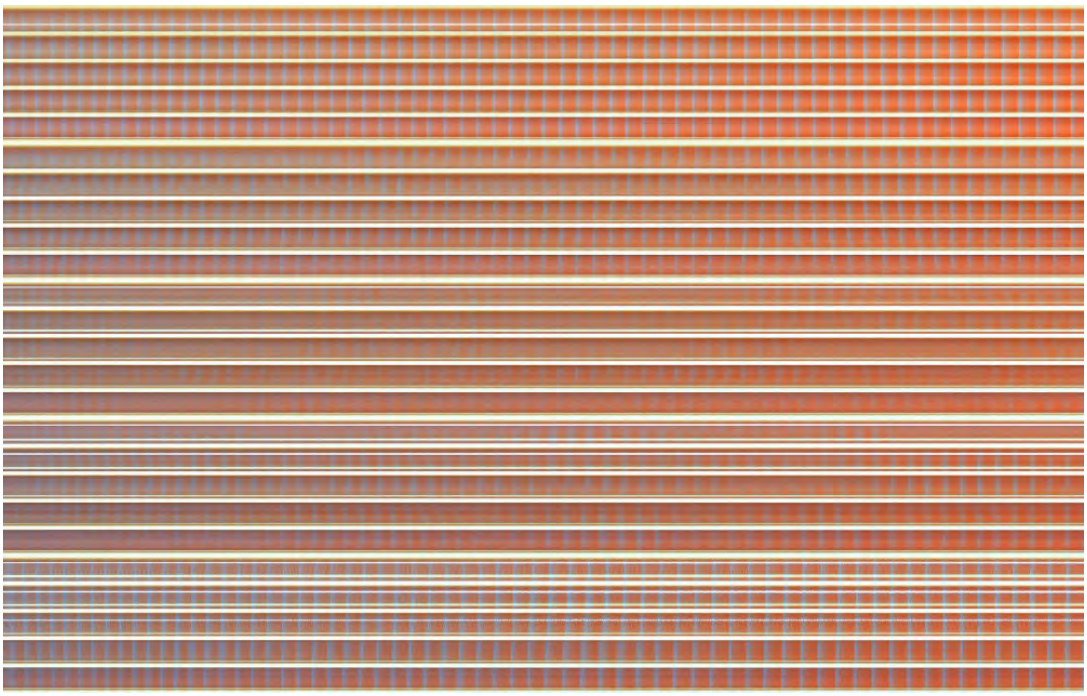

Figure S68: BZ experiments were only the left-most and right-most column were on, while all the other motors were off. This is the case 1-1 for the AND gate. Second repetition.

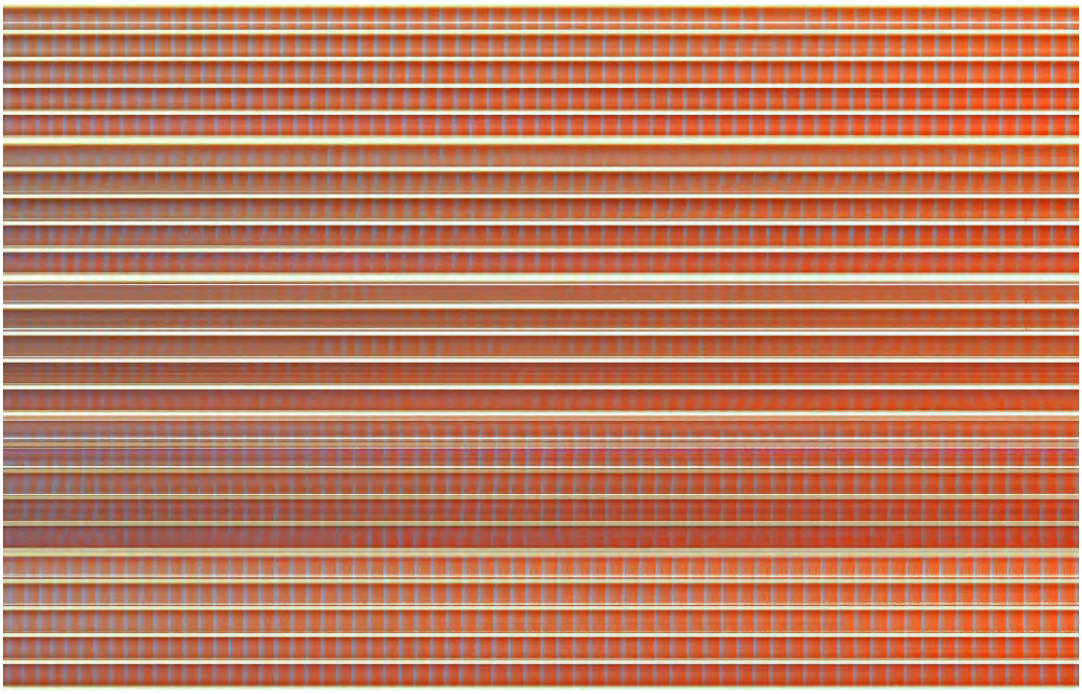

Figure S69: BZ experiments were only the left-most and right-most column were on, while all the other motors were off. This is the case 1-1 for the AND gate. Third repetition.

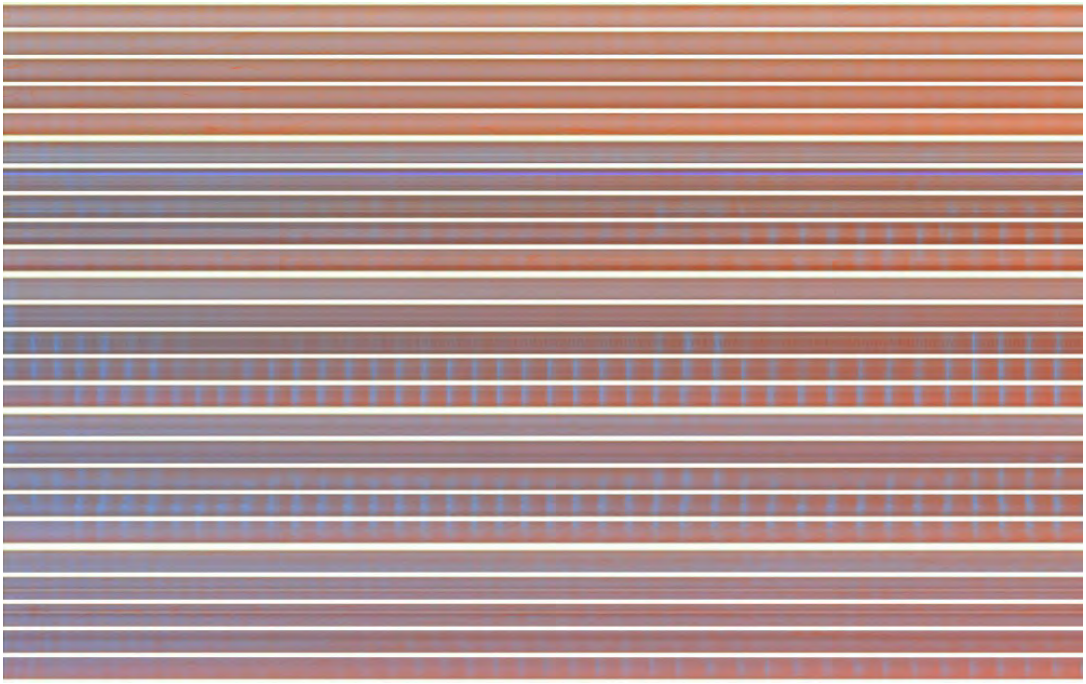

Figure S70: BZ experiments were only the center column was on, while all the other motors were off. This is the case 0-1 for the OR gate. First repetition.

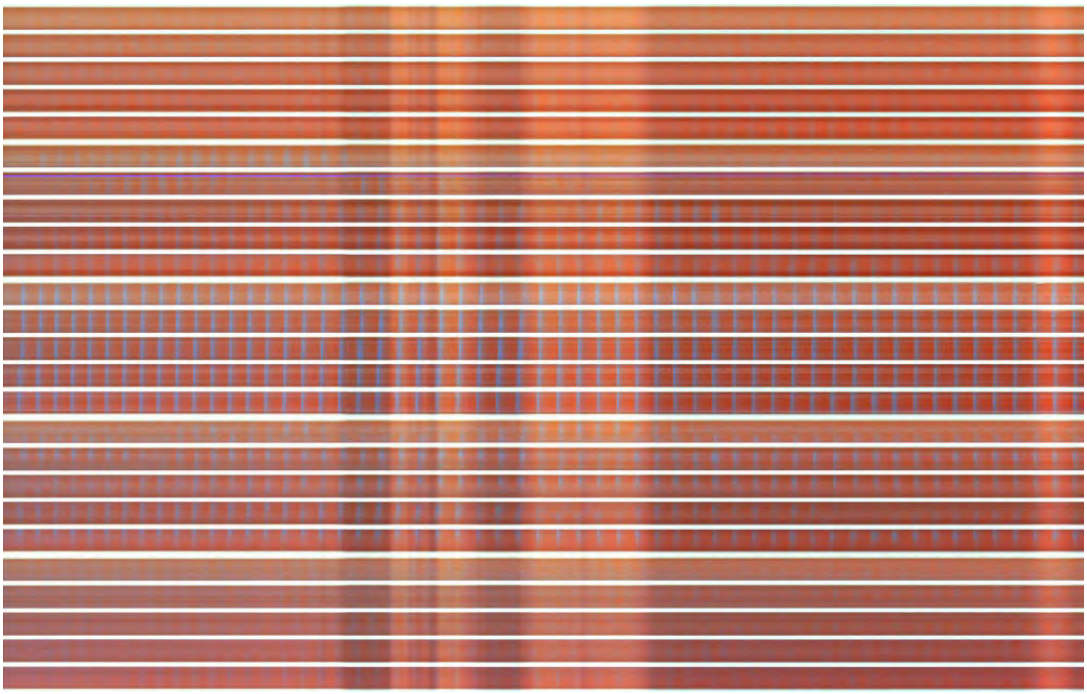

Figure S71: BZ experiments were only the center column was on, while all the other motors were off. This is the case 0-1 for the OR gate. Second repetition.

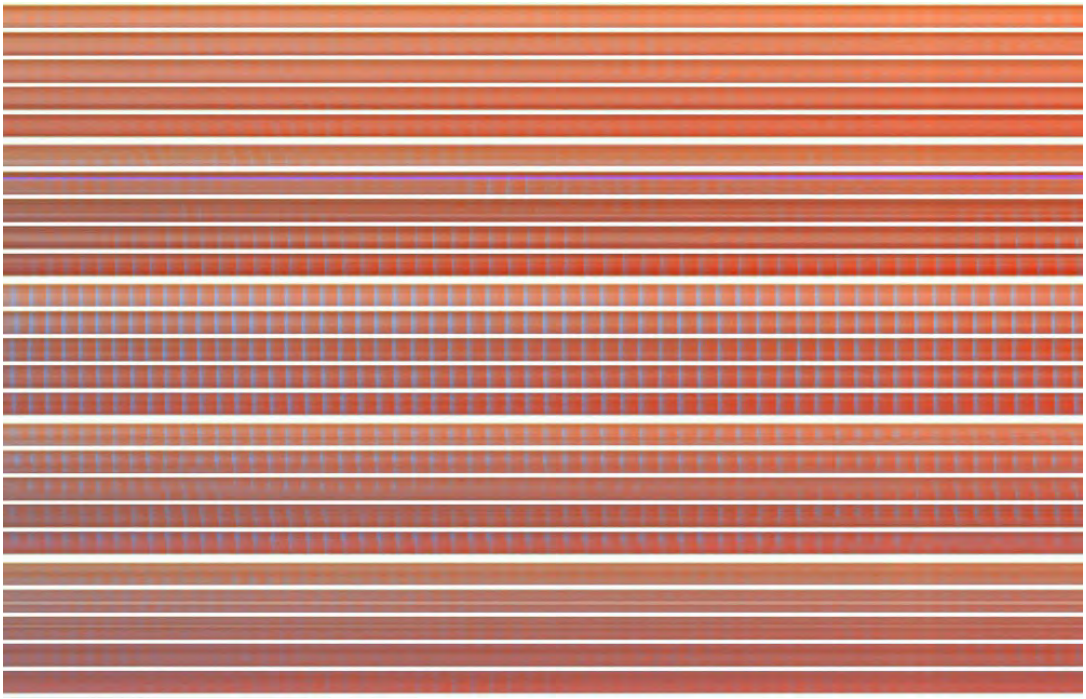

Figure S72: BZ experiments were only the center column was on, while all the other motors were off. This is the case 0-1 for the OR gate. Third repetition.

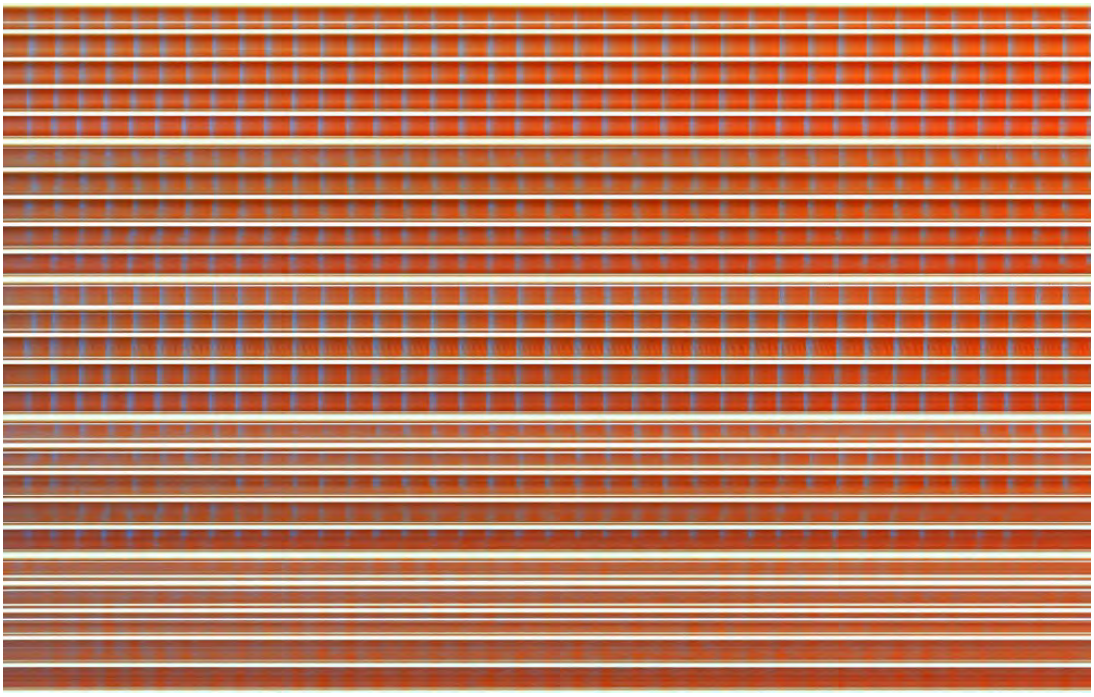

Figure S73: BZ experiments were only the center column was on, while all the other motors were off. This is the case 1-1 for the OR gate. First repetition.

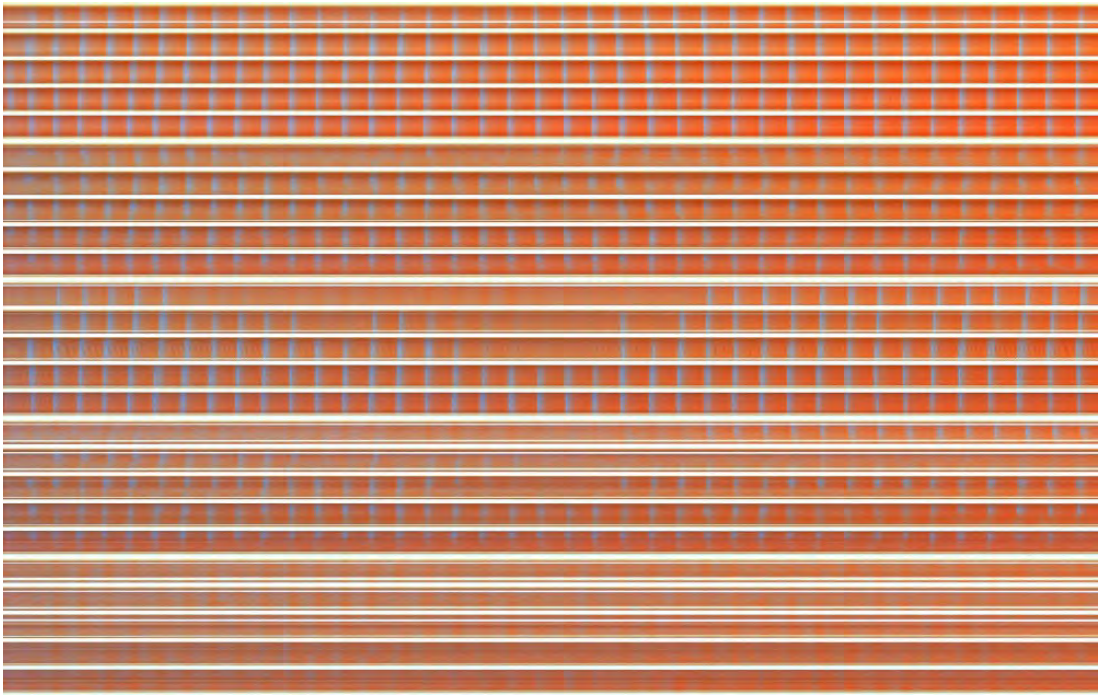

Figure S74: BZ experiments were only the center column was on, while all the other motors were off. This is the case 1-1 for the OR gate. Second repetition.

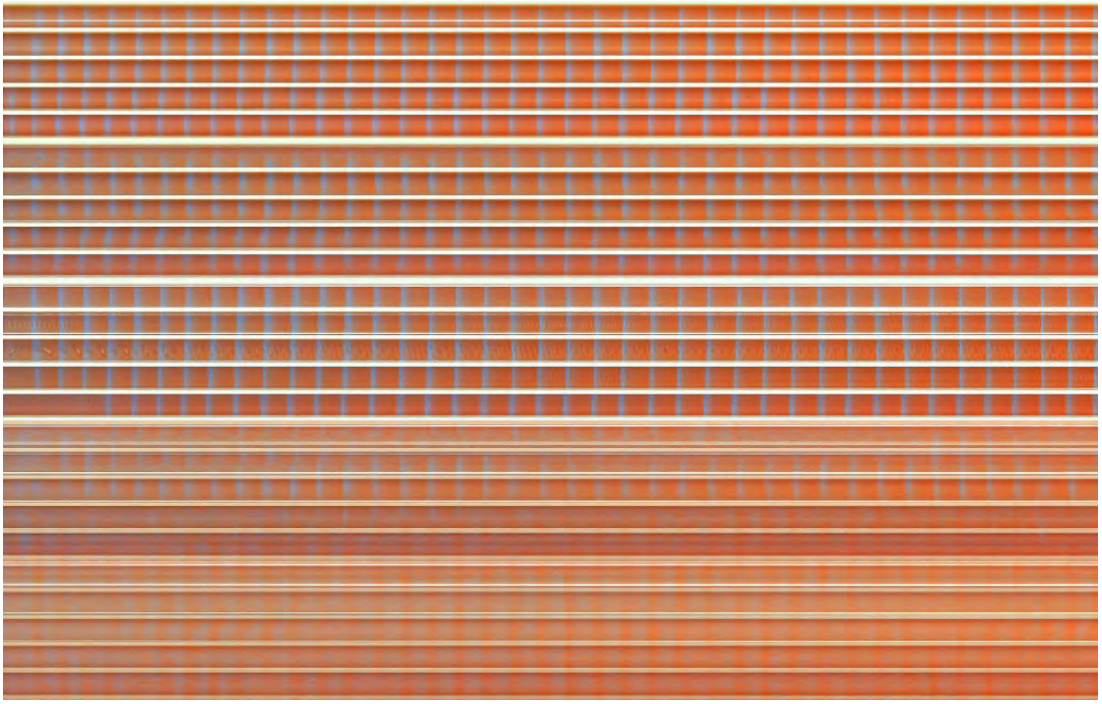

Figure S75: BZ experiments were only the center column was on, while all the other motors were off. This is the case 1-1 for the OR gate. Third repetition.

convolution: the BZ excitation waves generated at a cell propagate to neighbouring cells where another excitation waves are generated. The waves collide and convolve to form a synchronized oscillation. Thus, the whole BZ grid system can be viewed as a coupled oscillator system, or more in general, as a chemical dynamical system that consistently converts stirrer input patterns into patterns of excitation waves.

Figure S76 shows how the XOR was implemented by exploiting the BZ oscillations synchronization between cells. In the BZ grid, the leftmost and rightmost five cells were considered as inputs, X and Y, respectively. While the slow stirrer motion was fast enough to generate excitation waves in a cell and generate a globally-coherent wave pattern, the difference in rotation speed creates a specific flow pattern of BZ medium, which generated unique wave propagation patterns. If a column of five adjacent stirrers are rotated faster (the ON state), the stirrer motion generated a unidirectionally propagating wave pattern. This wave pattern was found to be symmetric, thus both (0, 1) and (1, 0) inputs give mirrored wave patterns. In contrast, the (0, 0) and (1, 1) inputs resulted in different yet reproducible wave patterns. To quantify these different wave patterns, we calculated the phase differences between the central cell and the other cells by cross correlation analysis (see Figure S76). The average phase difference between cells shows how the input pattern generated different phase difference patterns. In particular, (0, 1) and (1, 0) patterns show a bipolar pattern where one side (“0” or non-activated side) shows positively shifted phase (indicated in red) while the other side (“1” or activated side) shows negatively shifted phase because it was observed that excitation waves tend to propagate towards the cells with activated stirrers, thus the phase is delayed. On the other hand, the other cases, (0, 0) and (1, 1), showed different non-bipolar patterns. Therefore, the XOR gate can be implemented by defining the bipolar wave pattern as output “1” and the other pattern as “0”.

In order to emulate an XOR gate, the binarized data was used (see Figure S25). This data was read as 0’s and 1’s, and used to build a “Pandas” data-frame. The “correlate” function from Numpy was then used with this data in order to find the autocorrelation for all the wells. The results can be seen on Figure S77, S78 and S79. In this last image, there it can be seen how each cell oscillates at a different time. These oscillations were then plotted in a 5 by 5 matrix, similar to our platform, where there it can be seen the phase difference between cell oscillations. See Figure S80.

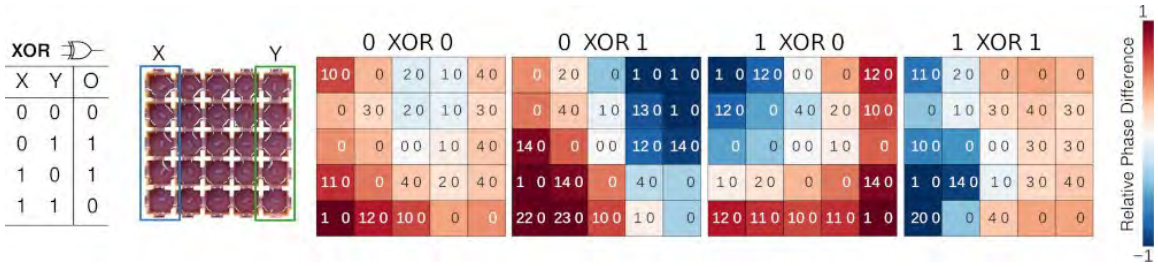

Figure S76: Designing “XOR” logic gates using the phase difference between localized oscillations. The leftmost and rightmost five cells are considered as inputs (X, Y) The heat maps show the

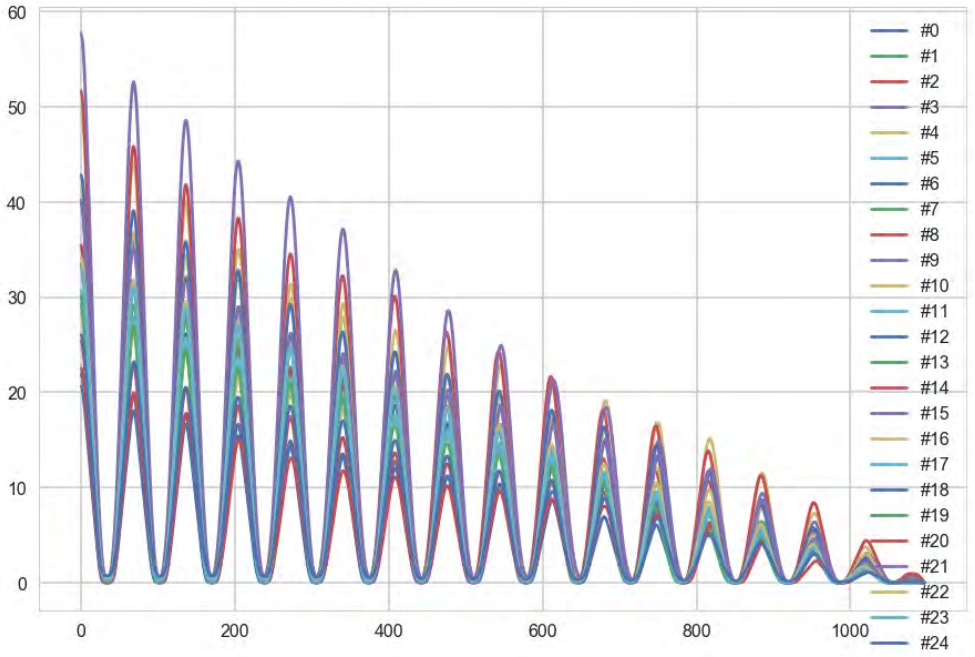

Figure S77: Using numpy correlation to calculate the correlation between wells.

5 Data analysis

5.1 Preparing the data in CSV format

In order to analyse the data from the videos, they were transformed into CSV (comma separate values) files. Unless stated otherwise, all the videos used in this section were 30 minutes long. The first step done was to speed them up by a factor of 15, meaning that the video would be instead 2 minutes long. This produced on average, at 30 FPS, 3600 frames. In the CSV files, columns represent time, while rows present location. Because our system has 25 cells, each file will have 25 rows and 3600 frames. In the case of binarised videos, like the ones shown on Figure S25,

each value in the CSV will be either 0 or 1. Zero if the cell is identified as red, and blue if the cell is identified as blue. In the case on non-binarised videos, like the one shown on Figure S23, each value in the CSV file will be the average blue channel value from a given cell. For example, in the very first value in a given CSV file will always be the average blue channel value of the first cell (top left cell) in the first frame. This will be a number between 0 and 255.

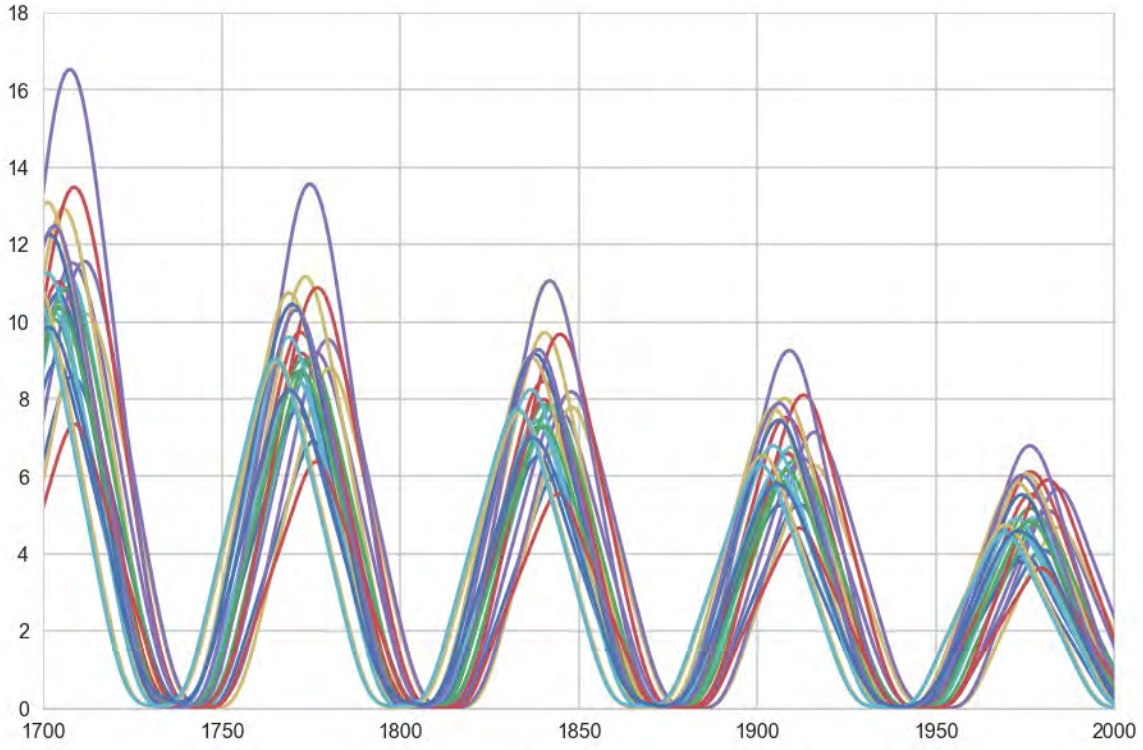

Figure S78: Focusing on Figure 77.

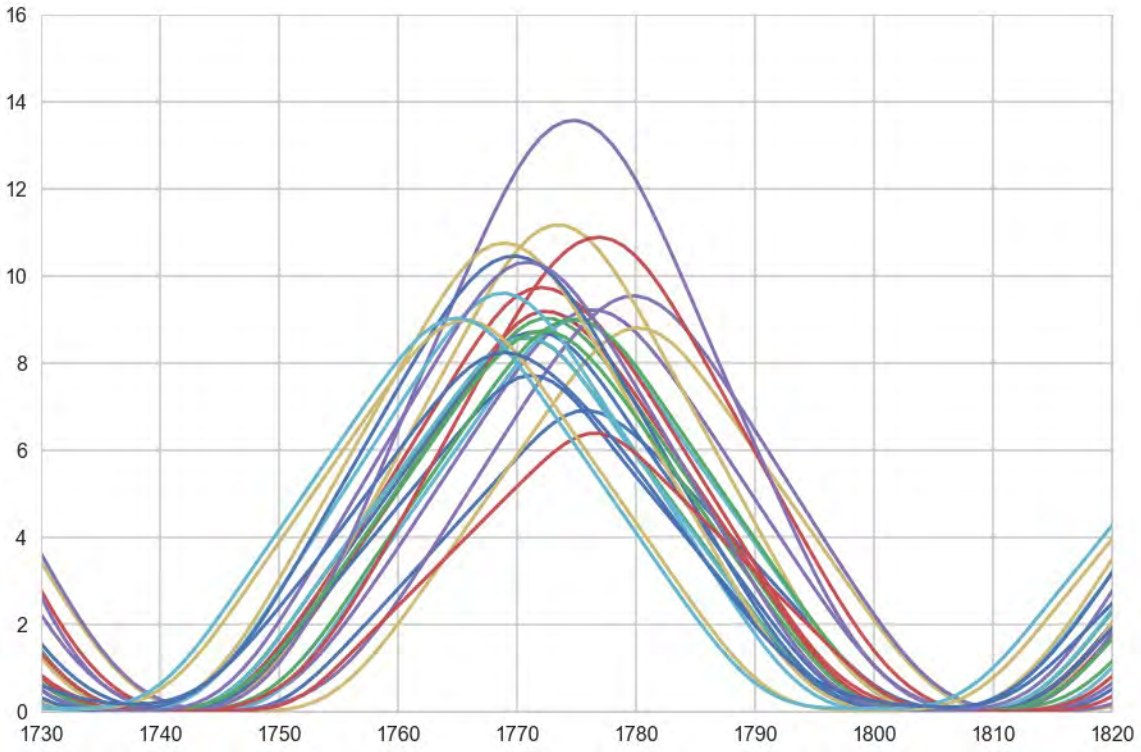

Figure S79: Focusing on Figure 78.

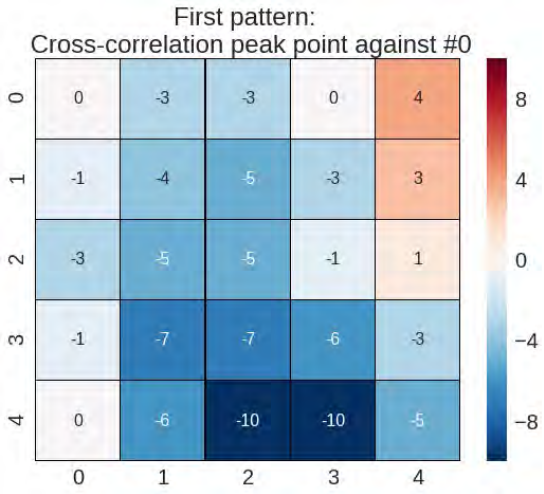

Figure S80: Show the phase differences from Figure S79. In this case, the base phase is the cell 0-0, and all the other cells are calculated against this one. When the number is negative, it means that cell oscillates before, while when the number is positive, it means the cell oscillates later. The number represents the difference in the number of frames between cell oscillations.

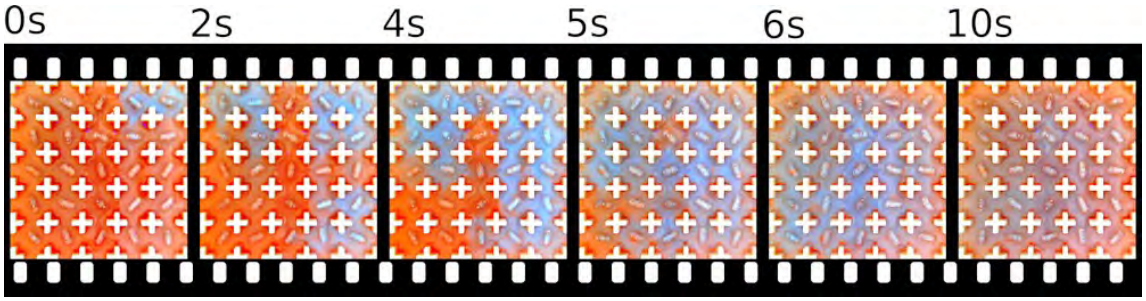

Figure S81: Different snapshots of the BZ wave oscillations for the case of XOR 1-0. Here it can be seen how the wave starts on the left and moves to the right.

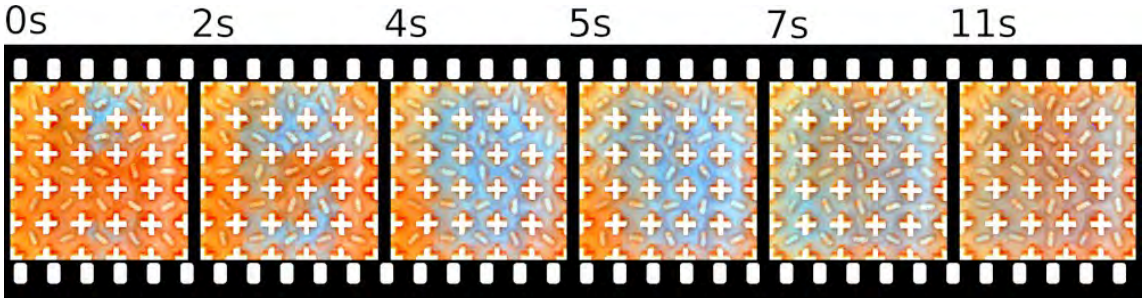

Figure S82: Different snapshots of the BZ wave oscillations for the case of XOR 1-1. Here it can be seen how the wave starts in the center and moves to both sides.

Source Code 7: MLP reservoir computer code

```
    # construct model
    model = Sequential() # input layer
    model.add(Dense(200, input_dim=25*wsize)) # hidden layer
    model.add(Activation('relu')) # activation func for hidden layer
    n_category = len(set(file_dict.values())) # number of categories at the output
    model.add(Dense(n_category, activation='softmax')) # output layer.

    # compile model
    model.compile('rmsprop', 'categorical_crossentropy', metrics=['accuracy'])
    model.fit(X_train, y_train, epochs=50, validation_split=0.001, verbose=False);

    # prediction
    y_train_pred = np.argmax(model.predict(X_train), axis=1)
    y_test_pred = np.argmax(model.predict(X_test), axis=1)
```

5.2 Machine learning for chemical reservoir computing system

The input patterns used are the ones showed on Section 4.2. After the binary CSV file was generated, it was input into a machine learning output layer of the chemical reservoir computing system. For the output layer, a multi-layered perceptron (MLP) was used. Although this is not a typical implementation for reservoir computing, where a single-layer network with no hidden layer is used, MLP was also used in several cases of reservoir computing systems to increase the computational capability for pattern recognition.[1] We used a MLP with only one hidden layer. Typically, 2500 input nodes and 200 hidden layer nodes. The size of the final layer was changed depending on the number of patterns to be classified. For activation function, rectified linear unit (ReLU) and softmax functions were used for the hidden and final layers, respectively. RMSprop was used for gradient descent optimization algorithm with categorical cross-entropy as cost function. Accuracy of predictions were measured by “accuracy score” function from “scikit-learn” library, defined as:

$$accuracy(\hat{y}, y) = \frac{1}{N} \sum_{N-1}^{i=0} 1(\hat{y}_i = y_i) \tag{1}$$

Where $\hat{y}_i$ and y_i are the predicted and true values of i-th sample, respectively. Computation was performed using a custom code written in Python (version 3.6 from Anaconda 4.3.0). Keras with TensorFlow backend was used to perform computation. A graphical processing unit, GTX1060 with 6GB memory, was used to speed up the computation. Source Code 7 shows how the model was built, compiled, and how the test and train predictions were obtained. Figures S83 and S84 show the confusion matrix of the test and training data. Figures S85 and S86 show the relation between the accuracy score and the size of the test data, and the size of the window used.

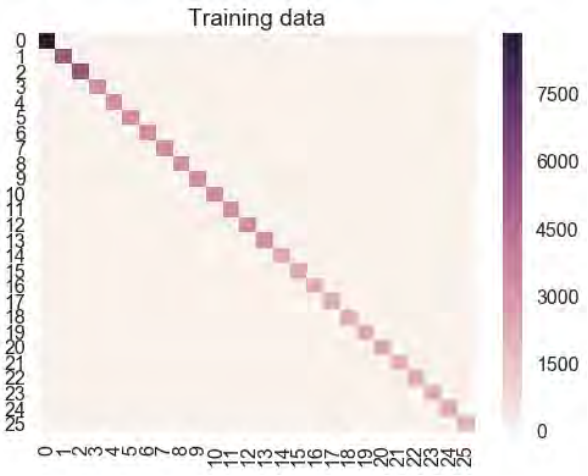

Figure S83: Confusion matrix for the training data used the model described in Source Code 7.

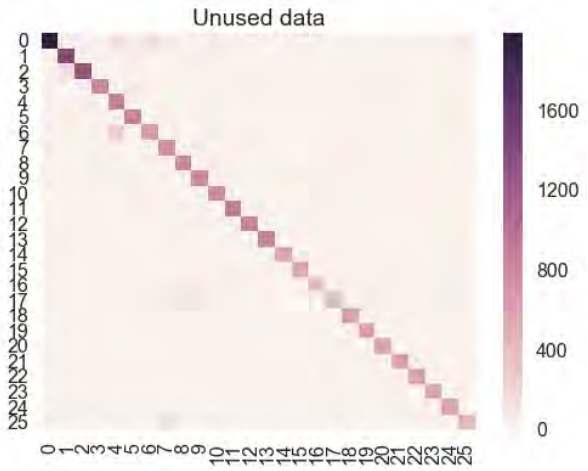

Figure S84: Confusion matrix for the test data used the model described in Source Code 7.

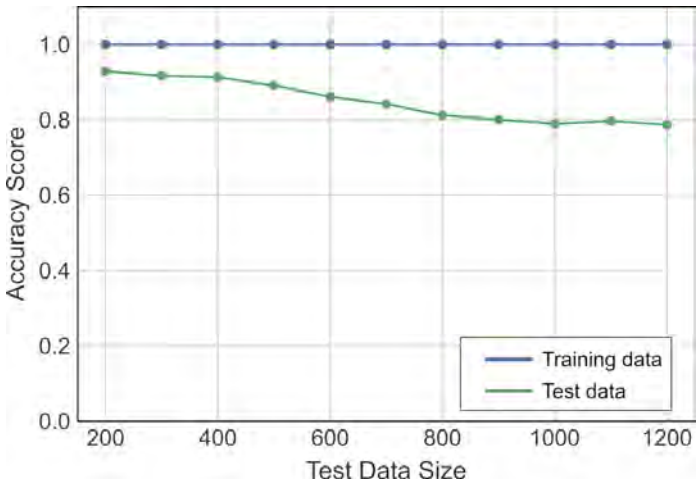

Figure S85: Plot comparing the test data size against the accuracy score.

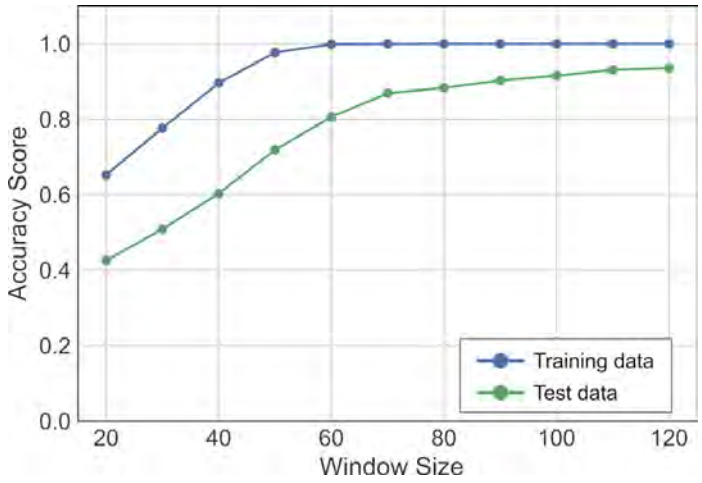

Figure S86: Plot comparing the window size against the accuracy score.

Source Code 8: CNN specification

```
height = 25
width = 25
channels = 1
n_inputs = height * width

conv1_fmaps = 2
conv1_ksize = 3
conv1_stride = 1
conv1_pad = "SAME"

conv2_fmaps = 2
conv2_ksize = 5
conv2_stride = 1
conv2_pad = "SAME"
conv2_dropout_rate = 0.5

conv3_fmaps = 1
conv3_ksize = 3
conv3_stride = 1
conv3_pad = "SAME"
conv3_dropout_rate = 0.5

n_fc1 = 16
fc1_dropout_rate = 0.5

n_outputs = 10
```

5.3 Using CNN to train the BZ medium

In order to extract the rules of the computation of the BZ medium, a Convolutional Neural Network (CNN) was used. The CNN implementation from Tensorflow was used. The scripts used are based on the book “Hands-on machine learning with Scikit-Learn and Tensorflow”[2]. In this case, in order to simplify the system, the patterns representing numbers from 0 to 9 were used (see Section 4.2). In this case, CSV used were the binarised ones. Therefore, each of these CSV had values 0 or 1. These CSV contain 3600 values. In this case, values from 1000 to 3600 were used. The window size used was 25. Therefore, the inputs to the CNN were 25 by 25, or 625 values. The test and train ratio were set to 30%. Three CNN layers were used. The first one uses 2 feature maps and a kernel size of 2. The second one uses 2 feature maps and a kernel size of 5. The third one uses 1 feature maps and a kernel size of 5. Finally, there is a fully connected layer with 16 neurons, and then 10 output neurons. See Source Code 8 and 9 for the CNN specification. The CNN was trained and executed following the code snippets shown in the CNN chapter of “Hands-on machine learning with Scikit-Learn and Tensorflow”[2]. Once the model was trained, the last step was to extract the feature maps the kernels from each of the layers.

5.4 Using an Autoencoder to digitally generate BZ oscillations

In order to create a neural network that could digitally generate BZ oscillations, we used a model similar to the Autoenconder, where the input of the network the motor array patterns (see Section 4.2) and the output of this network were BZ oscillations as generated from the medium. Therefore, this network will learn to given a motor configuration, generate a BZ oscillation.

The Tensorflow library was used. The scripts used are based on the book “Hands-on machine learning with Scikit-Learn and Tensorflow”[2]. In this case, in order to simplify the system, the patterns representing numbers from 0 to 9 were used (see Section 4.2) In this case, CSV used were the binarised ones. Therefore, each of these CSV had values 0 or 1. These CSV contain 3600 values.

The Autoenconder used had 25 inputs and 625 outputs. Three hidden layers were used of 50, 10 and 50 neurons. The code used to train this autoencoder was “Training One Autoenconder at a Time” from [2]. Each autoenconder was trained for 3000 iterations. The learning rate was 0.00001 and L2 regularization was used (0.00001). The output from this autoenconder was input into the CNN explained in Section 5.3.

Source Code 9: CNN layers declarations

```
with tf.name_scope("inputs"):
  X = tf.placeholder(tf.float32, shape=[None, height, width], name="X")
  X_reshaped = tf.reshape(X, shape=[-1, height, width, channels])
  y = tf.placeholder(tf.int32, shape=[None], name="y")
  training = tf.placeholder_with_default(False, shape=[], name='training')

conv1 = tf.layers.conv2d(X_reshaped, filters=conv1_fmaps, kernel_size=conv1_ksize,
↪  strides=conv1_stride, padding=conv1_pad, activation=tf.nn.relu, name="conv1")
conv2 = tf.layers.conv2d(conv1, filters=conv2_fmaps, kernel_size=conv2_ksize, strides=conv2_stride,
↪  padding=conv2_pad, activation=tf.nn.relu, name="conv2")
conv3 = tf.layers.conv2d(conv2, filters=conv3_fmaps, kernel_size=conv3_ksize, strides=conv3_stride,
↪  padding=conv3_pad, activation=tf.nn.relu, name="conv3")

with tf.name_scope("pool3"):
  pool3_flat = tf.reshape(conv3, shape=[-1, pool3_fmaps * heigth * width])
  pool3_flat_drop = tf.layers.dropout(pool3_flat, conv2_dropout_rate, training=training)

with tf.name_scope("fc1"):
  fc1 = tf.layers.dense(pool3_flat_drop, n_fc1, activation=tf.nn.relu, name="fc1")
  fc1_drop = tf.layers.dropout(fc1, fc1_dropout_rate, training=training)

with tf.name_scope("output"):
  logits = tf.layers.dense(fc1, n_outputs, name="output")
  Y_proba = tf.nn.softmax(logits, name="Y_proba")
```

5.5 Using a Recurrent Neural Network to emulate the behaviour of the BZ platform

In order to build a dataset to train a Recurrent Neural Network (RNN), experiments were performed where each stirrer was activated at a random speed for a random duration (minimum of 1 minute). For example, in some of the experiments the 30 minute experiments were divided in windows of 1 minute, and within these windows, each stirrer was activated a random speed. Several variations of this procedure were repeat where the window time was different (ie 1, 2 or 3 minutes) and the range of speeds was also different (ie the full range of PWM until 4000, or until 1000). Once the videos were generated, the data was inputted to the RNN by either only providing the average blue channel of each cell (values from 0 to 255), or by binarizing the whole video using the previously explained SVM (Section 3), and therefore providing to the RNN an array of 0s and 1s.

The RNN was built using Keras (Python). LSTM cells were used. The most common architecture used involved a first “Dense” layer using between 128 to 256 neurons, followed by 3 to 5 LSTM layers, using between 512 to 64 neurons, and finally 1 or 2 “Dense” layers between 256 and 64 neurons. A dropout of 0.2 was used after each layer. In the case of the non-binarized data, the loss function used was “mean seuqred error” and the optimizer used was “rmsprop”. Everything else was set using the Keras defaults. In the case of the binarized data, each “Dense” layer used a sigmoid activation function, the loss function used was “binary crossentropy” and the optimizer used was “rmsprop”.

5.6 Mutual information calculations

The mutual information calculations shown on Table S3 were performed using the function “normalized mutual info score” from “sklearn.metrics.cluster”.

	pat0	pat1	pat2	pat3	pat4	pat5	pat6	pat7	pat8	pat9
pat0		0.005	0.058	0.058	0.001	0.064	0.281	0.036	0.281	0.028
pat1	0.120		0.005	0.005	0.053	0	0.005	0.442	0.005	0.005
pat2	0.031	0.279		0.365	0.001	0.096	0.204	0.116	0.365	0.058
pat3	0.093	0.280	0.401		0.001	0.383	0.204	0.116	0.365	0.058
pat4	0.258	0.133	0.032	0.056		0.039	0.031	0	0.001	0.009
pat5	0.008	0.165	0.107	0.133	0.043		0.383	0.058	0.211	0.064
pat6	0.0375	0.219	0.125	0.081	0.090	0.234		0.036	0.597	0.058
pat7	0.101	0.376	0.199	0.161	0.183	0.219	0.326		0.0365	0.009
pat8	0.199	0.229	0.174	0.250	0.167	0.093	0.178	0.229		0.146
pat9	0.075	0.149	0.227	0.216	0.057	0.046	0.054	0.136	0.226	

Table S3: Top-right part of the table, mutual information of the motor patterns as described in Section 4.2. Bottom-left part of the table, mutual information of the BZ oscillations produced by said patterns, after being trained in an Autoenconder. Therefore, the data here being compared is the “outputs” from Figure 5B in the main manuscript.

6 Towards generalized computation using the BZ platform

The experimental platform consists of n x n cells in a square grid with nearest neighbours connected to each other with an interconnecting channel of the defined dimensions. Each cell consists of a magnetic stirrer together with the motor connected to PWM input. The oscillation amplitude and frequency of Belousov Zhabotinsky (BZ) reaction usually depend on the stirring rate and temperature. In this section, based on the certain assumptions, we explore the possible experimental observables in our experimental set-up which can be utilized for computational operations such as pattern recognition, neural networks etc.

6.1 Experimental inputs

The inputs of the BZ computational platform are defined by the vector with cell positions and the stirring rate of the stirrer placed in the cell. Activating a stirrer in a cell not only affects the amplitude and oscillating frequency of BZ reaction but also allows interaction between nearest neighbours, which can be seen as an operation for information transfer and processing. Assuming each cell (C_{ij}) can be activated with stirring action with k different PWM levels capable of creating distinct chemical oscillations. The total number of input possible combinations are given by k^{nxn}. For the case of two different levels (ON and OFF), the minimum number of combinations are 2^{nxn}. The scaling of the number of input states with n (number of cells in a row/column) is shown in the Figure S87A.

6.2 Chemical states

We define the chemical state of the BZ computational platform using an oscillation frequency and phase of each cell which can be utilized as a basic chemical information processing unit. The single chemical state of the system can be defined for a defined subset of the computational cell by defining an initial phase shift (at the time ($t = t_0$) of activating any subset of the inputs) between the different cells and the oscillating frequencies of each of the cells. Depending on the PWM input state and the state of the neighbouring cells, the oscillation frequency of the cell could be modified.

If we assume for simplicity, that each cell can oscillate between two different states (RED/BLUE) at p different frequencies, the maximum number of chemical states is given by $p^{nxn} \times 2^{nxn}$. Formation of synchronized global waves or independent oscillating regions are different combinations of phase differences and oscillating frequencies of BZ cells. The scaling of the number of chemical states with n (number of cells in a row/column) is shown in the Figure 87B. See also Figure S87. Table S4 shows estimated states and other parameters for BZ computational platform.

Parameter	Magnitude	Comments
Input States (MIN)	*ca.* 3.3×10^{7}	Assuming two different voltage levels (ON/OFF) for the stirrers (no PWM) on 5 x 5 grid.
Input States (MAX)	*ca.* 1.1×10^{15}	Assuming 4 different PWM levels on 5 x 5 grid, with each level capable of modulating the amplitude and frequency of BZ oscillations locally in the cell.
Chemical States (MAX)	*ca.* 3.7×10^{22}	Assuming two different phase states (RED/BLUE) at the time of input/processing event and four different oscillation frequencies of BZ reaction on 5 x 5 grid processing cells. [6, 7, 8, 9]
Chemical Memory	25 bits	Assuming 5 x 5 grid with one bit of information on each cell
Chemical Information readout rate	2.5 bits/s	Assuming the fastest oscillation frequency is 1/10 Hz with imaging full 5 x 5 grid.

Table S4: Relation between the input and the chemical states.

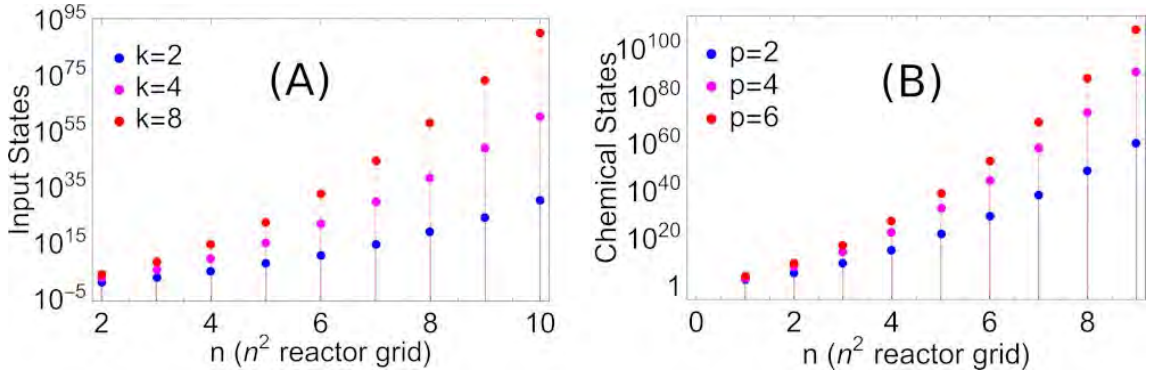

Figure S87: Scaling of the number of states in the BZ computational platform. (A) shows the scaling of the number of input states with the number of BZ cells on the experimental platform at different PWM stirring inputs (2,4 and 8). (B) shows scaling of the number of chemical states with the number of BZ cells on the experimental platform at a different number of measurable oscillation frequencies (2, 4 and 6).

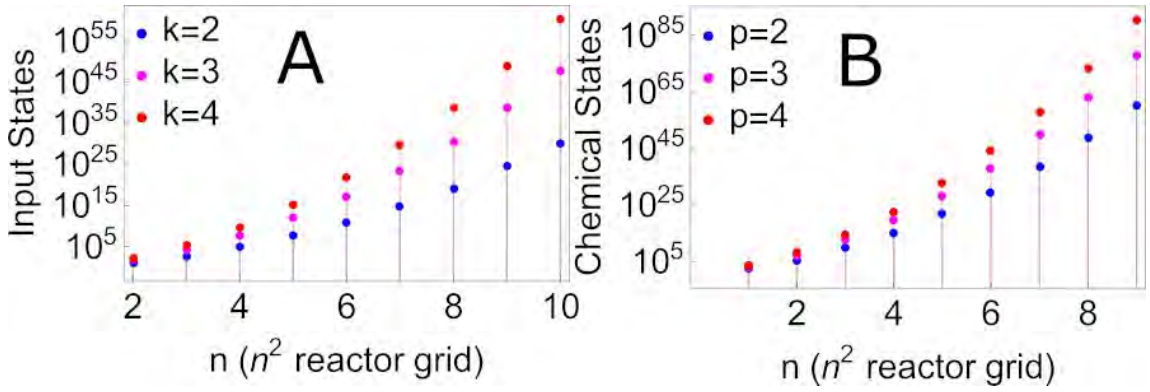

Figure S88: Scaling of the number of states in the BZ computational platform. (A) shows the scaling of the number of input states with the number of BZ cells on the experimental platform at different PWM stirring inputs (2,3 and 4). (B) shows scaling of the number of chemical states with the number of BZ cells on the experimental platform at a different number of measurable oscillation frequencies (2, 3 and 4).

6.3 Mathematical description of the dynamics of coupled BZ Oscillators

In this section, we discuss the coupling between various physicochemical effects expected in the experimental platform and describe a phenomenological model which can be used to develop the efficient and optimized design of the platform. BZ oscillations are often modelled using the mathematical description of autocatalytic reactions such as Brusselator or Oregonator. Due to the complexities of stirring effects which includes the effect of stirring rate on amplitude and frequency of BZ reaction as well as mass transfer between neighbouring cells, we use phase dynamics scheme often used for weakly coupled oscillators. Here, we define set of assumptions to simplify the complexity of coupling between chemical reactions with hydrodynamic interactions and define computation relevant operations on BZ grid.

1. **BZ Cell description:** The time-dependent state of each BZ cell is defined by the phase and amplitude of the oscillation. In the absence of an interaction between neighbouring cells, each cell oscillates at its natural frequency defined by the stirring rate which is also a timedependent operation. So, the complete experimental platform at any time is defined by stirring rate of each cell which defines the natural frequency and phase information. We assume only two different measurable states (RED/BLUE) and hence neglect the amplitude modulation, see Table S4.

2. **Defining Cell States: ACTIVE, PROCESS and INACTIVE** Similar to the experiments and to define different field-programmable computational operations, we categorized the cell into three different states, active, process and inactive.

    - **ACTIVE** cells have relatively faster stirring speed which initiates strong oscillations and influences the neighbouring cells. These cells act as inputs for information processing in the BZ grid.
    - **PROCESS** cells have lower stirring speed which is not capable of initiating strong oscillations but allows and enhances interaction between neighbouring cells. These cells transfer information and process information from the ACTIVE and other PROCESS cells.
    - **INACTIVE** cells have stirrers turn off which inhibits the information transfer and with the neighbouring cells. INACTIVE cells help in allowing parallel information processing in different regions on the grid.

3. **Cell-Cell Interactions:** The interaction between the neighbouring cells depends on the cell state as described above (2). Due to the different stirrer rates in ACTIVE, PROCESS and INACTIVE cells, there is asymmetric mass transfer between the neighbouring cells. We assume cell-cell interactions are confined to nearest-neighbours only, such that ACTIVE and PROCESSING cells can only influence the four nearest neighbours in a square grid.

4. **Coupling Constants between different cell types:** The coupling constant quantifies the cell-cell interaction between two cells neighbouring cells, which can be used as an interaction parameter in the mathematical description of phase evolution. The coupling constant ($K_{ij \rightarrow mn}$) between the two neighbouring cells (indicated by (i,j) and (m,n)) depends on the cell types as described above (2). As different cell types have different speed of the stirrers, there in an asymmetric information transfer between the neighbouring cells. So, depending on the different possible combinations of neighbouring cell types, we can define coupling constants which can be used as parameters which depends on the physical design and angular velocity of the stirrers.

$$K_{ij\to mn} = \begin{cases} K_1, & ij = ACTIVE\ and\ mn = ACTIVE \\ K_2, & ij = ACTIVE\ and\ mn = PROCESS \\ 0, & ij = ACTIVE\ and\ mn = INACTIVE \\ \\ 0, & ij = PROCESS\ and\ mn = ACTIVE \\ K_3, & ij = PROCESS\ and\ mn = PROCESS \\ 0, & ij = PROCESS\ and\ mn = INACTIVE \\ \\ 0, & ij = INACTIVE\ and\ mn = ACTIVE \\ 0, & ij = INACTIVE\ and\ mn = PROCESS \\ 0, & ij = INACTIVE\ and\ mn = INACTIVE \end{cases}$$

So, in the current model, there are only three different interactions, between two ACTIVE cells, from ACTIVE to PROCESS cells and between two PROCESS cells. Using $K_1(r_s)$, $K_2(r_s)$ and $K_3(r_s)$, we can construct a network of coupled oscillators and investigate the evolution of different chemical states.

5. **Memory effect:** As observed in experiments, once a pattern is created on the BZ grid, on deactivating the INPUT cells, the global periodic oscillations sustains for certain time which eventually dampens. The presence of this memory effect in oscillations could be utilized to apply time-dependent operations on the previous state which could be utilized to build a set of complex operations.

Based on the above description, each BZ cell of the grid is defined by an ordinary differential equation (ODE) for phase dynamics with coupling with nearest neighbours[5]. We consider a twodimensional array of coupled oscillators in a square lattice, so the evolution of phase of BZ cell $\varphi(i,j)$ is given by,

$$\frac{d\phi_{ij}}{dt} = \sum_{mn} H\left(\phi_{mn} - \phi_{ij}\right) K_{ij\to mn}\left(r_s\right) + \omega_{ij} + \xi(t)$$

where, φ_{ij} is the phase of cell C_{ij}, ω_{ij} is the natural oscillation frequency which is a function of the angular velocity of the stirring, $K_{ij\to mn}(r_s)$ is the coupling constant between the two neighbouring cells which also depends on the angular velocity of the stirrer (r_s) and the physical design of the interconnects between the two cells. The stronger the angular velocity of the stirrer, stronger the fluid flow and mass transfer between two interconnected cells, and hence larger the coupling constant. $\xi(t)$ is the common noise which satisfies $\langle\xi(t)\xi(t')\rangle = 2D\delta(t - t')$.

These set of coupled equations are complicated by the hydrodynamics between the cells and non-linearity of the Belousov-Zhabotinsky reaction. For simplicity, we assume H as a sinusoidal or a continuous rectangular wave function with a defined period, the above set of equations can be solved using an explicit finite difference scheme. Using these calculations, we can investigate the evolution of different chemical states together with operations and control over the BZ grid. See Figure S89.

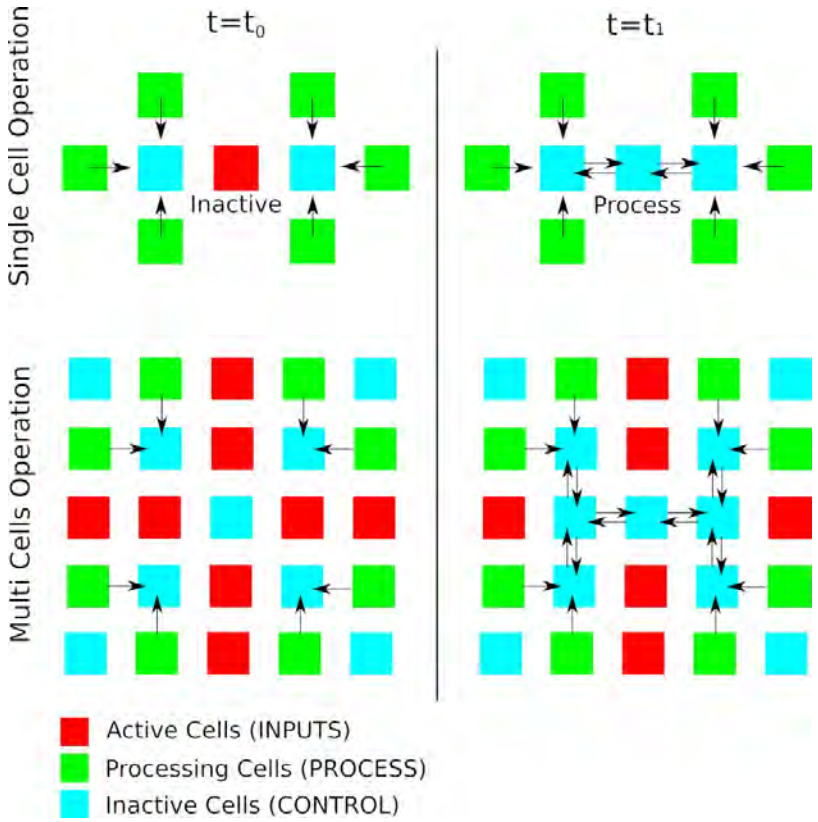

Figure S89: Operations on BZ grid. Figure shows time-dependent single cell or multi-cell operations on the BZ grid by tuning the stirring rates of individual cells.

7 Estimating number of operations and required logic gates

BZ Platform (5 by 5 array):

(Assumption: Two possible initial phases (Red/Blue) and four different oscillation frequencies)

- Total Number of Input Patterns (Binary Stirring Patterns): $2^{25} = 3.35 \times 10^{7}$
- Total Number of Chemical States (defined by Initial Phase and Oscillation Frequency): $2^{25}4^{25} = 3.77 \times 10^{22}$

Autoencoder: Three layers (50-10-50 Neurons):

- Estimated Gate Count for fast multiplication: 12928 [3]
- Estimated Gate Count for addition operation: 1440 [4]
- Possible Input Patterns to autoencoder: $2^{25} = 3.35x10^{7}$
- Possible Output Patterns from autoencoder: 2^{625} (25 cells x 25 time slices centred around oscillation peaks)

Layer 1:

- Number of Neurons: 50
- Number of Inputs: 25
- Total Multiplication Operations: 50 x 25 = 1250
- Estimated Total Number of Gates for Multiplication Operations: 1250 x 12928 = 1.616×10^7
- Total Addition Operations: 50 x 25 = 1250
- Estimated Total Number of Gates for Addition Operations: 1250 x 1440 = 1.8×10^6
- Total Number of Activation Operations: 50

Layer 2:

- Number of Neurons: 10
- Number of Inputs: 50
- Total Multiplication Operations: 10 x 50 = 500
- Estimated Total Number of Gates for Multiplication Operations: 500 x 12928 = 6.464×10^6
- Total Addition Operations: 10 x 50 = 500
- Estimated Total Number of Gates for Addition Operations: 500 x 1440 = 7.2×10^5
- Total Number of Activation Operations: 10

Layer 3:

- Number of Neurons: 50
- Number of Inputs: 10
- Total Multiplication Operations: 50 x 10 = 500
- Estimated Total Number of Gates for Multiplication Operations: 500 x 12928 = 6.464×10^6
- Total Addition Operations: 50 x 10 = 500
- Estimated Total Number of Gates for Addition Operations: 500 x 1440 = 7.2×10^5
- Total Number of Activation Operations: 50

Totals:

- Total Number of Neurons: 50 + 10 + 50 = 110
- Total Multiplication Operations: 1250 + 500 + 500 = 2250
- Total Addition Operations: 1250 + 500 + 500 = 2250
- Total Number of Activation Operations: 50 + 10 + 50 = 110
- Total Operations: 110 + 2250 + 2250 + 110 = 4610
- Estimated Total Number of Gates for Multiplication Operations: 2.9088×10^7
- Estimated Total Number of Gates for Addition Operations: 3.24×10^6
- Estimated Total Number of Gates: 3.23×10^7 (32.3 Mi Logic Gates)
- Assuming the minimum of 2 transistors per logic gate (3 for AND and OR, 2 for NAND and NOR), the total number of equivalent transistors are 32.3 Mi x 3 = 64.6 Mi or ca. 60 Mi
- Assuming the maximum of 3 transistors per logic gate (3 for AND and OR, 2 for NAND and NOR), the total number of equivalent transistors are 32.3 Mi x 3 = 96.9 Mi or ca. 100 Mi
- So, at the individual transistor scale there are a minimum of 60 Mi operations possible or a maximum of 100 Mi operations possible.
- Assuming that our BZ platform encodes similarly to the described Neural Network using 1 minute window of data, then it encodes an equivalent of 60 M/60s = $1Ms^{-}1$.

8 Power dissipation in BZ reaction

$$3CH_2(COOH)_2 + 4BrO_3^- \rightarrow 4Br^- + 9CO_2 + 6H_2O$$

Enthalpy of formation (from NIST database):

1. Malonic Acid (MA): -634.87 kJ/mol
2. Bromate: -342.50 kJ/mol
3. Bromide: -121.0 kJ/mol
4. Carbon dioxide: -393.50 kJ/mol
5. Water: -285.82 kJ/μmol

Using Hess' Law:

- For Reactants: 3 MA + 4 BrO_3^- = -3274.61 kJ/mol
- For Products: 4 Br^- + 9CO_2 + 6H_2O = -5619.42 kJ/mol
- Difference = -2344.81 kJ/mol (for 3 mols of Malonic Acid)
- For per mol of malonic acid, enthalpy of reaction is -781.60 kJ/mol

Concentration of Malonic Acid: 1 M
Total volume of Malonic Acid used: 18ml
Total time: ca. 2.5 hours **(Assumed)**

So, the total power dissipation is given by,
P = (781.60 kJ/mol x 1 M x 18 ml) / (2.5 x 3600s) = 1.56 J/s

If we use the BZ platform to run 50 x 10 x 50 neural network with the estimated speed of 1 Mi equivalent transistor operations per second, the power consumption per operation is 1.56 μJ. However, running a three-layer 50 x 10 x 50 neural network only uses a small subset of total possible chemical states (as most of the BZ cells oscillates at the same frequency with variable phase differences). So, with the similar power consumption, much more information processing is possible. So, accessing all chemical states (2 phase states, 4 frequencies give 3.77 x 10^{22}) can substantially reduce the power consumption per chemical operation. It is important to note that, by correctly defining a chemical operation, much more information processing is possible as compared to single transistor scale or logic operations.

If we assume that all chemical states are accessible in 2.5 hours, the estimated power consumption per chemical operation (switching form one chemical state to other),

$P = (781.60\ kJ/mol \times 1\ M \times 18\ ml) / (2.5 \times 3600s) \times (1/2^{25}4^{25}) = 4.13 \times 10^{-23}\ J/s$

Current state-of-the-art, Intel i9 processor with 7 Bn transistors all clocking at 4 GHz consumes 147 W. So, power consumption per operation is given by,

$P = 147\ W / (4\ GHz \times 7 \times 10^{9}) = 5.25 \times 10^{-18}\ J$

9 Figures enhancements

All the figures shown in the main manuscript and in this document were designed using Inkscape (inkscape.org).

On Figure 2 from the main manuscript, the top-down pictures of the device were the oscillations can be seen were manually enhanced in order to make the oscillations more visible. In the Supplementary Video these oscillations can be clearly seen.

Bibliography

[1] Lukosevicius, M., and Jaeger, M.: Reservoir computing approaches to recurrent neural network training, *Computer Science review*, 3, 127–141 (2009).

[2] Geron, A.: Hands-on machine learning with Scikit-Learn and Tensorflow, *O'Reilly* (2017).

[3] Jones, D.W.: CS:2630, Computer Organization Notes. Beyond Integer Addition and Subtraction, *The University of Iowa - Department of Computer Science*.

[4] Jones, D.W.: CS:2630, Computer Organization Notes. Arithmetic and Logic, *The University of Iowa - Department of Computer Science*.

[5] Hoppensteadt, E.M., Izhikevich, E. M.: Weakly Connected Neural Networks, *Springer, New York* (2007).

[6] Kalishyn, Y.Y., and Rachwalska, M., Strizhak, P.E.: Stirring Effect on the Belousov-Zhabotinsky Oscillating Chemical Reactions in a Batch. Experimental and Modelling, *A Journal of Physical Sciences*, 65a, 132–140 (2010).

[7] Ruoff, P.: Excitations induced by fluctuations: an explanation of stirring effects and chaos in closed anaerobic classical Belousov-Zhabotinskii systems, *The Journal of Physical Chemistry*, 97(24), 6405–6411 (1993).

[8] Dutt, A.K., Mueller, S.C.: Effect of stirring and temperature on the Belousov-Zhabotinskii reaction in a CSTR, *The Journal of Physical Chemistry*, 97(39), 10059–10063 (1993).

[9] Noszticzius, Z., Bodnar, Z., Garamszegi, L., Wittmann, M.: Hydrodynamic turbulence and diffusion-controlled reactions: simulation of the effect of stirring on the oscillating BelousovZhabotinskii reaction with the Radicalator model, *The Journal of Physical Chemistry*, 95(17), 6575–6580 (1991).